The University of Sheffield

Single Molecule Spectroscopy Studies on the Fluorescent Properties of PCDTBT

Author:
Adrian Razvan Mantsch

Supervisor:
Dr. Ashley Cadby

A thesis submitted in partial fulfilment of the requirements for the degree of Master of Philosophy

in the

Department of Physics and Astronomy

June 2018

"We never experiment with just one electron or atom or (small) molecule. In thought experiments we sometimes assume that we do; this invariably entails ridiculous consequences ... we are not experimenting with single particles, any more than we can raise Ichthyosauria in the zoo."

Erwin Schrödinger

THE UNIVERSITY OF SHEFFIELD

Abstract

Faculty of Science
Department of Physics and Astronomy

Master of Philosophy

Single Molecule Spectroscopy Studies on the Fluorescent Properties of PCDTBT

by Adrian Razvan Mantsch

Conjugated polymers are a class of materials which acquired an increasing scientific interest in recent decades, due to their distinct photophysical properties. A consequence of their unique chemical structure, characterised by a system of delocalised π-electrons, their properties makes them suitable for optoelectronic applications. In this project we studied the optical properties in single molecule domain of a polycarbazole type conjugated polymer, poly[N-9'-heptadecanyl-2,7-carbazole-alt-5,5-(4',7'-di-2-thienyl-2',1', 3'- benzothiadiazole)], commonly known as PCDTBT by means of single molecule spectroscopy and fluorescence blinking.

Photoluminescence spectroscopy, characterised by multiple chromophore fluorescence emission, and lifetime imaging of PCDTBT single molecules suggest an emission mechanism based on intrachain energy transfer. We then use photo blinking measurements to reveal the mechanism responsible for the intermittent fluorescence emission as well as the origin of the material's emission. Three fluorescent states were observed, which is an indication of intramolecular aggregates that allow direct energy transfer between various chemical groups composing the polymer backbone. A statistical analysis of the measured fluorescence time traces shows that a tunnelling mechanism is present in the sample which is likely responsible for the intermittent fluorescence emission.

Acknowledgements

This work was funded by the ACRITAS FP7 Initial Training Network (www.acritas.eu), in the form of a Marie Curie fellowship.

I would firstly like to thank my supervisor, Dr. Ashley Cadby, for his assistance, support and the opportunity to work on this project.

Next I wish to thank Cvetelin Vasilev (Department of Molecular Biology and Biotechnology, University of Sheffield) for his help in optimising the experimental set-up automation.

I also thank James Kingsley (Ossilla) for providing the conjugated polymer used in this study as well as Stuart Harris (Zeon chemicals Europe Ltd.) for supplying the Zeonex polymer matrix, used in sample preparation.

Lastly, I would like to thank my family for their support in my long endeavour at the University of Sheffield.

Contents

List of Figures

Chapter 1

Introduction

1.1 Outline of work

1.1.1 Importance and objective

The importance of conjugated polymers has increased in the last decades, due to their emergence as an attractive class of materials for the development of organic electronic devices, mainly biological and chemical sensors [1–3], solar panels [4–6], LED's [7–9] or field-effect transistors [8, 10, 11]. One conjugated polymer of interest in the field of optoelectronics is PCDTBT. Due to its low HOMO/LUMO levels, it has led to an increase in the efficiency of photovoltaic devices which can exceed the efficiencies reported for other conjugated polymers commonly used in optoelectronics [12, 13].

To use this class of polymers in the applications listed above, one must first understand their fundamental properties. Due to a certain degree of disorder in thin polymer films, there's a significant difference between the properties of polymers in bulk and at nanometer scale. To overcome this limitation, Single-Molecule Spectroscopy (SMS) has emerged. It was initially developed as a cryogenic technique [14] and it relies on the detection of photoluminescence (PL) emission of individual chromophores, deposited on an inert substrate [15, 16]. Figure 1.1 shows the basic principle on which SMS operates. Due to the limitations of optical microscopes,

in order to image the fluorescence originating from individual emitters the concentration of the deposited film must be low enough so that the physical separation between individual molecules is higher than the device's diffraction limit.

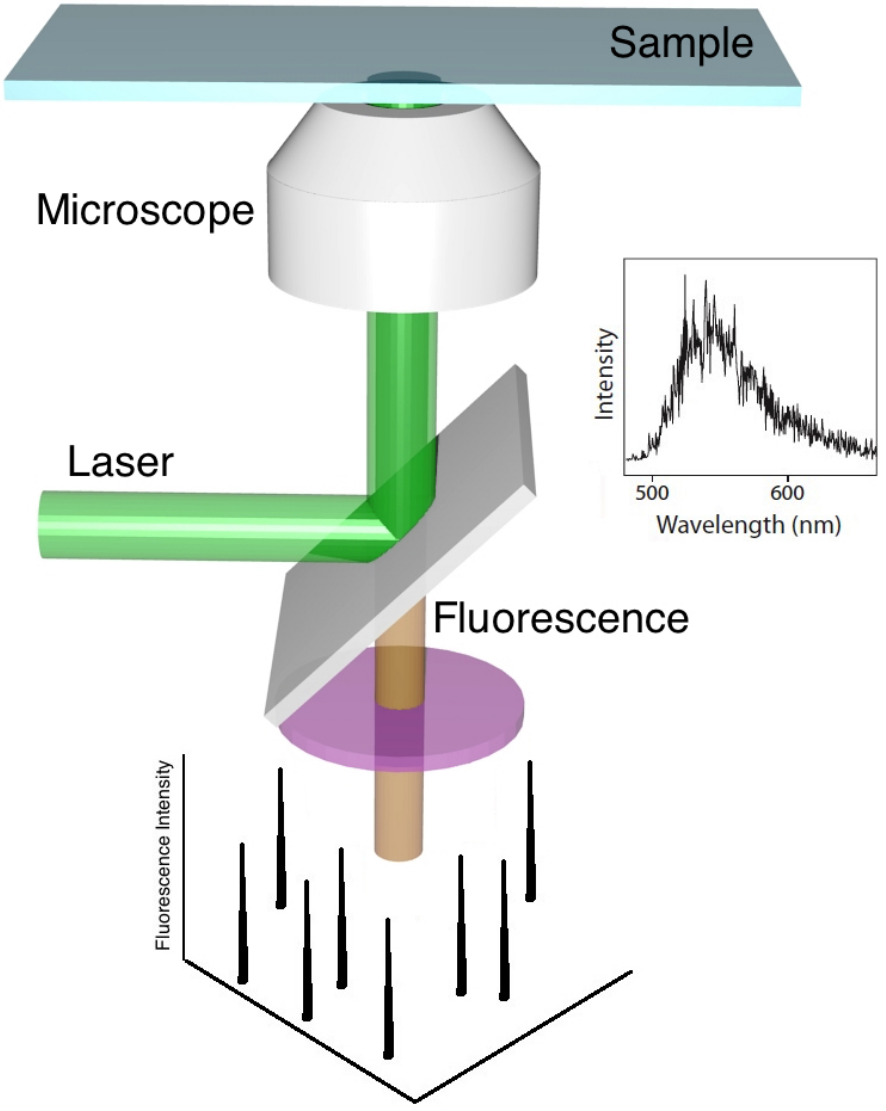

FIGURE 1.1: The basic principle behind single-molecular spectroscopy

Despite the recent developments in the optoelectronic device area, there is still a significant gap in understanding the photophysics of conjugated polymers. The final goal of the project is to gain knowledge on the likely mechanisms involved in the absorption and emission of light by a polycarbazole type conjugated polymer, in the single molecule domain. Since photoluminescence (PL) experiments take a long time and require the analysis of a large population of single emitters for any significant statistical characterisation, a secondary objective is to automate and optimise the

experimental procedure in order to allow acquiring and analysis of PL data for numerous molecules in a reasonable amount of time.

1.1.2 Thesis overview

The current thesis presents a Single Molecular Spectroscopy (SMS) study on a polycarbazole based conjugated polymer, namely PCDTBT, which is of interest in polymer electronics. It is structured in 6 chapters, as follows:

Chapter 1 gives an introduction in the field of semiconductor physics, a brief description of polymer semiconductors as well as the project goal and a list of publications.

Chapter 2 shows a theoretical overview on the subject discussed in this study. We offer a general overview of polymeric materials and a description of π-conjugated polymers. Emphasis is put on on the optical properties of π-conjugated polymers, more precisely the absorption process and a description of excited states (polarons, triplets, singlets) as well as the parameters that define the lifetime of excited states. Also, we review the previous work in the field on single molecule studies as well as a discussion on the technological importance of PCDTBT.

In chapter 3, besides the sample preparation procedure, we also describe the techniques used in this study as well as an overview of the experimental set-up. Also, we show initial design ideas regarding the automation of data acquisition a detailed description of the current automation system

Results are shown in chapters 4 and 5. Chapter 4 is dedicated for single molecule studies on PCDTBT, photoluminescence both in bulk and at single molecule level followed by fluorescence lifetime measurements and time-resolved analysis of the results. This chapter is followed by chapter 5, which is reserved for fluorescence time trace measurements on the studied conjugated polymer and an analysis of its molecular dynamics.

In chapter 6, we summarise the results and present the conclusions of our study as well as possible directions for future research. Since the experimental techniques result in a relatively large volume of data, we close this thesis with a series of appendices which present the codes used for automatically analysing the PL and time trace results.

1.2 Introduction to semiconductor physics

1.2.1 Semiconductors

Based on their resistivity values solid materials are separated into conductors (mostly metals, approximately 10^{-8} Ω·cm) and insulators (10^{18} Ω·cm). Semiconductors are intermediates between the two categories, with resistivity values in the 10^{-2} - 10^{8} Ω·cm range. Figure 1.2 shows this separation. Metals are materials that occupy the low range of the resistivity scale. Nevertheless, there are materials in this class that have relatively high resistivities compared to typical metals. Therefore, metals which exhibit this property are also known as semimetals. An important feature that needs to be mentioned is the behaviour of materials at the high end of the resistivity range. At high resistivities, semiconductors and insulators are hard to separate and temperature becomes an important factor. Since conductivity (and implicitly resistivity) depends strongly on temperature, the distinction between a semiconductor and an insulator depends strongly on the material's temperature at any given time. For this reason, semiconductors can be defined as a group of materials that have a measurable electric conductivity at room temperature or above [17].

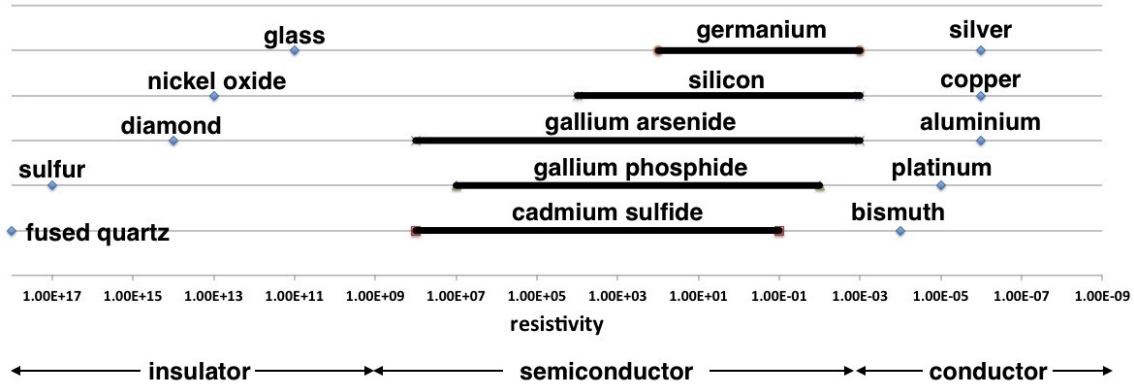

FIGURE 1.2: Common resistivity ranges for conductors, semiconductors and insulators.

The classification of materials into conductors, semiconductors or insulators is dictated by the band structure which is a direct result of the material's crystalline structure, more specifically on how the atoms composing the crystalline lattice are arranged. Since the potential energy of atoms vary with the interatomic distance, the

properties of a crystalline material can only be adequately described using quantum physics [18, 19].

A quantum mechanics treatment is more complex than needed in this context, therefore the formation of energy bands will be briefly explained by means of Bohr's theory [20]. By combining the classic planetary model with quantum mechanics, he was able to explain why and how electrons occupy stable "orbits" around a nucleus, by occupying certain pre-determined energy levels. When more atoms are approaching one another, the energy levels of each atom split into several separate (but close) levels. In the case of a crystal, these separate energy levels merge to form a single continuous band. When the interatomic distance within the lattice reaches equilibrium, this continuous energy and separates in two distinct components: the valence and conduction band, separated by a bandgap (also known as forbidden band). This band, more precisely its energy, represents the minimum required energy to create electron-hole pairs and it it the main property that determines a material's conduction properties.

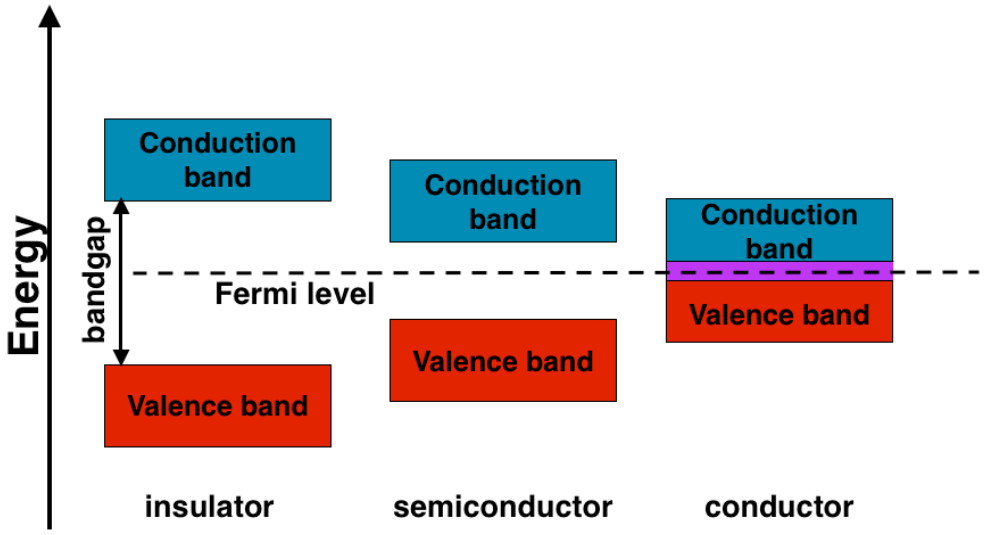

FIGURE 1.3: Schematic representation of energy bands.

In figure 1.3 we schematically show the conduction and valence bands for the above mentioned classes of solids. Electrons occupying the valence band are are unable to travel between various atoms sharing a crystalline network, as opposed to electrons occupying the conduction band which are free to move and act as charge carriers. For conductors, there are two possible situations: the energy levels in the conduction

band are partially filled or the valence band is fully filled and it also overlaps with the conduction band. In both these situations, the forbidden band is virtually non-existent and electrons are free to move between atoms with a minimal intake of energy. With regards to semiconductors and insulators, electrons completely occupy the valence band while the unoccupied conduction band is separated from the valence band by a bandgap. In this situation, electrons require a relatively large amount of energy, higher or equal to the energy of the bandgap, to bridge the separation between the valence and conduction bands and freely move between various atoms in a molecule or crystal. For insulators, the bandgap is very large and thermal energy or electric fields will be unable to supply sufficient energy to move an electron from the valence band to the conduction band without compromising the structure of the molecule or crystal. Semiconductors on the other hand, have a narrower forbidden band and thermal energy is usually sufficient to excite electrons. However, despite the narrower bandgap compared to an insulator, if the thermal energy supplied to the molecule is too low, the material will become an insulator as opposed to metals, which will have conductive properties practically at any temperature [17, 21].

1.2.2 π-conjugated polymers

Among semiconducting materials, organic and inorganic, polymers have gained interest in recent decades, due to the possibility of producing optoelectronic devices at costs lower than similar devices fabricated with silicon and well as the possibility of introducing new features and functionalities such as optical transparency or flexibility, features that are difficult and sometimes impossible to achieve in silicon based technologies [22–25].

In order to be suitable for fabricating optoelectronics, a polymer must have a conjugated molecular backbone, composed of alternating single and double bonds. Figure 1.4 shows a few examples of π-conjugated polymers. The single bond-double bond conjugation enables certain optical properties and enhances the transport of electrical charges [26, 27]. Also, functionalizing the polymer with certain unsaturated substituents, including simple olefins, heterocycles or aromatic hydrocarbons, in order to enable cheap manufacturing techniques (from solution) or to control certain properties such as optical absorption and PL [28].

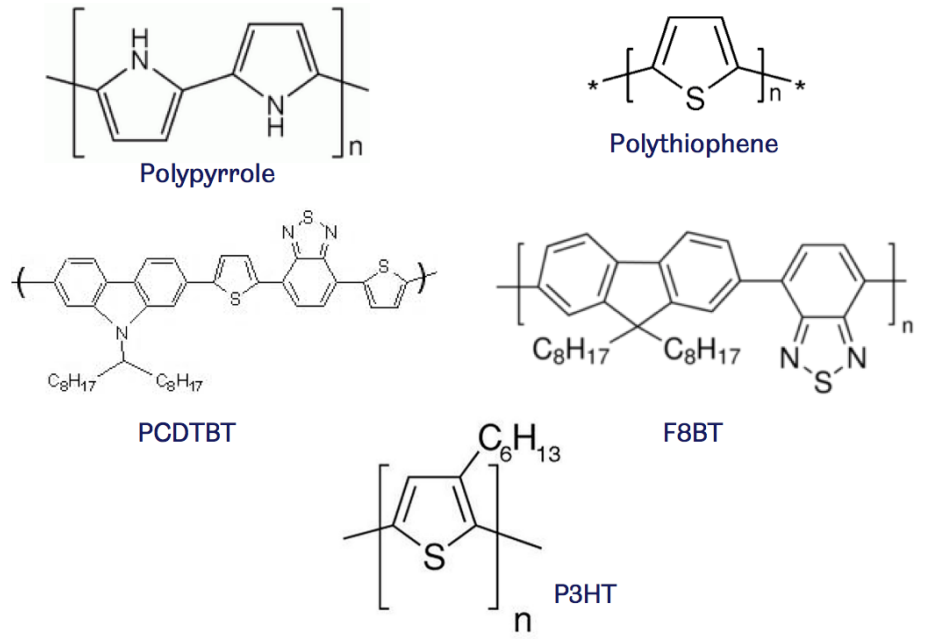

FIGURE 1.4: Examples of π-conjugated polymers used for fabricating optoelectronic devices.

Other properties that influence the formation of thin films as well as solubility or morphology are the polydispersity index (PDI) and the polymer's molecular weight (Mw). Modifying a polymer's molecular weight, will greatly change its thermal properties and electronic structure. Therefore it is important to achieve a certain equilibrium between the material's PDI and Mw, so that the properties of interest are stable and reproducible [29].

There are advantages for using π-conjugated polymers, compared to regular semiconductors [26]:

- Thin polymer films offer a uniformity which in turn offers increased control over structural characteristics. This will improve printing, since the process requires a high level of control over rheological properties.
- Due to the very small size of a polymer's crystalline domains, charge transport becomes isotropic which increases performance stability from one device to another.
- Since polymers have a very narrow solubility range and high viscosity in bulk, manufacturing multilayered devices is improved due to a higher range of material and solvent choices.

- Compared to classic semiconductors, polymers have little to no vapour pressure devices fabricated from polymers are less susceptible to diffusion during fabrication. Also, mechanical properties are more adaptive, which makes conjugated polymers suitable for flexible nanometer thick devices.

1.2.3 Morphology change with optical properties

The improvement of organic nanoscale electronic devices in recent years is linked to breakthroughs in synthesising new conjugated polymers. π-conjugated polymers are one of the most important group of materials due to their potential in developing a wide range of electronic devices such as light emitting devices (OLED), photovoltaics, field-effect transistors or photodiodes [30, 31].

Polymers in this class are formed of chains of alternating single and double bonds, a characteristic which dictates the colour of the material and its fluorescence properties. If such a molecule absorbs a photon, it will form an excited state in which a certain segment of the polymer chain contains an excited electron. If the length of the chain containing the excited electron increases, the energy of the excited state will be lower. Because exact calculations are difficult, this behaviour can be approximated by the quantum particle in a box problem: the longer the box, the lower the energy of the excited state and the peaks in the fluorescence spectrum will be shifted to red. But polymer chains are not straight and rigid rods. If the molecule is very long, the conjugated polymer chain will adopt various conformations, resulting in conjugated chains of different statistical lengths. For large polymer chains, due to its molecular conformation, the end-to-end distance of the excited chain (approximated by a quantum particle in a box) will be shorter than the physical length of the molecule, which will cause a fluorescence emission of higher energy than expected [32–34].

An example of such behaviour is seen in PFO (poly(9,9-dioctylfluorene). As seen in [35], the polymer has two main conformations: glassy PFO and "β-phase". When using chloroform, being a good solvent for the polymer, the fluorene units are free to rotate in order to accommodate the relatively long alkyl side chains. When exposed to toluene, the polymer adopts the β-phase conformation (figure 1.5). The solvent will induce a swelling of the polymer, thus elongating the polymer chains. this elongation forces PFO to twist and adopt a helix conformation, in which the angle

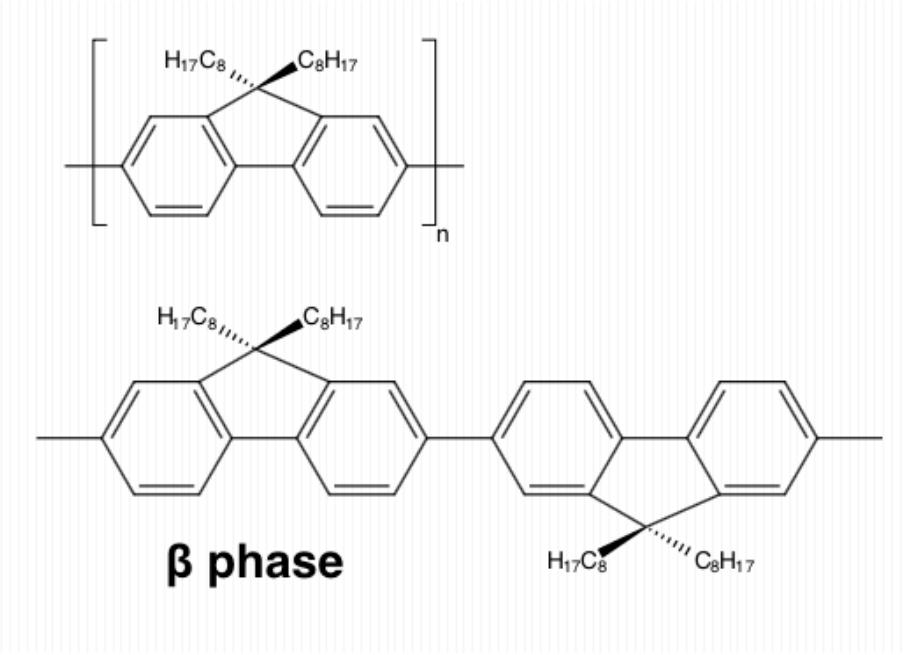

FIGURE 1.5: The chemical structure of PFO at different rotational angles.

between monomer units is fixed at 180°. This renders the polymer chains relatively planar and ribbon like. In figures 2 and 3 of [35] we see the absorption and emission properties of the polymer in both conformations. Although the absorption shows little change between the two phases, the PL spectra of the β-phase is red-shifted, which is consistent with an elongated molecule and subsequently a lower energy gap for the chains with fixed 180° angles.

1.3 List of publications

- **A. Mantsch**, A. J. Cadby, *Automated Microscopy System for Single Molecular Spectroscopy Measurements.* Focus on Microscopy, Goettingen, Germany, March 29 - April 1 2015, pp. 479, ISBN 978-3-95404-942-4.

- **A. Mantsch**, Ashley Cadby, *Correlating the Optical Properties pf Single Polymer Chains with Morphology*, ACRITAS Workshop "Imaging and controlling molecular assembly", Graz, Austria, February 10 - 11, 2016, pp. 28.

- **A. Mantsch**, A. Cadby, *Single molecular spectroscopy. Parallel lifetime and imaging of single molecules.* G.I.T. Imaging & Microscopy 2 (2016), pp. 21 - 23.

Chapter 2

Background

2.1 Polymers

2.1.1 Introduction

Polymers (Greek polus, "many" + meros, "parts") are macromolecules composed of a large number of repeating units, known as monomers. There are many examples of naturally occurring polymers, such as starch, cellulose or several macromolecules essential for life such as proteins, DNA and RNA. The earliest uses of these materials has involved the use of natural polymers to produce small artefacts. In the early 19th century scientists started to chemically modify natural polymers, in order to produce a wider range of materials, such as celluloid or gun cotton.

In the mid 19th century and early 20th century, synthetic polymers were first manufactured. Given the endless possibilities of fabricating synthetic polymers, possibilities limited only by chemical and physical laws, this class of materials has found applications in virtually all fields of science and industry as well as a wide variety of applications in every day life such as clothing, electrical components, packaging, cosmetics and so on.

2.1.2 Classification

The classification of polymers is based on several criteria, which will briefly be discussed below.

- Structure
- Chain architecture
- Miscellaneous criteria

2.1.2.1 Structure

The first classification criteria for polymers was proposed in 1929, and it separates polymeric materials into two main categories: addition polymers and condensation polymers. Both types are based on the structure of the repeating unit. For addition polymers, the repeating unit has virtually the same structure as the monomer. As opposed to addition polymers, in the case of condensation polymers, the monomers reacting in order to form the repeating unit will suffer a change in their chemical structure by forming a condensation compound (as seen in the case of polyester synthesis) [36].

Although this initial criteria was reasonable, some newer materials had a chemical structure similar to that of a condensation polymer but the synthesis mechanism did not form a condensation compound. In order to take into account these exceptions to the general rule, a series of conditions have been introduced. In order to be considered a condensation polymer, a material has to satisfy the following conditions [37]:

- during preparation, some of the monomer's constituents are lost and will form a small condensation molecule (such as a number of water molecules, as seen in polyesters);
- the polymer backbone contains functional groups such as amide or ester groups.

If a polymer does not meet any of these conditions, it will be categorised as an addition polymer.

2.1.2.2 Chain architecture

Despite the fact that some polymers have identical chemical structures, their chemical, physical and mechanical properties can radically differ based on the architecture of their main molecular chain. For this purpose, polymers can be classified as:

- **Linear** polymers - the main molecular backbone presents no side branches;
- **Branched** polymers - the polymer chain several branches of various lengths;
- If the side chains in a branched polymer are formed by a different monomer than the one forming the backbone, the polymer will be a **graft** polymer.
- **Crosslinked** polymers - small structures or chemical interactions will bond together different sections of a polymer's chain, or even several separate chains, thus forming a large three dimensional structure. Most of the times, the crosslinking process is irreversible, leading to a structure with high stability but limited solubility and mobility. an exception is the elastomer class, where the crosslinks are physical in nature, in the form of physical interactions or entanglements.

2.1.2.3 Miscellaneous criteria

Besides the above mentioned classification, there are other criteria on which polymers can be classified. This includes **biodegradability**, **origin**, **morphology** or **production size**. Based on their origin, polymers are classified into two main classes: natural (naturally occurring) and synthetic (manufactured in a laboratory). Additionally, based on the presence of carbon, synthetic polymers are divided into two categories: organic, the most studied of the two categories, and inorganic, such as silicone rubber. According to the morphology of the macromolecule, polymers are of two types:

- homopolymers - the polymer chain is formed of only one type of polymer.
- copolymers - the polymer molecule contains several different types of monomers. Based on the arrangement of these monomer unites, copolymers can be random (-A-B-B-B-A-A-B-A-B-B-A-A-B-), block (-A-A-A-A-A-B-B-B-B-B-) or alternating (-A-B-A-B-A-B-A-B-A-B-).

Another important classification criteria is the material's production size. Polymers produced in large quantities and with low profit margins per weight unit are commodities. Commodities include polymers with a very wide range of applications, such as polyethylene, polycarbonate, PMMA, PET or PVC [38]. Moreover, there are polymers produced in relatively small volumes, produced for very specific applications. There materials are specialty polymers.

2.1.3 Molecular weight

An important property of polymeric materials is molecular weight. As opposed to small molecules, which exhibit a fixed molecular weight, not all polymer chains will have the same length or molecular mass. Therefore, any given type of polymer will be characterised by a distribution of molecular weights or a series of average weights. As shown in [39, 40], the most common averages used to define a polymer's molecular weight distribution are the number average molecular weight ($\bar{\mathrm{M}}_\mathrm{n}$) and weight average molecular weight ($\bar{\mathrm{M}}_\mathrm{w}$). They are defined by the following equations:

$$\overline{M}_n = \sum_x f_x^n M_x \tag{2.1}$$

$$\overline{M}_w = \sum_x f_x^w M_x \tag{2.2}$$

where f_x^n and f_x^w are the number and weight fractions of chains containing x monomers and $\mathrm{M_x}$ represents the molecular weight of a chain with x monomers, which is:

$$M_x = xM_0 \tag{2.3}$$

M_0 represents the molecular weight of one monomer unit.

Another example of important and commonly used quantities are the weight average ($\bar{\mathrm{r}}_\mathrm{w}$) and number average ($\bar{\mathrm{r}}_\mathrm{n}$, also known as degree of polymerisation) chain lengths. These are properties related to the number average and weight average molecular weights and are defined as follows:

$$\overline{r}_n = \frac{\overline{M}_n}{M_0} \tag{2.4}$$

$$\overline{r}_w = \frac{\overline{M}_w}{M_0} \tag{2.5}$$

2.1.4 Nomenclature

Presently, there is no standard criteria for naming polymeric materials. Although rules for naming these materials have been introduced by IUPAC (International Union for Pure and Applied Chemistry), these naming rules are not widely used. Instead, for many polymers, their trade names are more popular than the IUPAC nomenclature. for this purpose, three main naming systems have been established [37]:

- source-based terminology;
- IUPAC nomenclature;
- abbreviations and trade names.

Conventional, source-based nomenclature

This is the most widely used naming criteria. Applied mostly for simple homopolymers, it uses the word "poly" and the name of the repeating unit. In case of copolymers, the name of the monomer unit is replaced by the chemical group formed by the two reacting monomer units. Examples of polymers named using this nomenclature are:

- Polystyrene - PS;
- Poly(vinyl chloride) - PVC;
- Poly(methyl methacrylate) - PMMA;
- Poly(ethylene terephtalate) - PET;

IUPAC naming criteria

Similar to the source-based criteria, the rules established by IUPAC are used for single strand polymers, built from constitutional units connected by an atom from each adjacent unit. In this case the naming is based on the prefix poly and the name of the smallest repeating unit (CRU - constitutional repeating unit). Most conventional polymers care considered single strand and therefore compatible with this rule. It is more powerful than other non-conventional naming procedures, since it gives information regarding the material's chemical structure. More details about the IUPAC nomenclature are presented in [41].

Abbreviations and trade names

Although the IUPAC and source-based nomenclatures are sufficient for naming polymeric materials, some materials have very well known trade names that will always take precedent over their IUPAC names. Such materials are

- nylons (belonging to the polyamide family);
- kevlar - poly(paraphenylene terephtalamide);
- teflon - poly(tetrafluor ethylene);

Also, due to the impractically long names of some polymers, especially conjugated polymers, abbreviations are widely used. Such examples are:

- P3HT - poly(3-hexylthiophene-2,5-diyl);
- F8BT (sometimes known as PFBT)- Poly(9,9-dioctylfluorene-alt-benzothiadiazole);
- PCDTBT - Poly[N-9'-heptadecanyl-2,7-carbazole-alt-5,5-(4',7'-di-2-thienyl-2',1',3'-benzothiadiazole)];

2.2 Introduction to conjugated polymers

As mentioned in a previous section, polymers can be classified according to various criteria such as origin, biodegradability or production volume. Besides widely used

commodity polymers, there are specialty polymers which are characterised by small production batches. Among these specialty polymers a class that holds particular importance to several fields of research are π-conjugated polymers.

Conjugated polymers are polymer macromolecules characterised by a delocalisation of the double bonds in their main chain. First discovered in the early 20th century with the preparation of polyacetylene [42], the materials gained interest in the 1970's, when the Nobel prize for chemistry was awarded in 2000 for the discovery of their conductive properties [43, 44]. In the awarded paper, the authors measured the conductivity of halogenated cis and trans isomers of polyacetylene, which showed a semiconductor-like behaviour of polyacetylene halides.

Due to their peculiar optical and electrical properties (properties resulting from the alternating single and double bonds in their backbone) this class of materials has gained importance in optoelectronics, mainly the production of new and improved devices such as LED's [7–9], solar cells [4–6] or field effect transistors [8, 10, 11]. Other, more recent applications, include their use as active materials in batteries [45, 46], optical switching devices due to third-optical nonlinearity of these conjugated polymers [47] or sensors and actuators for artificial muscles [48].

Examples of such polymers are polythiophene or p-doped poly(3,4-ethylenedioxythiophene).

2.2.1 Main characteristics

The first and simplest π-conjugated polymer was polyacetylene. It was discovered in 1958 as a linear polymer [42] and it was of little scientific interest until 1977, when its conductive properties were demonstrated [43]. For this purpose, polyacetylene will be used to present the main characteristics of conjugated polymers.

With the structure $(\text{-CH=CH-})_x$, this very basic linear conjugated polymer can be considered a 1D analogue of graphite , due to its hybridised carbon atoms. One difference between a conjugated polymer's main chain and graphite is the fact that the polymer's single carbon bonds are not of equivalent length. Due to this variation in bond length the electronic properties are altered and a bandgap between the HOMO (an occupied πband) and LUMO (unoccupied π^* band) levels is opened. Thus, these materials can be included in the semiconductor category, with a bandgap of 1 to 3 eV, due to their distinct electronic properties. Also, the π-π^* optical transition

(corresponding to the bandgap) will give the polymers colour, which translates to a strong spectral component in the visible range [45, 49]. This is shown in figure 2.1

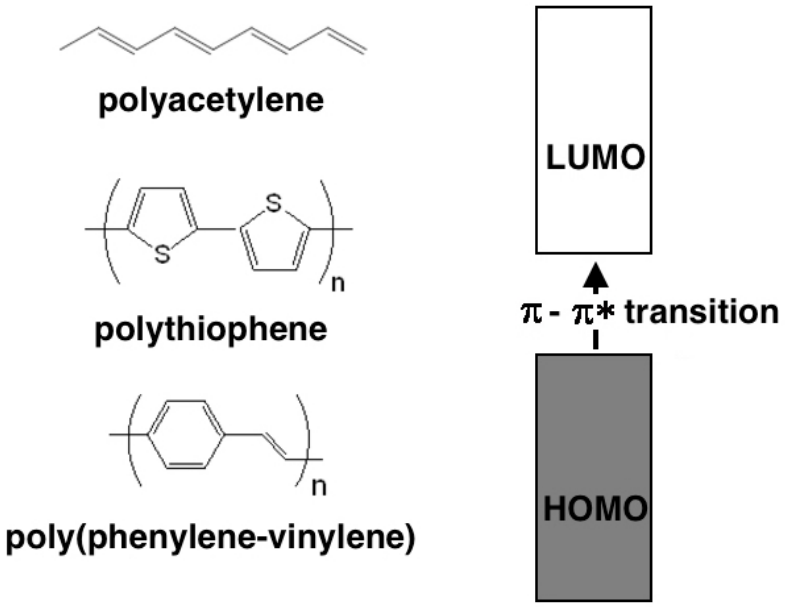

FIGURE 2.1: Examples of common π-conjugated polymers and the optical band gap.

In essence, optical properties can be controlled by the length of the bandgap. Functionalizing the main polymer chain by selecting proper electron donor and acceptor chemical groups will result in π-conjugated polymers with narrow bandgaps and small variations in the bond length. Historically, the narrow bandgap conjugated polymer was poly(isothianaphtene), prepared in the mid 1980's through electrochemical polymerisation [50]. The polymer has a bandgap of 1 eV, approximately half of the value for the commonly used polythiophenes.

Although these materials have gained significant interest in the last decades and dozens of conjugated polymers with narrow bandgaps have been synthesised, a π-conjugated polymer with overlapping conduction and valence bands and negligible bandgap has not yet been discovered.

2.2.2 Synthesis

There are many routes for synthesising conjugated polymers, involving typical polymer chemistry procedures in addition to electrochemical and organic chemistry

methods. One example is the preparation of poly(acetylene), the simplest conjugated polymer, which can be prepared from cyclooctatetraene (COT)through a ring opening polymerisation reaction in the presence of a catalyst [45, 51]. One such reaction was proposed by Edwards and it involves a multiple step procedure, which is presented in figure 2.2. Firstly, COT reacts with hexafluoro-butyne forming the monomer, which is then traded with an appropriate catalyst (Ziegler-Natta or metathesis). The result of this catalytic reaction is a precursor polymer which leads to poly(acetylene) through thermal decomposition [52].

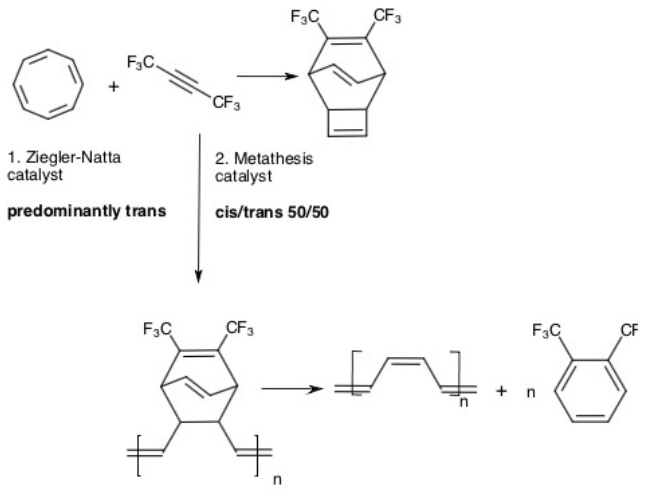

FIGURE 2.2: The synthesis of poly(acetylene) from cyclooctatetraene.

In the case of heterocyclic polymers (such as poly(thiophene), convenient synthetic routes involve electrochemical methods or the chemical oxidation of the appropriate monomer, thiophene in the case of poly(3-alkylthiophene)s (PAT). Due to the nature of the monomer used for PAT polymerisation, there are three means of coupling: head-to-head, head-to-tail and tail-to-tail. Initial methods were cross-coupling or electrochemical oxidation but the obtained poly(thyophene)s were not regioregular [53, 54]. Fgure 2.3 shows two preparation methods for PATs, namely the Kumada cross-coupling reaction and electrochemical oxidation.

To solve the regioregularity problem, several other preparation paths were proposed. One such method is the McCullough method, shown in figure 2.4. It is a 4-step process, which starts from 3-bromothiophene, which yields 3-alkylthiophene by means of Ni(dppp)Cl_2. The monomer is then brominated with NBS (N-bromosuccinimide) and lithiated with LDA (lithium diisopropylamide). A Grignard reagent is then obtained which will condense regioregular PAT [55, 56].

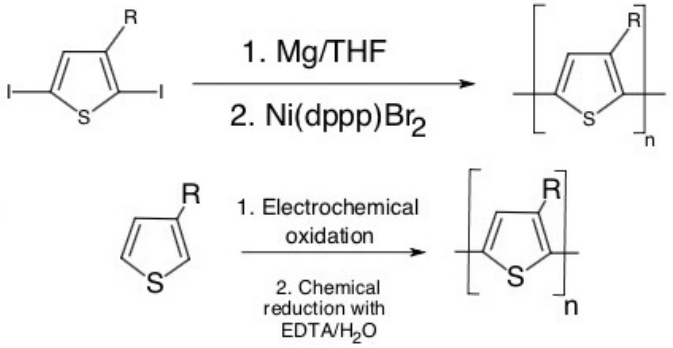

FIGURE 2.3: The synthesis of polythiophenes.

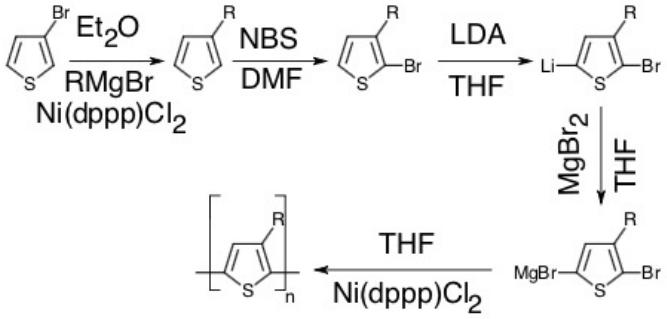

FIGURE 2.4: Regioregular poly(thipohene) synthesis method proposed by McCullough.

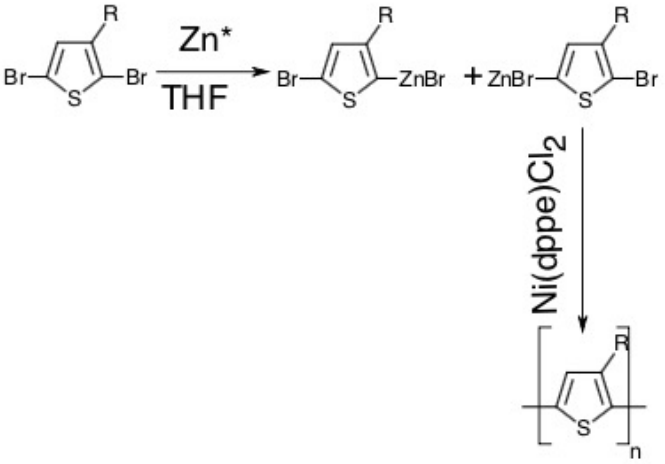

FIGURE 2.5: Regioregular poly(thipohene) synthesis method proposed by Rieke.

An alternative method, presented in figure 2.5, was proposed by Chen and Rieke [57, 58]. It starts from 2,5-dibromo-3-alkylthiophene and in the presence of zinc . The result will be a mixture of two isomers which, with the help of $Ni(dppe)Cl_2$ will give regioregular PAT.

2.3 Properties of π-conjugated polymers

2.3.1 Absorption of light

The most important components in a molecule, regarding its optical properties, are the chromophores. Also known as fluorophores, they are the section of a molecule that absorbs and emits light at specific wavelengths which is characteristic for the material absorbing energy. This property usually depends on the fluorophore's chemical structure and environment. It needs to be noted that although the terms are interchangeable, they define separate roles. Chromophores are components that are responsible for the absorption of light while fluorophores are the section that emits the absorbed energy. In figure 2.6 we show the electromagnetic spectrum of light as well as the corresponding range of energies.

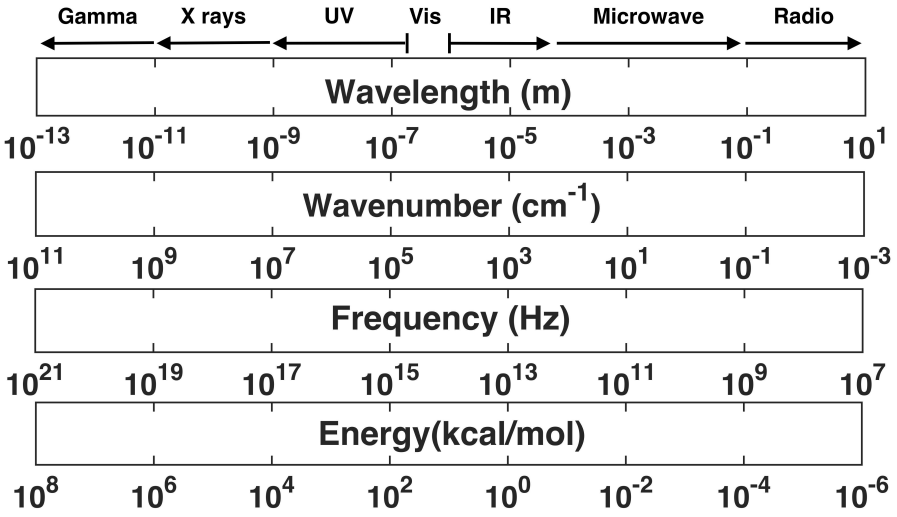

FIGURE 2.6: The electromagnetic spectrum and energy of an absorbed photon.

Depending on energy and wavelength, molecules can behave in various ways upon absorbing a photon. For wavelengths lower than 200 nm (UV and higher energy radiation), photons have sufficient energy to ionise the molecules absorbing them, thus resulting in photochemical degradation [59–61]. This degradation effect is more common in unsaturated materials (compounds formed with σ bonds) when absorbing a photon with an energy higher than 6 eV. In the case of double and triple bonds, besides σ bonds, π electrons are also used to form chemical bonds. Compared to σ

bonds, those formed by π electrons are generally weaker due to the parallel orientation of the respective molecular orbitals, which is translated into lower energy photons required for excitation. Besides the shift in the absorption wavelength caused by the presence of π electrons, conjugation (alternating single and double bonds) will result in a further red shift in the absorption spectrum. A strong absorption in the visible section of the electromagnetic spectrum can serve as an indication that fluorophores in a studied material are conjugated.

For wavelengths of 200 nm and above, absorbed photons can only trigger one of two energy transitions: n - π^* and π - π^*. When a molecule is excited with light of sufficient energy, an electron occupying the sample molecule's Highest Occupied Molecular Orbital (usually in the ground state S_0) to a position in the Lowest Unoccupied Molecular Orbital thus forming an excited state (S_1). For molecules that absorb in the visible spectrum, the energy gap between the ground state and excited state will be in the range of 35 - 70 kcal/mol [59]. In conjugated molecules, the delocalisation of π electrons translates into a high mobility of these charges along the molecular backbone. Considering this, the energy transitions inside the molecule can be approximated by a simple theoretical model by assuming that π electrons don't interact (they're evenly spread over the conjugated system, minimising repulsions). In this case, the energy landscape of a molecule can be approximated with a quantum particle in a box. In such a situation, an electron's potential energy is considered constant along the length of the box and approaching infinite at both ends of the conjugated section. By using Schroedinger's equation, we can define the waveform and energy with equations 2.6 and 2.7:

$$\psi = \sqrt{\frac{2}{L}} sin\left(\frac{n\pi x}{L}\right) \tag{2.6}$$

$$E_n = \frac{n^2 h^2}{8mL^2} \tag{2.7}$$

where n represents the quantum number (the antinodes of the eigenfunction along a molecular chain); L shows the length of a molecular box; m is the mass of an electron; h - Planck's constant and x is a spatial variable, showing the displacement along the chain.

A molecular orbital will be characterised by a waveform and an energy. By applying the Pauli exclusion principle [62], only two electrons (with opposite quantum spins) can occupy an energy level or waveform. So, for a system with an even number of electrons, the lower energy states will each be filled by two electrons while the higher energy states will remain unoccupied. Thus, in order to formulate a system with a higher energy, an electron from the HOMO level (characterised by a quantum number n) to the LUMO level (characterised by a quantum number $n+1$), the result of which being an excited singlet S_1. In this case, the wavelength of the absorption will be given by equation 2.8 and the energy of the excitation photon will be given by the Planck equation (equation 2.9).

$$\Delta E = E_{LUMO} - E_{HOMO} = \frac{h^2}{8mL^2}\left(n_{LUMO}^2 - n_{HOMO}^2\right) \tag{2.8}$$

$$E = h\nu = \frac{hc}{\lambda} \tag{2.9}$$

where h represents Planck's constant; ν is a frequency; c is the speed of light and λ represents the wavelength.

Given that the ground state S_0 for a compound with N electrons is characterised by N/2 occupied levels, the quantum numbers defining HOMO and LUMO can be written as n_{HOMO}=N/2 and n_{LUMO}=N/2+1. Inserting this in equation 2.8 will give equations 2.10 and 2.11.

$$\Delta E = \frac{h^2}{8mL^2}\left(N+1\right) \tag{2.10}$$

$$\lambda = \frac{8mc}{h}\frac{L^2}{N+1} \tag{2.11}$$

In conclusion, a molecule's absorption bands can be roughly estimated from its length and number of π electrons.

2.3.2 Excited states

2.3.2.1 The Jablonski diagram

The processes which take place during light absorption and emission are best shown by the Jablonski diagram [63]. In figure 2.7 we show a typical diagram, showing the electronic states and transitions for organic molecules. Upon absorbing a photon, a molecule will form an excited singlet state, usually an S_1 or S_2 singlet. Through internal conversion, followed by a vibrational relaxation, the formed excited state will relax to a lower vibrational level in S_1 and will eventually return to the ground state with emission of fluorescence. The process that controls the formation of the higher singlet states is the interaction of the transitioning electron with the electric component of the light used for excitation [59, 64].

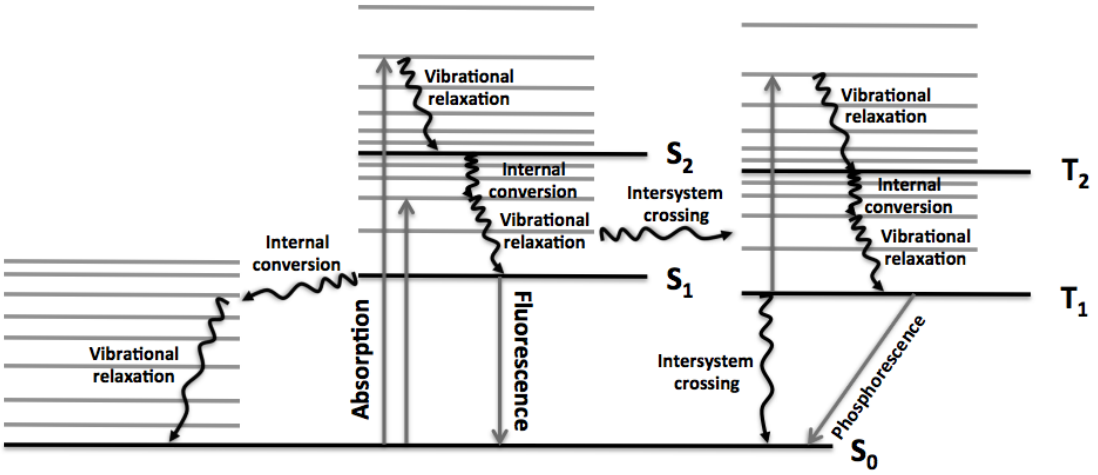

FIGURE 2.7: The Jablonski diagram, showing electronic transitions for organic molecules.

Another possibility for S_1 singlets is to sustain a spin conversion to a T_1 triplet state, through a process called intersystem crossing. The T_1 triplet will also return to the S_0 ground state with emission of phosphorescence, an emission which is usually shifted towards higher wavelengths compared to fluorescence. For most organic molecules, intersystem crossing is a very improbable and inefficient process with crossing rate constants significantly lower than those for fluorescence. Nevertheless, the presence of heavy atoms such as halogens will aid intersystem crossing and the formation of triplet states, making the majority of these molecules phosphorescent [65].

Upon absorbing a second photon, molecules excited both in singlet and triplet states can be further excited to higher vibrational levels (S_n or T_n), resulting in ionisation and photobleaching. Unlike singlet states, the triplet - singlet transition is forbidden which will result in a much higher average lifetime for an excited triplet state, compared to singlet states.

2.3.2.2 Singlet and triplet states

The properties of organic semiconductors emerge from a delocalisation her the whole molecule of their π and π^* molecular orbitals. After a photon is absorbed, an electron from HOMO will be advanced to LUMO, generating an excites state. This coulombically bound electron-hole pair will migrate through the material subjected to photoexcitation until the two charges are located on the same molecule, the result of which being an intramolecular exciton, or adjacent molecules, the result being an intermolecular excited state. There are two ways of generating excited states: optical excitation, which creates only singlet excited states [66, 67], and electrical excitation, creating both singlet and triplet states [68]. For clarification, a singlet is the state with anti-parallel electron spins in the π and π^* orbitals. Similarly, triplets are the excited states with parallel spins for the electrons in π and π^* orbitals. For both singlet and triplet states, the total spin adds to zero. Figure 2.8 shows the molecular orbital configuration for singlet and triplet states.

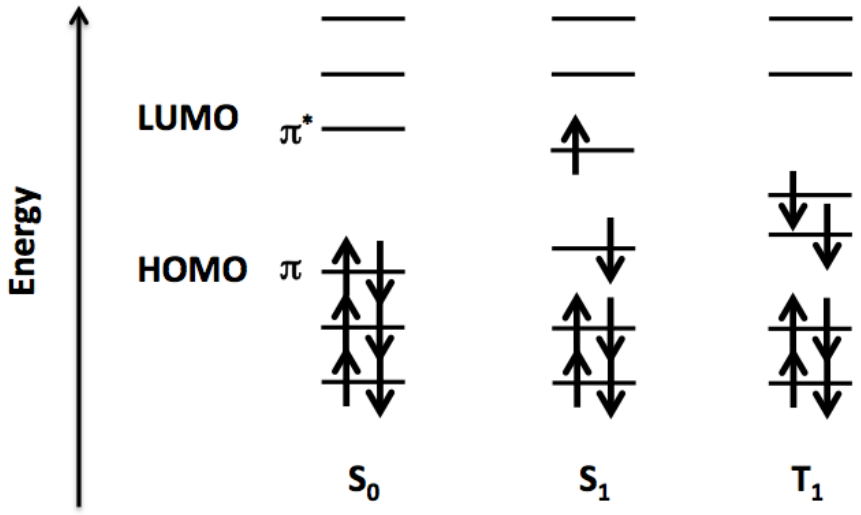

FIGURE 2.8: The electronic configuration of singlet and triplet states.

As seen in figure 2.8, the excited state which resulted after photoexcitation is formed by unpaired electrons in HOMO and LUMO, forming a system of two particles. From a quantum mechanics perspective, any two particles characterised by a spin angular momentum will have two eigenstates and two eigenvalues. For a two particle system, there are four eigenstates, who's wavefunctions can be written as follows [69]:

$$\alpha_1\alpha_2, \quad with \quad S = 1; \quad M_s = 1 \tag{2.12}$$

$$\beta_1\beta_2, \quad with \quad S = 1; \quad M_s = -1 \tag{2.13}$$

$$\frac{1}{\sqrt{2}}(\alpha_1\beta_2 + \alpha_2\beta_1), \quad with \quad S = 1; \quad M_s = 0 \tag{2.14}$$

$$\frac{1}{\sqrt{2}}(\alpha_1\beta_2 - \alpha_2\beta_1), \quad with \quad S = 1; \quad M_s = 1 \tag{2.15}$$

where α and β are are the spin wavefunctions of the two electrons forming the excites state, S and M_s are the eigenvalues characterising the two particles' eigenstates. The first three spin wavefunctions (equations 2.12 to 2.14) denote a triplet state because the only difference is in the z component of the spin momentum. The remaining spin wavefunction (equation 2.15) characterises the singlet state [70]. Figure 2.9 shows the vector diagram of singlet and triplet states .

One aspect of importance in figure 2.9 is the orientation of the spins in singlet and triplet states. For triplet states, the spins of the two unpaired electrons in HOMO and LUMO are in phase and coupled with antisymmetric spatial wavefunctions. For singlet states, the opposite is true. the spins are out of phase and they are coupled with symmetric wavefunctions.

The nature of singlet and triplet states described above was discussed for simple molecular films (for simplicity). But of all organic semiconductors, the most complex from the perspective of their electronic structure are π conjugated polymers. In simpler organic semiconductors, where the molecules are linked by van der Waals bonds, the excited states will only form on a molecule and its immediate neighbours.

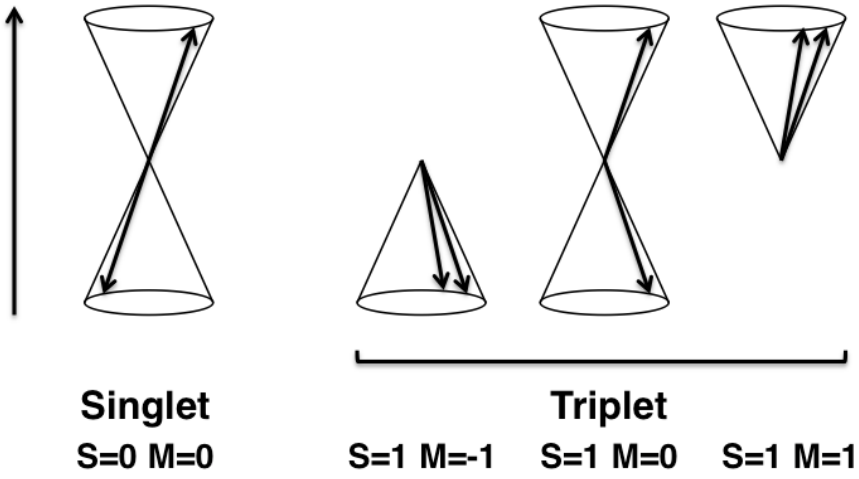

FIGURE 2.9: The orientation of singlet and triplet spins and the corresponding eigenvalues, in a local magnetic field (indicated by the arrow).

As opposed to these simpler cases, excited states formed in polymers will extend across several molecular chains, extent which depends on several factors [69]:

- coulomb interactions, which reduce the distances in the electron-hole pair;
- the distortion of bonds in the molecular backbone;
- the increase in the energy of electrons for large excited states.

Since electron-hole pairs are not point charges, they are characterised by decaying and overlapping wavefunctions. One factor that influences the wavefunctions of electrons and holes is the mean distance between these two particles ($\langle r_{eh} \rangle$), which is approximately equal to the size of an exciton. The average $\langle r_{eh} \rangle$ for conjugated polymers has been calculated and values of somewhat below 1 nm have been obtained for a singlet and approximately 30% lower for triplet states [71, 72].

Besides intra-molecular excited states, inter-chain excitons (excited states residing on neighbouring polymer chains) can also form. For these inter-molecular excitons (termed exciplex, excimer or poltroon pair), the characterising wave function (containing covalent and ionic terms terms) can be written as:

$$\Psi = c_1\Psi(A^*B) + c_2\Psi(AB^*) + c_3\Psi(A^-B^+) + c_4\Psi(A^+B^-) \tag{2.16}$$

where Ψ represents the excited state wavefunction, A and B are the polymer chains over which the excited state is delocalised, c is a constant and *, - and + are the excited states. Covalent bond contributions are characterised by the constants c1 and c2, while ionic contributions are characterised by c3 and c4. When the chains holding the exciton are identical and covalent interactions are dominant, intermolecular excited states are named excimers. For dominant ionic contributions, the excited states take the name "charge-transfer exciton" [69].

2.3.3 Excited state lifetime

As shown in [73], exciton diffusion in polymers (the energy migration through a film via energy transfer) depends on the lifetime of excited states, in the sense that longer excited state lifetime will yield longer diffusion lengths. In its own term, exciton lifetime is linked to the fluorescence quantum yield - Φ_f - the ratio between the absorbed and emitted photons (in other words, the probability of an exciton to be neutralised through fluorescence). Φ_f is described via equation 2.17:

$$\Phi_f = \frac{k_r}{k_r + k_{nr}} \tag{2.17}$$

where k_r is a radiative decay rate constant and k_{nr} is a non-radiative decay rate constant which describes all exciton deactivations means, such as intersystem crossing or intra- and intermolecular energy transfers [74].

Since the lifetime of an excited state also depends on radiative and non-radiative processes, the average time spent in an excited state before spontaneous fluorescence emission is determined by equation 2.18 [75]:

$$\tau_f = \frac{1}{k_r + k_{nr}} \tag{2.18}$$

where τ_f is the average exciton lifetime. Also, the fluorescence lifetime - a decrease of excited fluorophores ($F(t)^*$) in time upon excitation with an infinitesimal optical pulse is

$$\frac{d[F(t)^*]}{dt} = -(k_r + k_{nr})[F(t)^*] \tag{2.19}$$

By integrating between 0 and time t, equation 2.19 becomes

$$I(t) = I_0 exp\left(-\frac{t}{\tau_f}\right) \tag{2.20}$$

As seen in equation 2.20, fluorescence lifetime is time in which the fluorescence intensity reaches 1/e of its intensity at time t=0, following excitation with an infinitesimally short light pulse. In the case of heterogeneous samples or materials containing more than one fluorophore, fluorescence lifetime can be determined by means of a multi exponential function [59]:

$$I(t) = \sum_i a_i \left(-\frac{t}{\tau_i}\right) \tag{2.21}$$

where τ_i is the lifetime of the i-th component of a sample and a_i represents the contribution of the i-th component to the total fluorescence intensity.

There are two major methods of measuring fluorescence lifetimes [64]:

- time-domain (photon counting method), discussed in another chapter;
- frequency-domain (phase modulation).

As opposed to light pulses, the frequency-domain method provides excitation by means of sinusoidally modulated light. In this case, excitation can be written as

$$E(t) = E_0[1 + M_E cos(\omega t)] \tag{2.22}$$

where ω is the angular frequency of the modulated light and M_E is a modulation factor, corresponding to the AC to DC ratio of the signal. The same frequency is used to modulate the fluorescence [76]. Due to the lifetime of the excited state, the fluorescence signal will suffer a decrease of the modulation factor (M_F) as well as a phase delay and it's characterised by equation 2.23.

$$F(t) = F_0[1 + M_F cos(\omega t - \Phi)] \tag{2.23}$$

where Φ is the phase delay between the excitation and fluorescence signals. By measuring the phase angle Φ we get the basis for determining the fluorescence intensity, through sine and cosine Fourier transforms [76, 77] as equation 2.24.

$$I_f(\omega) = \int_0^\infty I_f(t) exp(-i\omega t) dt \tag{2.24}$$

Considering a species with a single fluorescence lifetime, the expression for the fluorescence intensity is now given by

$$I_f(\omega) = \frac{1}{\tau} \int_0^\infty exp\left[-\left(\frac{1}{\tau} + i\omega \right) t \right] dt = \frac{1 - i\omega\tau}{1 + \omega^2\tau^2} \tag{2.25}$$

This expression, formed of a real and imaginary component, is related to the experimentally determined quantities

$$\begin{aligned} M_C &= (1 + \omega^2\tau^2)^{-1/2} \\ tan(\Phi_C) &= \omega\tau \end{aligned} \tag{2.26}$$

From equation 2.26, two lifetimes can be obtained:

$$\begin{aligned} \tau_1 &= \frac{1}{\omega} tan(\Phi_C) \\ \tau_2 &= \frac{1}{\omega} \left(\frac{1}{M_C^2} - 1 \right) \end{aligned} \tag{2.27}$$

If the fluorescence decay is a single exponential, the two individual lifetimes will have identical values. If, when considering the single exponential decay model gives different lifetimes, a multi exponential decay model must be considered instead. Compared to time-domain measurements, the frequency domain method cannot be applied for single-molecule fluorescence measurements.

2.4 Single molecule spectroscopy

In 1952, Erwin Schrödinger said *we are not experimenting with single particles, any more than we can raise Ichthyosauria in the zoo* [78]. Once a true statement, the quote is no longer valid, due to advancements in microscopic techniques. One such technique is single-molecule spectroscopy. It was developed in the late 1980's and early 1990's [79, 80] and gained popularity due to its ability to study biological samples [81, 82].

With regards to organic semiconductors, the method was first applied to conjugated polymers in 1997 by David Vanden Bout and colleagues [83] when studying the fluorescence intensity jumps of a poly(p-phenylene vinylene) - poly(p-pyridylene vinylene) copolymer (PPV-PPyV). Their report shows the presence of reversible fluorescence switching for a molecule with very large molecular weight. This indicates that, despite the large number of repeating units in a polymer chain, the molecule acts as one entity and a single defect can be responsible for quenching the emission of an entire molecule. The discovery helps scientists in understanding the limitations of organic semiconductors for the fabrication of LEDs through a reduction of their quantum yield due to the presence of photochemical defects.

Conjugated polymers are very diverse materials, characterised by various degrees of disorder [84–86]. The length of a polymer chain is characterised by polydispersity (a measure of a material's molecular weight distribution) as well as various conformations. All these characteristics and variations in a conjugated polymer's structure will give rise to a broad region of energies for excited states.

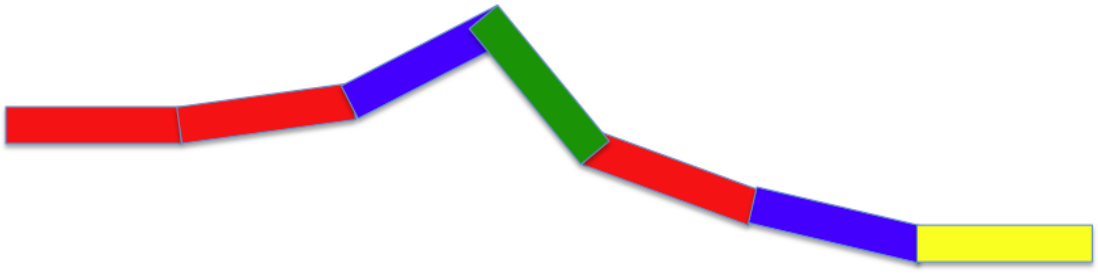

FIGURE 2.10: Schematic representation of a single polymer chain.

Figure 2.10 shows a schematic representation of a single π-conjugated polymer chain, based on Raman [87–90] and fluorescence spectroscopy [91–93]. Conjugated polymer chains are characterised by a system of delocalised π electrons, which can be

disturbed by the various conformation adopted by the molecule. These disruptions, such as sharp bends in the molecular chain, give rise to chromophores (chemical units with distinct optical properties). Since the presence of chromophores dictates a material's optical properties, spectroscopy measurements is performed on the present chromophores, even though a single molecule is formed by many (sometimes thousands) of repeating monomer units.

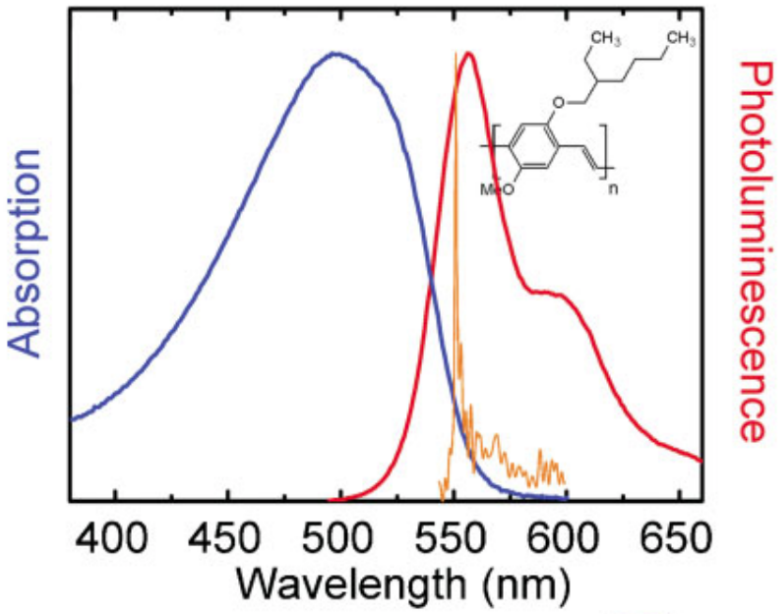

FIGURE 2.11: Absorption and PL spectra of MEH-PPV. The narrow feature represents the photoluminescence spectrum of a single chromophore. Reproduced with permission from [94]. Copyright 2010 WILEY-VCH Verlag GmbH & Co. KGaA, Weinheim

As opposed to absorption, where all optically active species are analysed, emission spectra are characteristic only for chromophores that emit light. Absorption is usually relatively featureless and characterised by a large range of wavelengths in the visible portion of the spectrum. By comparison, emission originates from longer sections of the molecule (with the lowest energy of the excited state) and the vibronic structure of the analysed polymer is sometimes visible. Figure 2.11 shows the absorption and emission properties of Poly[2-methoxy-5-(2-ethylhexyloxy)-1,4-phenylenevinylene], commercially known as MEH-PPV.

Experimentally, there are two means of performing SMS, wide-field [95–97] and confocal microscopy [98, 99]. Wide-field microscopy relies on imaging a large area of the sample, greatly improving data acquisition, while confocal imaging is based on scanning a single spot at a time, improving signal to noise ratio.

Typically, a sample for single molecule experiments is composed of a polymer diluted with a polymer matrix (such as Zeonex) which is then spincoated on a glass or quartz substrate. The sample is then placed underneath an objective lens which collects the light originating from the sampled focuses it on a monochromator which, by means of a mirror or diffraction grating, can image the entire scanned region or the spectrally resolved PL.

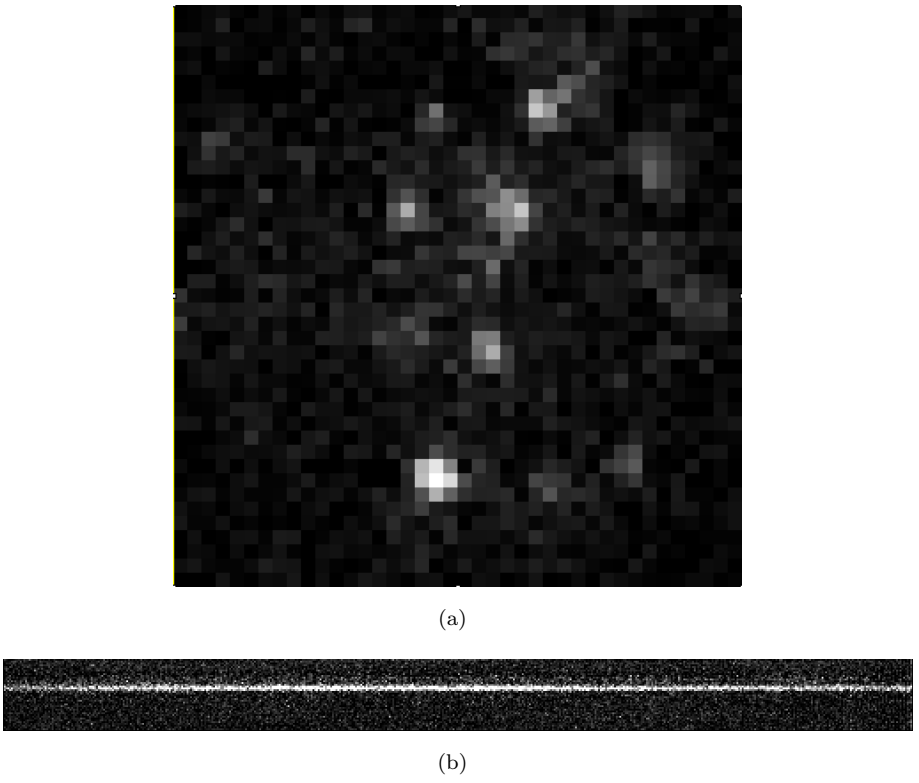

(a)

(b)

FIGURE 2.12: Typical data recorded in single molecule experiments. a) Image of a sample region containing several molecules; b) Spectrally resolved emission of a single molecule.

Figure 2.12 shows the typical data acquired in single-molecule experiments. Figure 2.12(a) shows a wide-field image of a sample region containing several single polymer molecules. The data was acquired by sending the light collected by the objective lens straight to a CCD camera by means of a mirror. The x and y direction can be restricted, by means of a slit and by defining a region of interest around an emissive feature of interest. If the mirror is replaced by a diffraction grating, the emission spectrum of the chosen region of interest is collected, as seen in figure 2.12(b).

2.4.1 Identifying single molecules

In order to perform single-molecule experiments, one must first identify the presence of single molecules within a sample. The first step in achieving this goal is a proper sample preparation procedure. The fluorescence of a single polymer chain can be measured by by diluting the analysed sample to nanogram regime (or lower if needed). Slowly reducing the concentration of the deposited solutions will lead to increasingly thinner films and a lower fluorescence intensity. Eventually, a critical dilution step is passed and individual emitters can be identified (as seen in figure 2.12(a)). The number and density of individual emissive features will vary with concentration but their emission intensity will remain relatively stable with increasing dilution.

A second piece of evidence for associating emissive spots with single molecules comes from the presence of fluorescence intensity fluctuations in time. This fluorescence intermittency is called photoblinking and it has been studied abundantly for various fluorescent systems [83, 100–103]. Although photo blinking is an indication of single emitters, by itself it is not sufficient for showing the presence of single molecules. Similar PL transients are encountered for mesoscopic emitters such as multichain molecular aggregates [104, 105], or perovskite nanocrystals [103]. Furthermore, the emission spectrum of a single molecule will randomly vary in time. This property is called spectral diffusion [106, 107] and it is a signature characteristic of single or multiple chromophore emission.

Clear evidence for the presence of single molecules can also be provided by photon correlation techniques. Single systems, such as simple atoms, are capable or absorbing and/or emitting a single photon at any particular time depending on wether the electron going rise to an excited state is in its ground state or not [108]. For this purpose, the photon detection distribution is characterised by the following expression [109]:

$$g^2(\tau) = 1 - \left(\frac{1}{N}\right) exp(-(W_p + \Gamma_f)\tau) \tag{2.28}$$

where $g^2(\tau)$ is the fluorescence intensity correlation function, W_p represents the pumping rate, N is the number of emissive sites and Γ_f shows the fluorescence decay rate. This technique (called photon antibunching) can not only detect single

molecules, but also determine the number of emissive sites. For a large number of emissive sites the correlation function g^2 approaches 1, while for single emitters it approaches zero. The method was first used in [110]. For this purpose, single photons can be generating by passing the PL originating from a single emitter through a beam spitter and observed by two detectors. As shown in [110], when measuring the fluorescence intensity correlation vs the delay time between the two detectors for a single conjugated polymer molecule, the value of the correlation function at zero delay time is very close to zero. This is direct evidence that PL emission originates from only one emissive site inside a polymer molecule.

2.4.2 Single molecule fluorescence spectroscopy

2.4.2.1 Room temperature single molecule spectroscopy

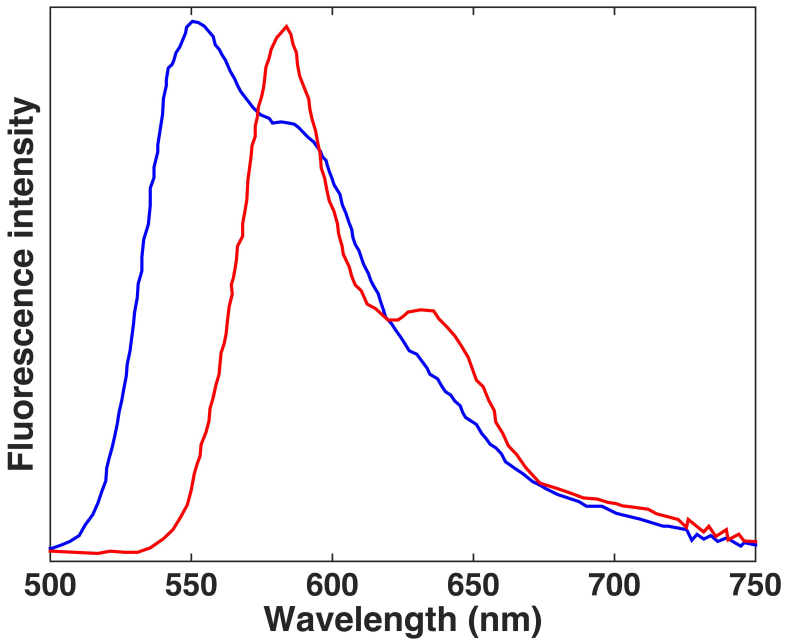

FIGURE 2.13: Examples of two single molecule fluorescence spectra of MEH-PPV. Adapted from [111].

While the emission spectra of a film presents itself as broad and relatively featureless, PL spectra of a single molecule originates from a much smaller number of emissive spots compared to ensemble emission. Therefore, single molecule fluorescence is a good tool for analysing the high degree of disorder which characterises conjugated polymers and regulates their optical properties.

Figure 2.13 shows two examples of single-molecule emission spectra (in this case belonging to MEH-PPV [111]). As opposed to ensemble PL, SM spectra are usually somewhat narrower and have a radically different structure compared to the bulk material [112]. While ensemble emission is generally featureless, SM emission is characterised by a more complex structure and peak distribution which can be correlated with various conformations adopted by a polymer molecule, such as rods, coils or defect cylinders [91, 113]. Single chains that adopt a more collapsed conformation will show enhanced intrachain energy transfers and a lower energy of the emitted light, as exhibited by the β conformation of PFO [35].

Besides fluorescence emission, information regarding the excitation process can also be provided by the lifetime of an excited state. Furthermore, fluorescence correlation spectroscopy can can give information of an excited state's dynamics [114]. In this method, the fluorescence properties of single molecules are analysed against time.

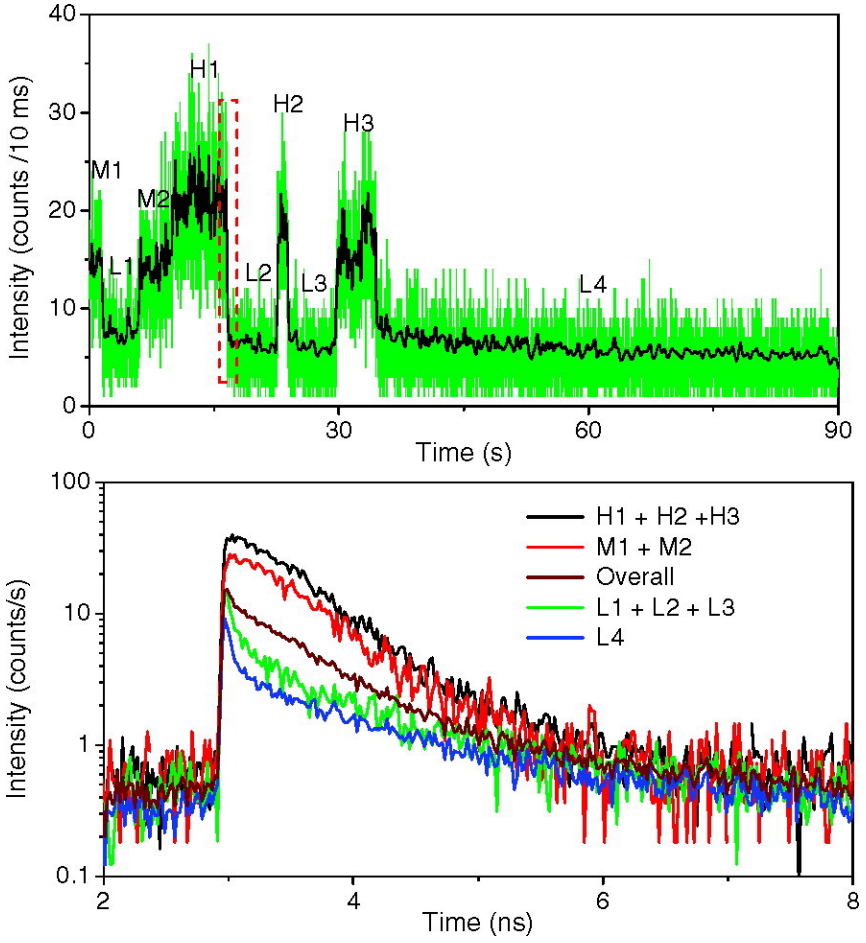

FIGURE 2.14: Fluorescence blinking and lifetime of a MEH-PPV molecule. Reprinted with permission from [115]. Copyright (2008) American Chemical Society.

First applied to conjugated polymers in 2000 [111], fluorescence dynamics measurements were further developed in recent years by reporting fluorescence transients in the lifetime of single molecules [115]. Figure 2.14 shows a fluorescence transient and lifetime of a single conjugated polymer molecule. As seen in the top panel, an on/off blinking behaviour can be observed, a characteristic of fluorescence emission originating from a single molecule [83]. The bottom panel shows shows fluorescence lifetime decays measured at various times in the above transient. Two intensity levels are noticed, in the form of alternating bright and dark states. The high fluorescence emission in the time trace is characterised by a long lived single exponential fluorescence decay while the dark state is defined by a fast multi exponential decay. As reported by the authors in [115], the blinking features are explained by fast quenching of the excited states while the rapid drops of the determined fluorescence lifetimes are characteristic of excitons occupying a quenching site on the molecular backbone.

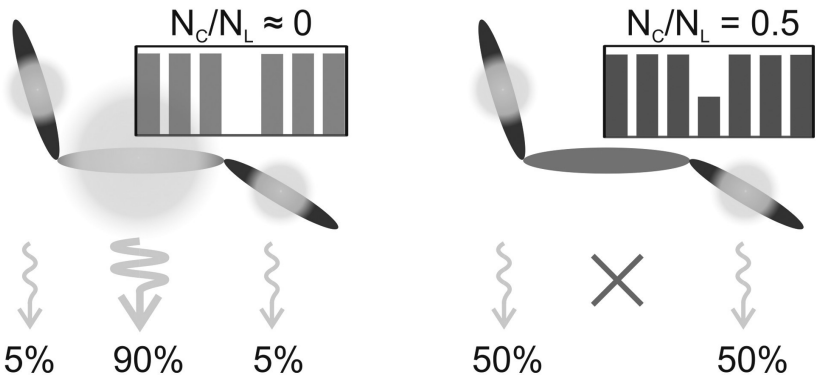

FIGURE 2.15: The quenching of a single polymer chain. Reprinted from [116], with the permission of AIP Publishing.

Similar results were reported by Lupton and co-workers in [116], where the influence of charge carriers on the PL properties of MEH-PPV are reported. Figure 2.15 schematically shows the quenching of a single MEH-PPV molecule. The quenching of the dominant chromophore results in an fluorescence intensity drop. The consequence of this charge injection process and subsequent quenching also translates into a blue shift of the remaining fluorescence as well as a sudden fluorescence lifetime reduction.

2.4.2.2 Low temperature single molecule spectroscopy

As seen in the previous sections, the fluorescence properties of a conjugated polymer are highly dependent on temperature. Fluorescence spectra at low temperatures, figure 2.11 inset, are significantly narrower and have a different structure compared to the PL spectrum of the same material acquired at room temperature (figure 2.13). By lowering the temperature, the line width of a fluorescent feature is drastically reduced and insight regarding the photo physical properties of individual chromophores is gained, namely the vibrational modes of an excited state become observable. Also, chromophoric coupling is reduced and the Zero-Phonon Line (characteristic of the difference between the ground and excited state of a molecule) can be observed [80, 117, 118].

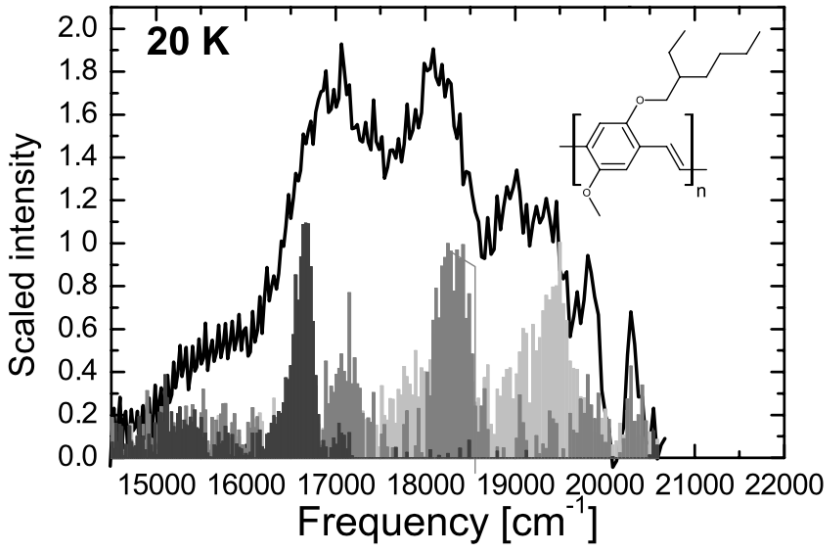

FIGURE 2.16: Low temperature fluorescence emission of MEH-PPV. The solid curve is the cumulated PL originating from a group of MEH-PPV single chains. The gray bars are examples of SM fluorescence spectra. Reprinted from [119], Copyright (2004), with permission from Elsevier.

With an increasing number of chromophores in a polymer chain and a high degree of disorder, the more difficult it is to detect and analyse narrow narrow spectra. The first instance of high resolution PL spectroscopy at low temperature for a single conjugated polymer chain was performed on polydiacetylene in a crystal diacetylele monomer matrix, reasonably approximating semiconducting organic nanowires [120], the authors reporting a high degree of order in the system. Following this study, low-temperature studies on more realistic systems have been performed. The first low-temperature single molecule fluorescence analysis on MEH-PPV (one of the most

widely studied conjugated polymers) has been performed in 2004 [119]. The authors reported a large range of wavelengths, over 100 nm (figure 2.16), for low-temperature emission peaks, which is a characteristic of the polymer's high degree of disorder - each analysed chain presented a distinct conformation, a characteristic responsible for the high spread of the emission peaks.

Since the first low temperature analysis of MEH-PPV, considerable effort has been given in order to clarify the origins of (blue or red) single chromophore emission. One such study was performed by Thomas Basche and colleagues in [121]. The authors investigated the fluorescence properties at 1.2 K of single MEH-PPV molecules. Emission spectra of different chains showed the presence of strictly red or blue emitting molecules. Fluorescence emission and TCSPC analysis showed no significant difference in the spectral range of both emissive species, thus ruling out interchromophoric transitions as a possible origin for red sites. There are two possible origins for the presence of red features: large chromophore units or interactions between chromophores due to a folding molecular backbone which leads to the formation of intrachain aggregates [122]. Since transitions between neighbouring chromophores has been excluded, red emission sites are due to longer chromophoric conformations leading to extended sections of uninterrupted π delocalisation.

2.5 The technological importance of PCDTBT

In recent decades, low bandgap conjugated polymers became increasingly more popular in the field of optoelectroncis, mainly for solar cells or other photovoltaics. One technologically important material for developing efficient solar cells is poly[N-9'-heptadecanyl-2,7-carbazole-alt-5,5-(4',7'-di-2-thienyl-2',1',3'-benzothiadiazole)], a polycarbazole derivated conjugated polymer commercially sold as PCDTBT. Due to its elevated red absorption, the polymer is able to collect solar radiation more efficiently thus increasing device performance [12, 13]. Another factor which influences the performance of photovoltaic devices is the HOLO-LUMO bandgap value. With a high ionisation potential, characterised by a HOMO level of -5.35 eV, PCDTBT displays open-circuit voltages of more than 0.8V, a value notably higher than that obtained for P3HT [13, 123, 124].

A consequence of the material's HOMO level, is an increased thermal stability [125–127]. In [125], the authors characterised the polymer's stability in N_2 and air. No

important chemical changes in the material's structure were observed. PCDTBT showed thermal stability at high temperatures. As seen in figure 2.17. the absorption spectrum of a PCDTBT thin film remains relatively intact up to 150°C in air. In N_2, the absorptiop bands of PCDTBT are unaffected when exposed to temperatures as high as 350°C.

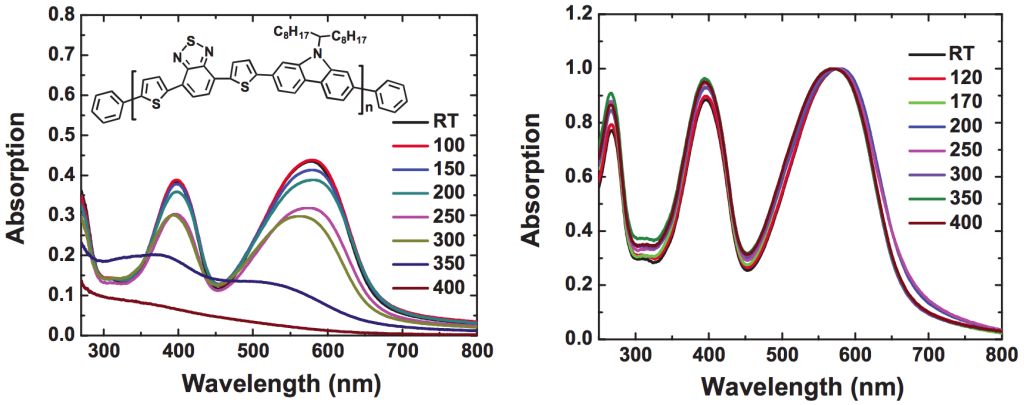

(a) (b)

FIGURE 2.17: The absorption spectra of a PCDTBT thin film exposed to high temperature in a) air b) N_2. Reproduced with permission from [125]. Copyright 2010 WILEY-VCH Verlag GmbH & Co. KGaA, Weinheim

Due to its high ionisation potential and thermal stability, the fabrication of solar cells with increased lifetimes (up to 4000 h) was possible [126].

Besides the increased thermal stability and open circuit voltage of the pure material, PCDTBT is also capable on increasing the efficiency of solar cells when incorporated into devices comprised of other polymer blends [128, 129]. A higher content of PCDTBT into a PTB7-Th:PCDTBT:$PC_{70}BM$ ternary bulk heterojunction cell can increase efficiency, compared to the PTB7-Th:$PC_{70}BM$ reference. By incorporating 20% PCDTBT, the power conversion efficiency (PCE) of the ternary blend solar cell was increased to 7.86%, compared to 6.91% efficiency for the reference sample [128]. The authors also observed improved open circuit voltages(V_{OC}) and short circuit current densities (J_{SC}).

Also, binary systems incorporating a third PCDTBT component show improved energy levels. This will induce a more potent charge transfer, due to PCDTBT's lower energy levels compared to PTB7 (as indicated by [128, 129]).

Chapter 3

Experimental Design

3.1 Automation

The experimental set-up for single Molecule Spectroscopy (SMS) experiments is a custom built optical microscope, based on Zeiss optics. It has been equipped with a Princeton Instruments Acton series 150 spectrometer and an electron-multiplying charged couple device (EM-CCD) camera. The spectrometer is composed of a slit, for minimising collection on the horizontal axis, and a multi-grating turret with a mirror for conventional imaging as well as a set of gratings (150 and 300 grooves/mm respectively) for spectroscopy measurements. Sample position is controlled by two separate devices:

- A Zaber A-series microscope stage and controller, for rough sample movement, in steps of several microns;
- A piezo stage and nPoint LC400 series controller, for finer position control (sub-micron steps).

The optical measurements required for Single Molecular Spectroscopy (SMS) can, at times, be very slow and time consuming due to the manual operation of the experimental set-up. In order to automate the experimental procedure and allow real-time SMS measurements, a series of automated applications have been implemented. The applications consist of several individual modules, which speed up the

optical measurements with minimal user intervention. A schematic representation of the automation system is presented in figure 3.1.

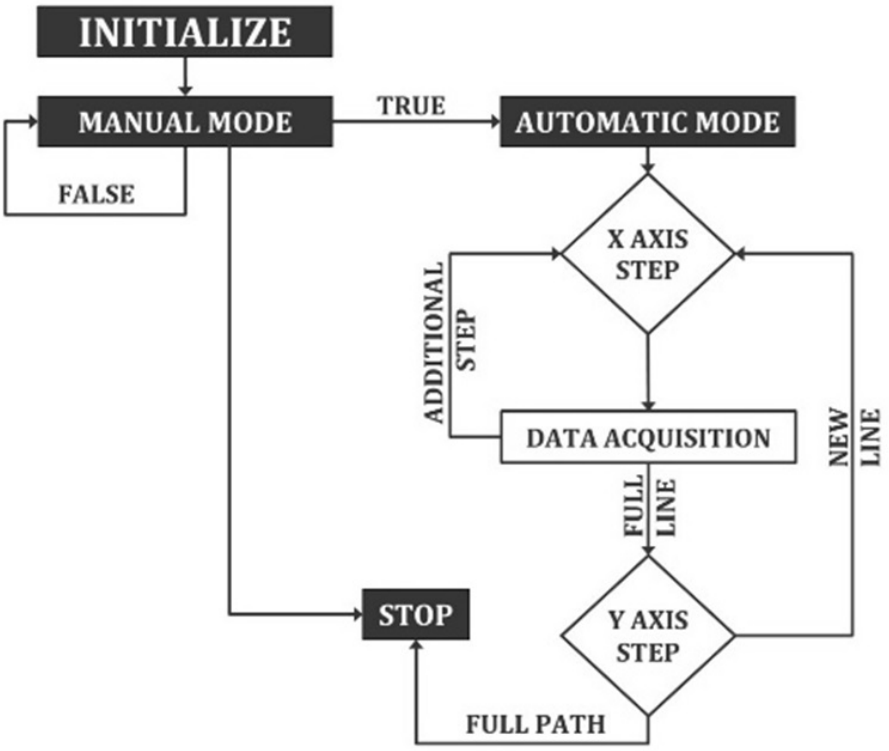

FIGURE 3.1: Automation software flowchart.

3.1.1 LabVIEW software

As mentioned earlier, SM measurements are usually very slow. The main reason for this problem is the large number of emitters that need to be measured, in order to perform a meaningful analysis. One of the main tasks of the current study is to automate the experimental procedure, in order to optimise the measurements and shorten the time required for acquiring a large volume of data.

The initial step in automating the experimental set-up was to test the feasibility of the task. For this purpose a LabVIEW based application has been designed and implemented, comprised of several interconnected modules, such as sample position controls and an imaging interface.

The operating principle of the LabView software is simple. After initialisation, the sample will automatically be moved (in steps of known size) in the horizontal plane, predominantly on one of the axes, considered for convenience as X. After each

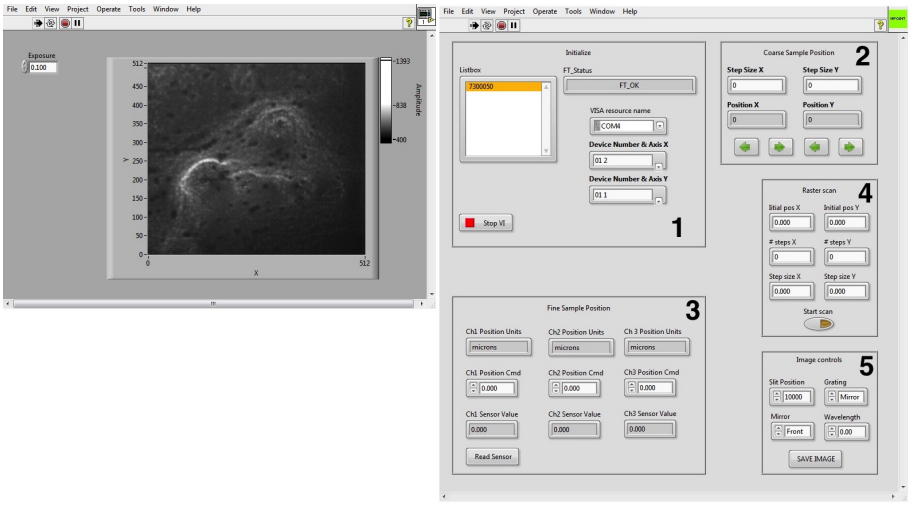

FIGURE 3.2: Control software front panels: camera (left); sample position (right). The sample position front panel contains: 1-initialize; 2-coarse sample position; 3-fine sample position; 4-raster scan; 5-image and spectrometer controls.

step motion on the X axis, the program automatically acquires and saves data in various modes (fluorescence intensity, lifetime measurements or photoluminescence spectroscopy). When motion on the X axis has been completed the sample will be moved one step on the perpendicular direction, noted as Y, and the entire cycle is repeated. Upon completing the preset motion pattern, the application is automatically stopped. The LabView software makes the experimental set-up extremely flexible, allowing various experiments, such as lifetime measurements and fluorescence spectroscopy on single molecules. Al the major components of the application will be described briefly below.

Figure 3.2 shows the front panels of the control software for SMS experiments. It is made of two separate virtual instruments (VI): one for for the EM-CCD camera (figure 3.2 left) and one for sample position commands (figure 3.2 right).

3.1.1.1 Sample position controls

An important function of the software is to accurately control the position of the sample in the experimental set-up. This can be achieved by means of two separate modules: coarse and fine sample position (segments 2 and 3 respectively, in figure 3.2).

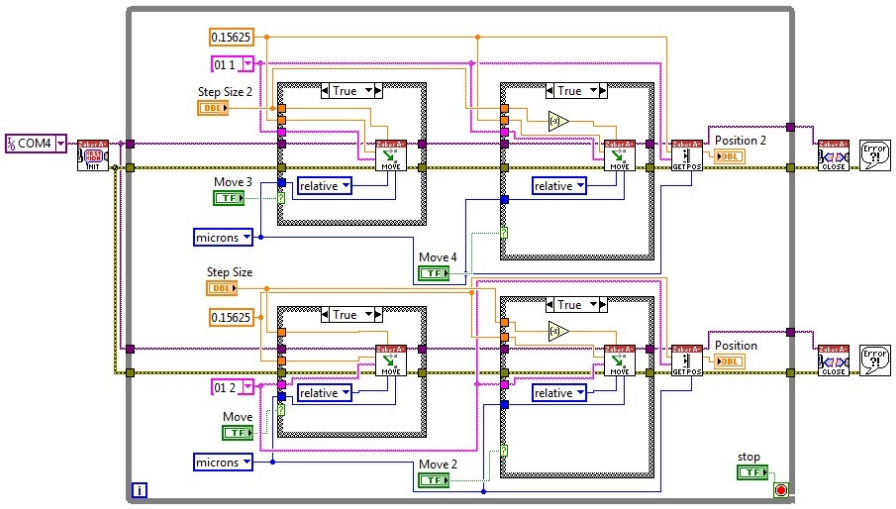

FIGURE 3.3: Block diagram for coarse sample position control.

Coarse Sample Position (figure 3.3) is responsible for controlling the position on both horizontal axes. Due to the relatively low sensitivity of the Zaber microscope stage, this segment is only used for moving the sample in rough steps of several microns.

Fine Sample Position (figure 3.4) controls the focusing of the camera image and the sample position in finer sub-micron steps, depending on the size of the laser spot used as excitation source.

3.1.1.2 Raster scan

There are two main modes of operation: manual and automatic. In the manual mode, the user is allowed to freely move the sample on all three axes for precisely positioning the sample. A camera control is also present in the manual stage.

A second operating mode (figure 3.5) involves the automatic movement of two of the motors, responsible for controlling the horizontal position of the sample (x and y axis). For this purpose, a motion pattern can be configured in the motor control front panel, by programming the start position, as well as the number and size of motion steps on both axes.

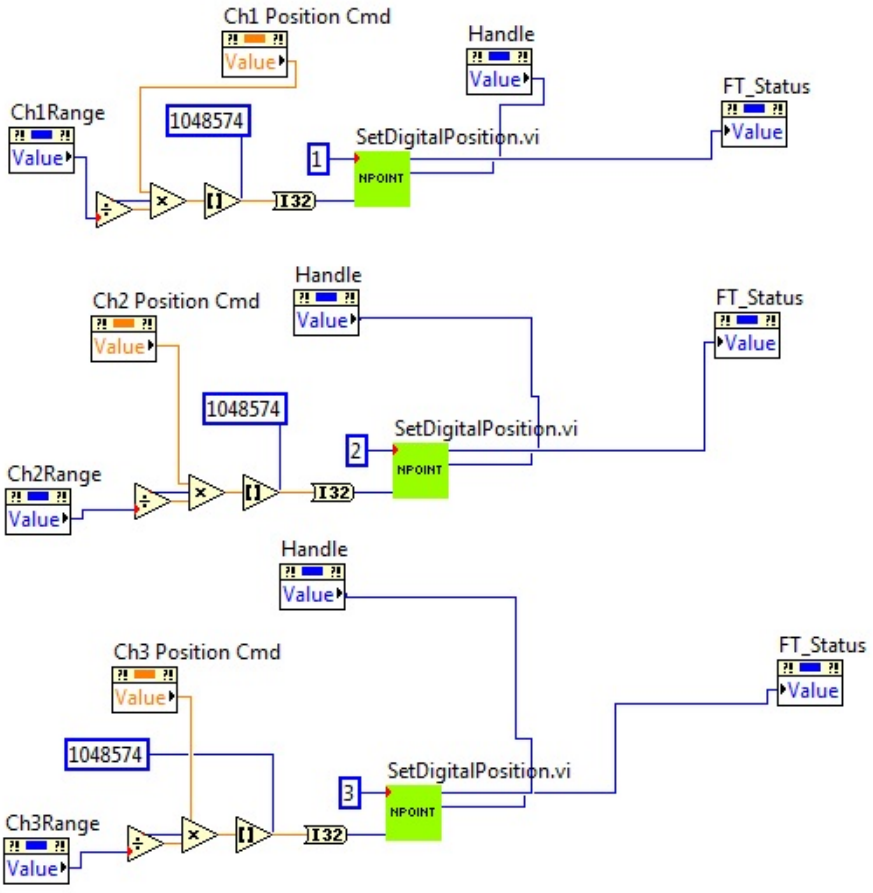

FIGURE 3.4: Block diagram for fine sample position control

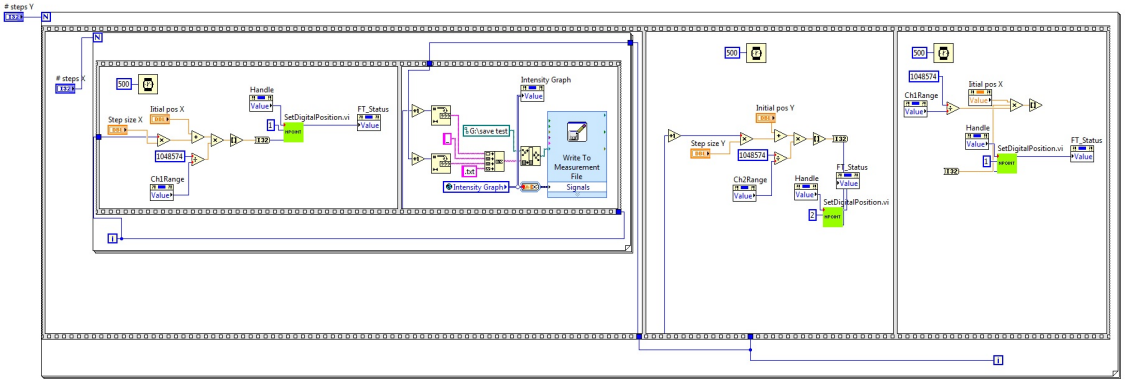

FIGURE 3.5: Block diagram for raster scan

3.1.1.3 Image capture and fluorescence spectroscopy

An important part of the data acquisition software is the image capturing module, which acquires camera images of the sample surface. The CCD camera connected to the microscope is being controlled by means of an R Cubed Software Scientific

Imaging ToolKit (SITK) specifically designed to allow LabView control of various scientific cameras and spectrographs, including the ProEM CCD camera used in our system. Figure 3.6 shows the block diagram of the camera module. The program is capable of displaying in real time the acquired camera images, as well as saving the mentioned images in the form of a data file, for further analysis.

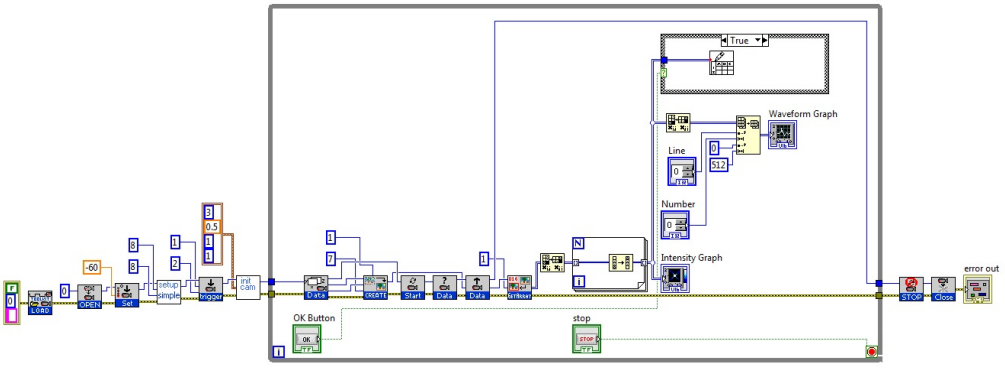

FIGURE 3.6: Block diagram for image capture.

3.1.2 Current automation

Although automating the experimental procedure was feasible, there were several inherent problems with the custom LabVIEW application, most importantly communication issues between the various toolkits, drivers and libraries used in the LabVIEW, which made our application slow and relatively difficult to operate. For this purpose, the custom software was replaced in later work with a series of dedicated software packages, which work together with the set-up's components in order to replicate the functionality of the previous LabVIEW application.

Sample position The position controls described in the previous section have been replaced with two applications, namely a Zaber console and the nPoint piezo stage control software (nP Control). The current sample control system presents an increased flexibility, since it allows the user to control all aspects of the raster scan (numbers of scan lines and points on each line as well as the size of the scanning steps and dwell time between steps. Also, the system offers the same flexibility on the vertical axis, which is useful for acquiring data in slices, thus creating a 3D image of the analysed sample.

Imaging Imaging the sample is now achieved through LightField, a data acquisition platform designed by Princeton Instruments. The platform offers user-friendly control over both the ProEM 512 EMCCD camera as well as the Acton series 150 fluorescence spectrometer used in our set-up. Also, it allows the user to control a wide range of experimental parameters as well as exporting the acquired data to many common file formats.

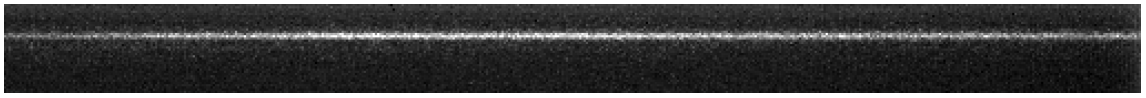

FIGURE 3.7: An example of frame generated by the experimental set-up. The bright line is a fluorescence spectrum.

Another important aspect of the described software platform is its integration with the piezo stage software mentioned above. After each motion step in the raster scan, the piezo stage will send a trigger to the LightField software which will automatically collect data (in the form of an image or a photoluminescence spectrum) for the spot excited by the laser at that time. This allows the user to rapidly scan and acquire data from a large area of the analysed film. Figure 3.7 shows an example of data acquired by the experimental set-up. In order to acquire the shown image, a region of interest containing an emitter is selected on film surface (in order to limit data collection to the region of interest) and the spectrometer grating is positioned at a centre wavelength (of 650 nm in this case). Following this, a spectral image is recorded for the selected region of interest. The bright feature in figure 3.7 represents the PL spectrum of the fluorescence emitter present in the selected region of interest.

After acquiring similar frames for each step in the raster scan, the data will then be integrated and a map of the film's surface is built. In the example shown in figure 3.8(a) each pixel in the obtained image represents a PL spectrum (figure 3.8(b)).

Fluorescence lifetime

Besides spectroscopy and imaging, the microscope stage responsible for controlling the sample position is also integrated with an APD detector (avalanche photo diode), and used for fluorescence lifetime measurements. For this purpose, we use the time-correlated single photon counting technique (TCSPC).

Similar to fluorescence image acquisition, each step in the raster scan triggers the APD diode which collects a fluorescence decay curve. After completing the raster

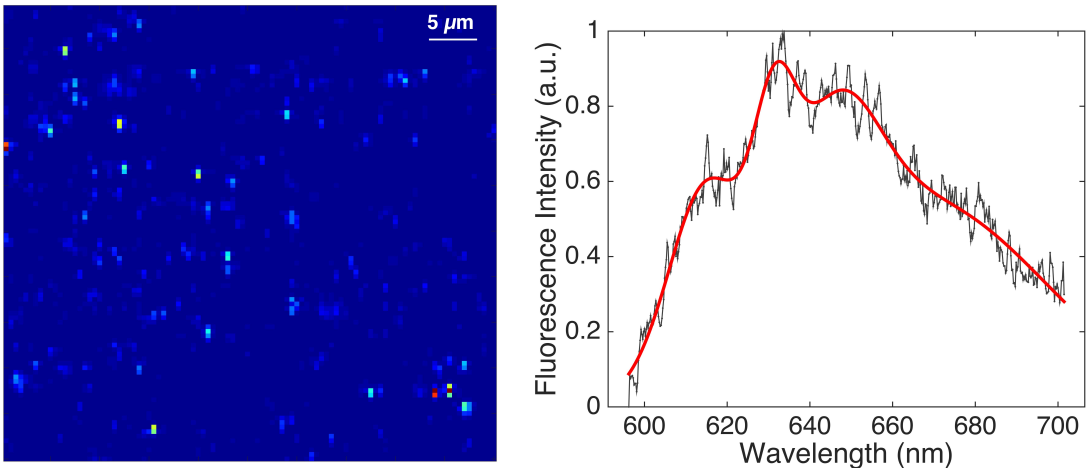

FIGURE 3.8: Fluorescence intensity map built from data acquired by the set-up's imaging module (a) and example of PL spectrum (b).

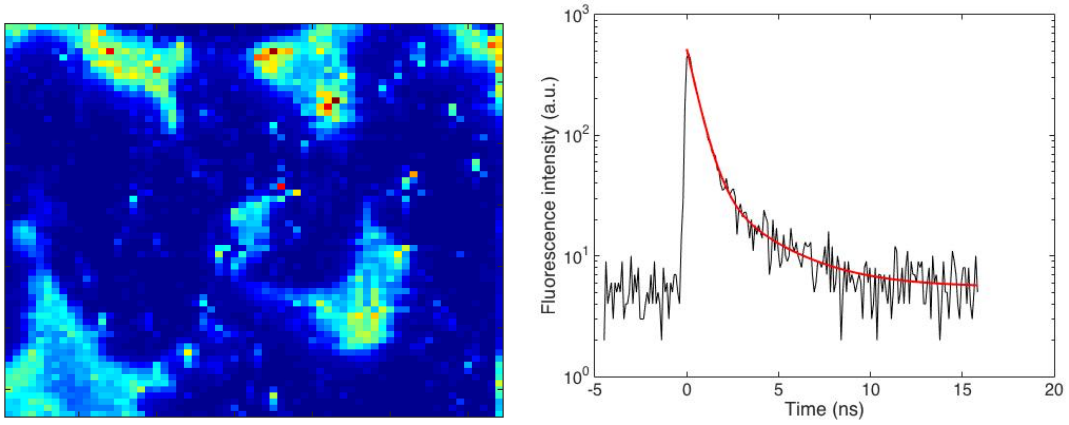

(a) Fluorescence lifetime map of a 400 µg/l PCDTBT thin film

(b) Typical fluorescence decay curve

FIGURE 3.9: Example of data acquired by the fluorescence lifetime mode

scan, the software accompanying the APD detector (software developed by Becker & Hickl) will build from the acquired decay curves, a fluorescence lifetime map of the sample surface. Figure 3.9 shows an example of data collected in this mode of operation.

3.1.3 Data analysis

3.1.3.1 Analysing photoluminescence data

Since single-molecule (SM) fluorescence requires the analysis of a large number of emitters for an adequate characterisation, we have designed and implemented a data analysis code, in order to automatically characterise the SM fluorescence result in a reasonable amount of time. There are several functions built into the code, that will be discussed individually:

- building the fluorescence intensity images
- detecting the points of interest
- generating the fluorescence spectra
- detecting the peaks of interest
- building the desired histograms

The entire data analysis code is shown in appendix A. The first function of the analysis code is **generating fluorescence intensity maps** (appendix A.2.1). Each frame in the data file generated by the software accompanying the experimental set-up (spe image file) is acquired in the form of a spectral image (figure 3.7). Each frame in the above mentioned data file (figure 3.7) is summed to a single numerical value and arranged into a matrix (a 100 x 100 px grid in this case), thus obtaining a fluorescence intensity map of the sample surface (figure 3.8).

After generating the image, the next step is **detecting the points of interest**. The data generated by this function is presented in figure 3.10. For this purpose, an intensity threshold is defined. After defining a value for the intensity threshold, the function presented in appendix appendix A.2.2. will build a matrix containing the regions in the previously built fluorescence intensity map, that have a fluorescence intensity above the specified threshold (figure 3.10(a)). After building the new matrix, the points of interest (in the form of the points with he highest intensity in each individual domain) are selected and matched with positions on the fluorescence intensity map (figure 3.10(b)). These selected points correspond to single molecules

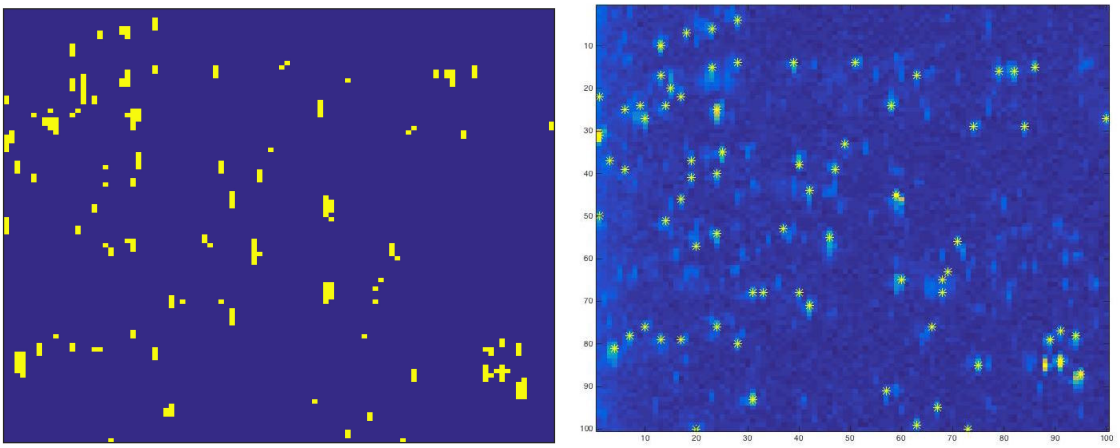

(a) (b)

FIGURE 3.10: Regions of interest, determined by the intensity threshold (a) and selected points of interest (b)

TABLE 3.1: Sample data collected after fitting each single molecule

#	a1	a2	a3	a4	b1	b2	b3	b4
1	0.289	0.313	0.336	0.506	611.889	630.096	649.263	663.075
2	0.279	0.261	0.583	0.550	613.293	630.752	643.361	697.004
3	0.737	0.396	0.647	0.309	608.946	630.403	647.081	672.689
4	0.332	0.216	0.447	0.349	612.104	630.296	648.683	699.999
5	0.562	0.496	0.589	0.500	615.209	631.654	646.421	672.634
6	0.211	0.405	0.243	0.368	613.532	632.175	655.229	666.701

* parameters a1 - a4 represent the peak amplitude;
** parameters b1 - b4 are the positions of each emission peak, in nm.

. Finally, a background is calculated (chosen as 10% of the lowest intensity) and subtracted from the fluorescence data (appendix A.2.3.).

The next step in the data analysis procedure is **generating the photoluminescence (PL) spectra** (appendix A.2.4). Frames corresponding to the points of interest previously determined are selected and the bright line observed in figure 3.7 (corresponding to the fluorescence emission) is plotted against the wavelength. The obtained PL spectrum is then normalised and fitted with four gaussian functions, to determine the position and amplitude of each emission peak (appendix A.2.5). Table 3.1 shows and example of data collected in this manner.

The next step in analysing the data is **detecting the peaks of interest**. After the points of interest have been analysed as described above, the fit parameters

are collected. The dominant peaks are then determined, by selecting for each PL spectrum the gaussian peak with the highest amplitude compared to the other three.

Finally, **the desired histograms are built**. For this purpose, the positions for the dominant maxima earlier determined are calculated. The resulting data will then be plotted against the occurrence and a histogram is thus generated.

3.1.3.2 Analyzing fluorescence time trace data

An important measurement in this study was fluorescence time trace measurements. This experiments involves the monitoring of the fluorescence intensity of an excited spot and plotting the acquired data over time. The excited emitter will undergo certain changes, corresponding to transitions between different states. This translates to discontinuities in the emitted fluorescence intensity (in the form of "on" and "off" times), the presence of this two-level system being an indicator that the detected fluorescence emission originates from a single molecule [83, 130, 131]. The goal of type of analysis is to determine the time each emitter spends in the two states. For this purpose, we have used a Matlab application, designed by the Department of Computer Science at University of North Carolina [132] to detect edges in 1D fluorescence time trace data. The data analysis code is presented in appendix B.

The data analysis code contains two main components: a main script for controlling certain experimental parameters (appendix B.1) and a utility function for detecting edges in the experimental data (appendix B.2). After loading the experimental data, two parameters (threshold and scales) designed to indicate how evident a step needs to be in order to be considered a step, are added to the workspace. The values of these two parameters are important. If the provided steps are too fine, the code will detect false transitions (due to sample noise). If the parameters are too coarse, the edge detection would not be precise and short transitions will be missed.

Figure 3.11 shows an example of fluorescence time trace data analysed with the described code. After the experimental data was input, the utility function shown in appendix B.2 will construct a series of scaled derivatives in order to determine the maxima and minima of local sharp edges. If the maxima and minima are persistent, they will be tracked through other scaled derivatives and recorded, giving us a reasonable measure of where edges occurred in our experimental data.

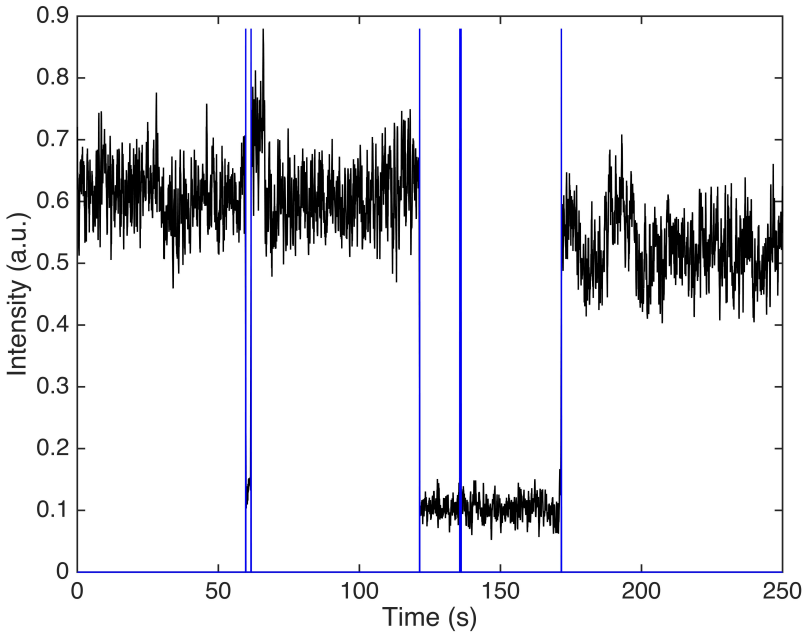

FIGURE 3.11: Figure generated by the edge detection code. The detected edges are shown in blue

The code is based on a Gaussian kernel derivative [133]. Ideal 1D step functions have sharp and distinct on/off transitions, which are easy to detect. But in real situations, ideal data sets never occur. The kernel on which the presented code is based handles noisy data by smoothing the data set. The scale parameter determines the level of noise suppression that needs to be applied. This is an essential parameter and its value determines how the data is analysed. A small value will blur the boundary between noise and actual data and false transitions will be detected. Large scale values will make the data too smooth and edge detection becomes very imprecise.

3.2 Techniques

Fluorescence is an emission process arising from the relaxation of excited states, involving transitions between various electronic states of fluorophores. This process is shown schematically in figure 3.12.

A fluorescent molecule is characterised by electronic states, split into several sub-levels depicting the fluorophore's various vibrational and rotational modes. Due to the energy gap between the ground and excited states, being much larger than

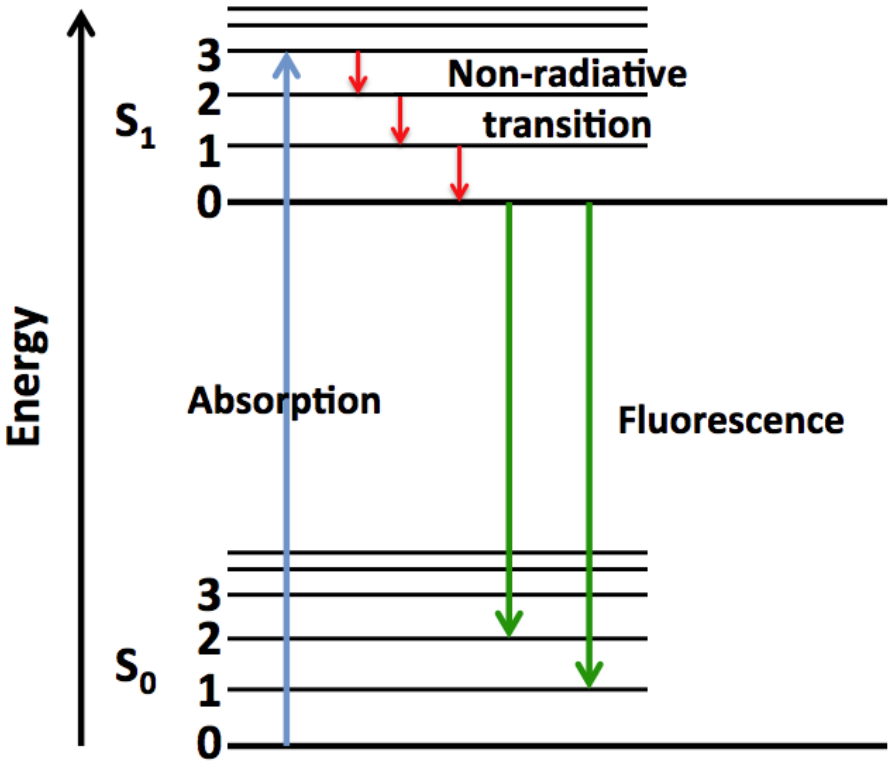

FIGURE 3.12: The Jablonski diagram, showing the absorption and fluorescence process.

thermal energy, photons in the UV or the blue-green region of the electromagnetic spectrum are needed for a transition. Upon exciting a molecule, the fluorophore presenting itself as an excited state will relax to a lower vibrational level. After a period of several nanoseconds, the molecule will decay from the singlet excited state back to the ground state and the energy excess is released in the form of a lower energy fluorescence emission [134].

3.2.1 Absorption

Absorption was measured with a custom experimental set-up, which is schematically shown in figure 3.13. Excitation was provided by a DH-2000 deuterium-halogen light source provided by Ocean Optics [135]. Light from the excitation source is collimated and focused on the sample surface. After passing through the sample, the transmitted light is again collimated and focused on an Andor Shamrock CCD spectrometer.

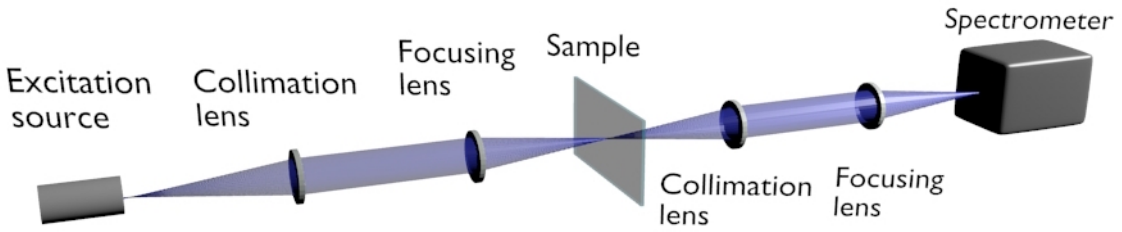

FIGURE 3.13: Schematic arrangement of the experimental set-up used for measuring the absorption spectrum of PCDTBT.

For determining the sample's absorption, transmission through a blank glass substrate is first measured which will be taken as reference. Afterwards, the sample of interest in measured and the following expression is used for determining the normalised absorption of the material:

$$Abs = \frac{Ref - Tran}{Ref} \tag{3.1}$$

3.2.2 Photoluminescence

Photoluminescence experiments (fluorescence and single molecule spectroscopy) were performed on a custom built optical microscope, based on Zeiss optics (figure 3.14). The set-up has been equipped with an Acton series 150 spectrometer and a ProEM 512 electron-multiplying charged couple device camera, both provided by Princeton Instruments [136].

The spectrometer contains a multi-grating turret composed of a mirror and a set of two gratings (150 grooves.mm and 300 grooves/mm), allowing conventional imaging or spectroscopy measurements at different wavelength optimisations. Molecule excitation is provided either by a Thorlabs M470L2 LED light source, or an ultrafast laser. The light from the excitation source is filtered by a 472/20 nm bandpass filter and reflected by a 500 nm long pass dichroic beamsplitter, to an oil immersion objective lens, thus reaching the sample. The fluorescence originating from the sample is then filtered by a 490 nm longpass filter and coupled into the spectrometer by a tube lens.

Sample position is being controlled by the A series microscope stage (for coarse movements) as well as an nPoint piezo controller, for finer position control. The

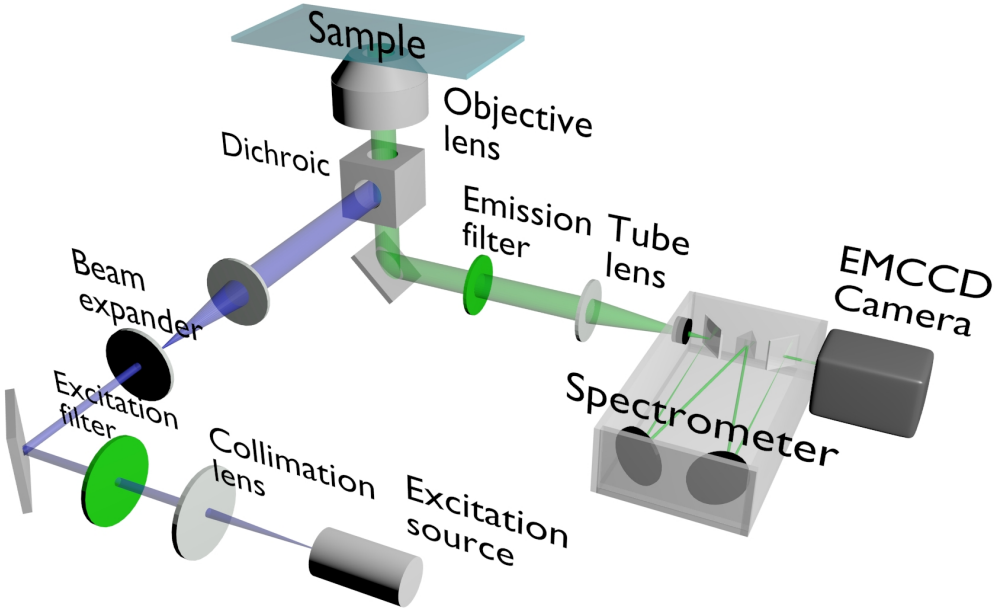

FIGURE 3.14: Schematic arrangement of the experimental set-up.

goal of our experiments is to measure, with a satisfying degree of accuracy, the individual optical properties of a large number of single molecules and correlate these properties with topographical data.

3.2.3 Time-correlated single photon counting

Fluorescence lifetime measurements discussed in this study have been measured by means of the Time-Correlated Single Photon Counting, using an Avalanche Photo Diode (APD) detector provide by Photonic Solution and a data acquisition software package (SPCM) provided by Becker & Hickl. The APD detector and data acquisition software were integrated with the automation software described in section 3.1. Reference [137] offers a detailed description of all the functions accompanying the SPCM software.

Developed 50 years ago [137–140], the TCSPC method is a technique which is based on detecting a single photon originating from a light signal as well as other characteristics such as the detection time and how the time measurement's waveform is reconstructed. The operating principle of this method is shown in figure 3.15.

Since the fluorescence intensity is very low for high repetition rate, low level signals, the probability of picking up multiple photons is very low. After exciting a sample

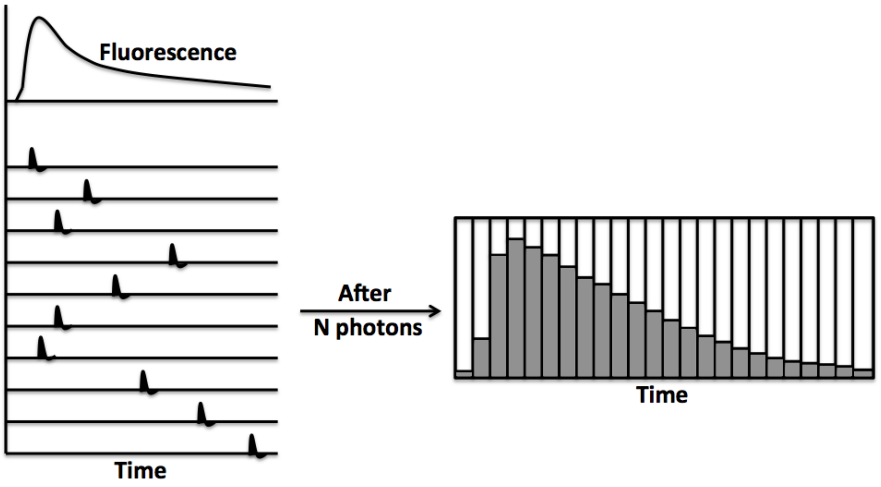

FIGURE 3.15: The operating principle of Time Correlated Single-Photon Counting

with a pulsed laser of known repetition rate, the detector will measure a train of pulses which have been associated with single photons originating from the sample's fluorescence. After a set number of signal periods (when a sufficient number of photons has been detected), a waveform is built with the arrival times of the single photons detected in each period. This distribution of arrival times represents the fluorescence decay curve.

Although the method is complex, it does hold several interesting features which shows its reliability and advantages over older, analog methods.

Time resolution

In the case of analog techniques, the resolution is strongly dependent on the pulse conveyed by the detector upon identifying a single photon (SER, single electron response). For TCSPC, the time resolution is not limited by the detector's SER, but on the arrival times of the single photons. The accuracy at which these photons are detected is called TTS (transit time spread). Since for any given detector the TTS is significantly shorter than the SER, TCSPS has significantly better time resolutions than classical analog techniques.

Counting efficiency

Ideally, the system should record all photons equally, which translates to infinitely small response functions, negligible background and time channels that cover the

entire detected signal. In these conditions, the signal to noise ratio (SNR) of a single exponential lifetime would be directly proportional to the number of photons (N), which corresponds to the signal to noise ratio for measuring the intensity o a similar number of photons [141]:

$$SNR = \sqrt{N} \tag{3.2}$$

In TCSPC, all emitted photons will contribute, resulting in no counting loss. Coupled with the very short instrument response function, the method is very close to an ideal counting efficiency [142, 143]

Acquisition time

One important feature of the method is the acquisition time. Due to the low repetition rates of early excitation sources and the level of electronics technology in the 1980's, earlier methods were relatively slow and needed several minutes of acquiring even one fluorescence lifetime curve.

However, modern sources have rates in the order of tens of MHz, which allows the acquisition of fluorescence lifetimes in mere milliseconds thus allowing high speed applications and real time measurements, important in biological studies.

3.3 Sample Preparation

PCDTBT (poly[N-9'-heptadecanyl-2,7-carbazole-alt-5,5-(4',7'-di-2-thienyl-2',1',3'-benzothiadiazole)]) was purchased from Ossila. The material had molecular weight of 38,800 g mol^{-1} (for PCDTBT) and a value for the polydispersity index of 1.8 [144]. The chemical structure of PCDTBT is shown in figure 3.16.

Single Molecule samples were prepared by dissolving the polymers in chlorobenzene, containing polynorbornene (commercially known as ZEONEX and provided by Zeon Chemicals), at a concentration of 4 g/L. The concentration of the polymers of interest varied between 4 g/L and 5 ng/L. After preparing the polymer blends as above, the solutions were spin-coated onto glass coverslips, for 60 seconds at 2000 rpm. A schematic representation of a basic spincoating process is shown in figure 3.17:

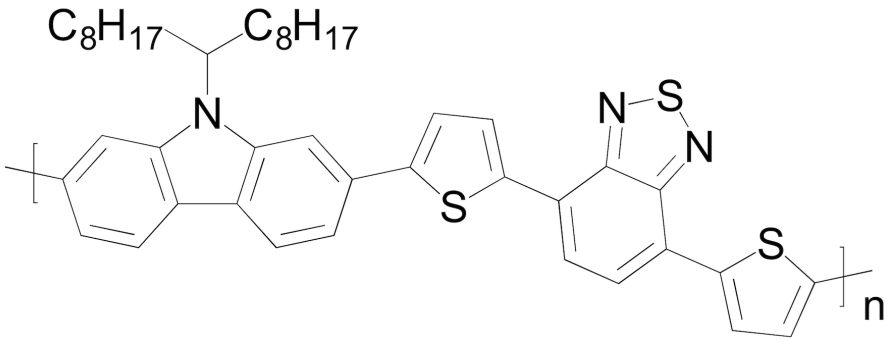

FIGURE 3.16: The chemical structure of the polymer used in this study.

- The substrates, in this case glass coverslips, is coated with 100 µl of a solution chlorobenzene containing 4 g/L Zeonex (used as a polymer matrix) and the polymer of interest (PCDTBT) at concentrations between 4 g/L and 5 ng/L (figure 3.17a);
- The coated substrate is then rotated at a constant speed, in order to remove the excess material and obtain a film of constant width (figure 3.17b);
- The airflow by the substrate rotating at high speed in the previous will dry the solvent used to dissolve the polymer of interest, leaving on the surface of the substrate a thin filmed containing only the molecules of interest (figure 3.17c).

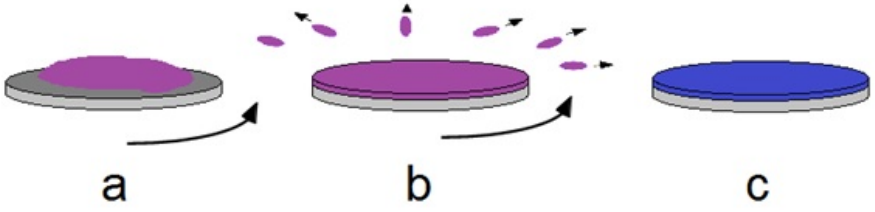

FIGURE 3.17: Schematic representation of the spincoating procedure.

The spincoating method has the advantage of being simple, it has fast drying times for the prepared substrates, as well as consistency and highly reproducible samples. Since the thickness of a spincoated film is inversely proportional to the square root of the angular velocity (2000 rpm in this case), the result is an thin and uniformly coated substrate with a thickness of 60 to 100 nm [145].

For testing the functionality of the experimental set-up and of the control software, a series of samples with known fluorescent properties (excitation/emission peaks at

540/560 nm) have been prepared, which contained orange carboxylate microspheres of 100 nm diameter purchased from Life Technologies [146–148].

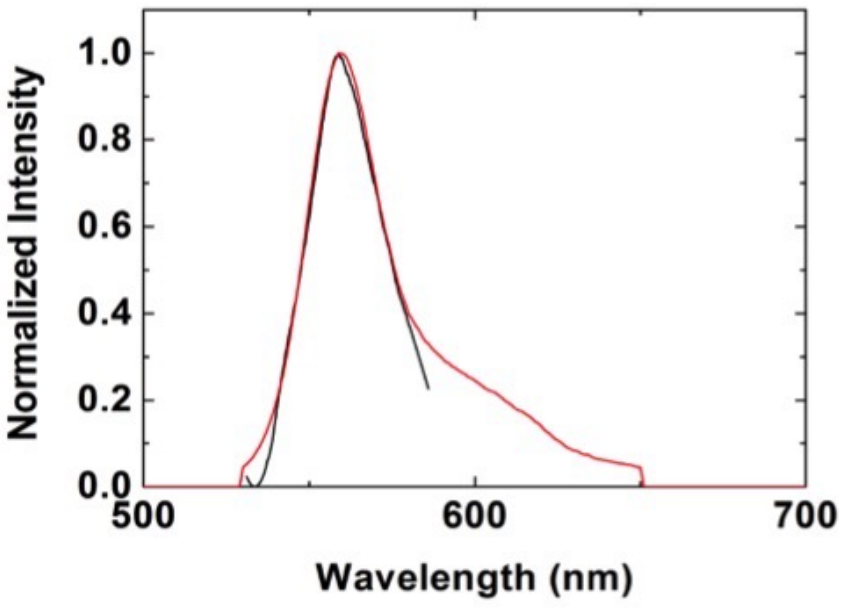

FIGURE 3.18: PL spectra of a single orange bead. Comparison between experimental data (red curve) and data provided by the manufacturer (black curve).

The samples were deposited on cover slips from the stock solution, using 10^2 and 10^3 dilutions. According to the Molecular Probes product information catalogue, the concentration of microspheres can be calculated using the equation below:

$$N = \frac{6C \times 10^{12}}{\rho \times \pi \times \phi^3} \tag{3.3}$$

where N is the number of spheres/mL; C is the concentration of spheres in solution, in g/mL (0.02 in this case); ρ is the polymer density, in g/mL (1.05) and φ represents the sphere diameter in µm. The formula gives us a concentration of 3.6 x $10^{11}$and 3.6 x 10^{10} beads/mL for the 10^2 and 10^3-fold dilution respectively.

For testing the functionality of the experimental set-up, a series of SM experiments were performed on samples coated with microspheres, as described above. According to the Molecular Probes Catalogue, the 0.1 µm orange beads had an emission maxima of 560 nm [149, 150] which, as seen in figure 3.18, matches the PL spectrum recorded by our experimental set-up.

Chapter 4

The fluorescence properties of PCDTBT

4.1 Single molecule photoluminescence

4.1.1 Introduction

As mentioned in an earlier chapter, scientific interest in conjugated polymers has increased recently due to their utility in developing and improving optoelectronic devices. The defining characteristic for these polymeric materials is their main molecular chain, composed of conjugated double bonds, a property which influences the material's conductivity and optical properties - characteristics which are relevant for optoelectronic applications.

When a photon is absorbed, the segment absorbing the photon's energy will form an electron-hole pair, in an excited state. The energy of the chromophore containing the exciton will strongly depend on the polymer's nature, varying inversely with the length of its backbone chain. Elongated polymers will contain low(er) energy excited states. Furthermore, when a molecule's length increases sufficiently, its conformation becomes a determining factor [32]. A very long molecule has the tendency of folding on itself, the result of which is a shorter statistical length compared to the polymer's physical length. Long molecules also tend to form sharp bends in their structure. Such collapsed conformations will cause sharp bends in the chain, angles that produce traps which will restrict the transport of excited states [151].

These factors, shorter statistical length and collapsed conformations, will cause the emission of the excited state in the form of fluorescence at a higher energy (lower wavelength) than one would initially expect [32–34].

There are several methods for studying the properties of conjugated polymers that overcome the limitations imposed by the fundamental differences between macro- and nanoscale. One such technique is SMS. As mentioned in chapter 1, the technique was first a low-temperature method but advances have allowed for the method to be applied at room temperature [14]. Another method for studying the properties of conjugated polymers is fluorescence lifetime imaging, a method which emerged in the late 1980's [152]. The most common practical method for studying the lifetime of excited states is TCSPC. A more detailed description of the method has been given in section 3.2.3 but in principle the method relies in exciting a molecule with very short laser pulses and measuring the arrival time of the photons emitted after excitation. When the arrival time of a large enough number of photons has been measured, a decay curve for the fluorescence emission is determined.

In this chapter we discuss the optical properties, studied by means of SMS and fluorescence lifetime imaging, of PCDTBT.

4.1.2 Properties in bulk

Figure 4.1 shows the absorption and PL spectra in bulk for a thin PCDTBT film. As it can be seen, the absorption spectrum of the polymer is comprised of two broad bands, peaking at 380 and 570 nm, which have been attributed to S_0-S_1 transitions, in the case of the 570 nm peak, and S_0-S_2 transitions, for the 380 nm peak [153].

These features are characteristic to polymers of similar structure and have been attributed to π-π^* transitions between the donor and acceptor units [154–157]. The splitting of the polymer's electronic structure into two distinct bands has been attributed to the large size of the monomer unit.

The blue curve in figure 4.1 represents the PL spectra for a PCDTBT film dissolved in Zeonex at a concentration of 4 g/l. It presents itself as a broad spectrum with a peak at 700 nm and several broad shoulders at lower wavelengths. The shoulders observed in the bulk PL are vibronic brands, due to the C=C double bonds. Both the

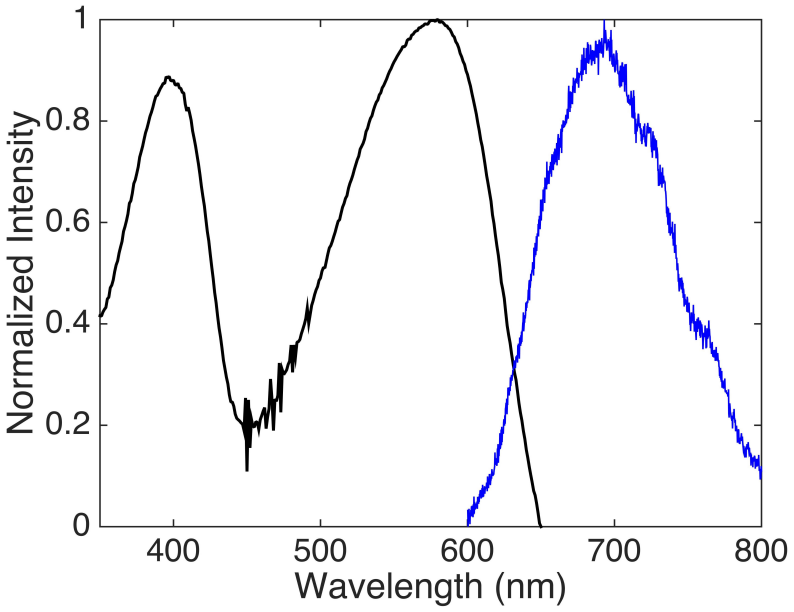

FIGURE 4.1: The bulk absorption (black) and photoluminescence (blue) properties of a thin PCDTBT film

absorption and bulk PL properties are in good accordance with the data previously reported in literature [157–160].

4.1.3 PL properties at different concentrations

Conventional microscopy techniques do have the capability of studying single molecules to a limited extent. The factor that reduces the resolution of single molecule data acquired by conventional means is the limit imposed by the instrument's optical components. This diffraction limit is defined as an inability to detect features smaller than a theoretical limit, which is directly proportional to the wavelength of the light used for exciting the sample.

There are several means to circumvent this limitation. One method is to lower the concentration of the polymer films, PCDTBT in this case, until the physical separation between individual emitters is larger than the instrument's diffraction limit. In figure 4.2 we show PCDTBT films at various dilutions. Figure 4.2(a) reveals a pure polymeric film. The materials shows itself as a continuous domain with few observable characteristics. As we lower the concentration, sample morphology shifts from a still relatively continuous film but with reduced intensity (figure 4.2(b)) to isolated islands (figure 4.2(c)) and finally fully resolved individual emitters, in figure

4.2(h). The bright spots observed in figure 4.2(h) exhibit on/off blinking, a behaviour characteristic for PL emission originating from single molecules.

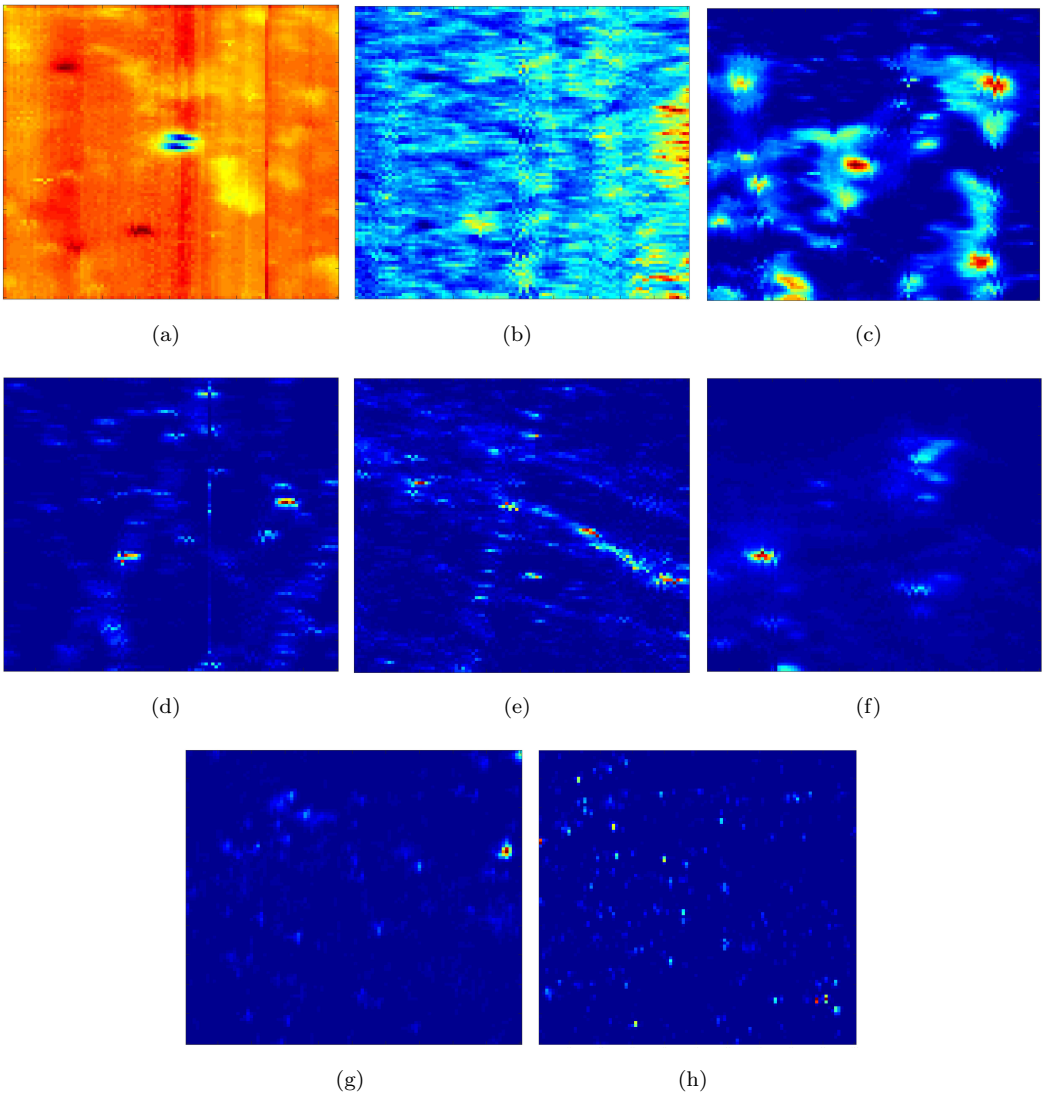

FIGURE 4.2: Fluorescence intensity maps of a PCDTBT film at various stages of dilution: a) 4 g/l; b) 4 mg/l; c) 400 µg/l; d) 40 µg/l; e) 4 µg/l; f) 400 ng/l; g) 40 ng/l.

Another side effect of increased dilution is a visible change in PCDTBT's photoluminescence properties. Figure 4.3 shows a series of PL emission spectra recorded for PCDTBT films dissolved in Zeonex at several dilutions. As mentioned in the previous section, the pure film (concentration 4 g/l) has a PL emission characterised by a broad peak at 700 nm and several narrower shoulders at lower wavelengths. When concentration is lowered, interchain energy transfer and interactions with the host matrix (responsible for the polymer's red emission) gradually diminishes. Eventually, the contribution of individual polymer chains becomes dominant, which is seen

as an increase in the intensity (compared to the intensity of the previously clearly dominant feature) of peaks at lower wavelengths. This is shown in figure 4.3 by the blue and red curves.

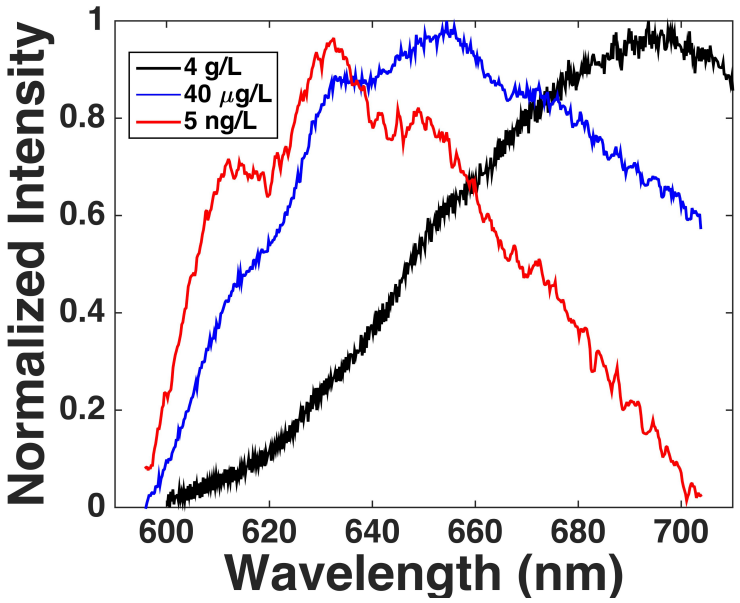

FIGURE 4.3: Series of bulk PL emission spectra recorded for PCDTBT thin films dissolved in Zeonex.

4.1.4 PL and images at single molecule level

In figure 4.4 we show a typical fluorescence emission map originating from a thin PCDTBT film at a concentration of 5 ng/l. Unlike the fluorescence emission maps shown in figure 4.3, at this low concentration individual emitters are resolved and can be easily observed. These features correspond to single polymer chains, although a moderate portion of the emissive features may be attributed to small molecular aggregates.

In order to study the polymer's PL properties in SM domain, the intensity of each of the bright features observed in the previously shows fluorescence map (identified with PCDTBT single molecules) was plotted against wavelength and fitted with a series of four gaussian functions.

Figure 4.5 presents the fluorescence emission spectra of two PCDTBT chains, recorded in Zeonex at room temperature. Upon a closer examination, the PL properties of PCDTBT single molecules differs from the emission observed in bulk for the pure

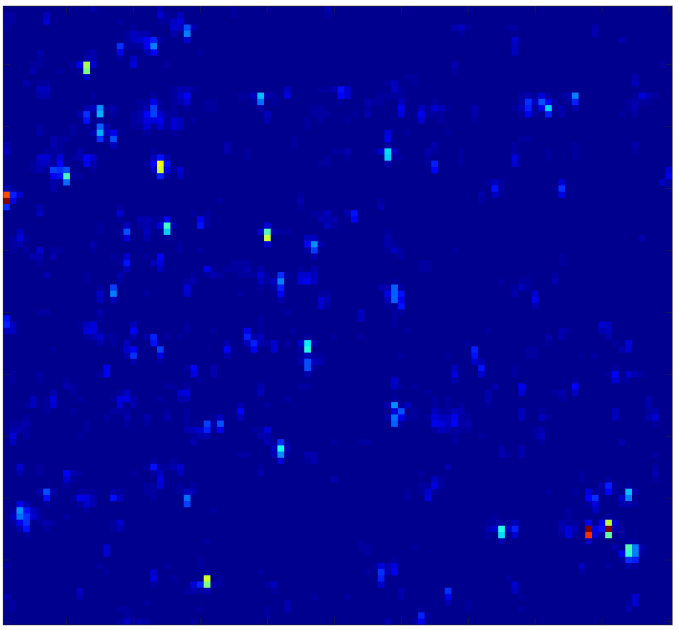

FIGURE 4.4: Typical map of PCTBT single molecule fluorescence emission, dispersed in Zeonex at a concentration of 5 ng/l.

polymer. Instead of one broad peak and several shoulders, in all cases the spectra now have several narrower peaks at relatively lower wavelengths compared to the clearly dominant feature at 700 nm observed for the pure material.

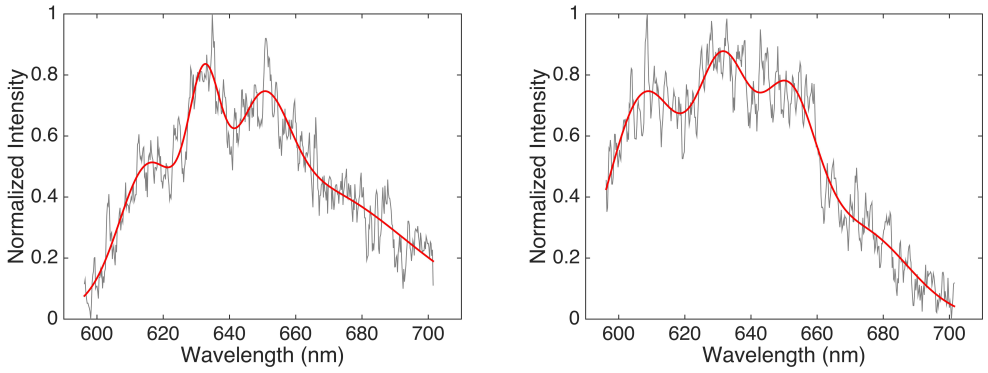

FIGURE 4.5: Photoluminescence spectra of two PCDTBT single molecules

After recording the emission spectra for approximately one thousand emitters, the recorded data was investigated in order to quantify the PL properties of PCDTBT at nanometer scale. By using a gaussian fit, the dominant feature of each fluorescence spectrum was determined. After collecting data for all one thousand SM's, a statistical distribution was built, by plotting the occurrence of each dominant peak at the

corresponding wavelength with an accuracy of 2 nm. Over the obtained histogram, a bulk PL spectrum recorded for a 5 ng/l film was overlapped.

Figure 4.6 shows the results of this statistical analysis. As it can be seen, the statistical distribution of the studied SM's presents itself a complex function with several distinct peaks. We indicate that only a small fraction of emitters, approximately 10% of the studied PCDTBT SM's, are characterised by a dominant emission in the range of 680 - 700 nm which corresponds to that of the ensemble PL. This occurrence is usually assigned to molecular clusters, formed by two or more intertwined chains. The rest of single molecules are blue shifted and split into four distinct regions peaking at 609 nm, 632 nm, 647 nm and 675 nm respectively.

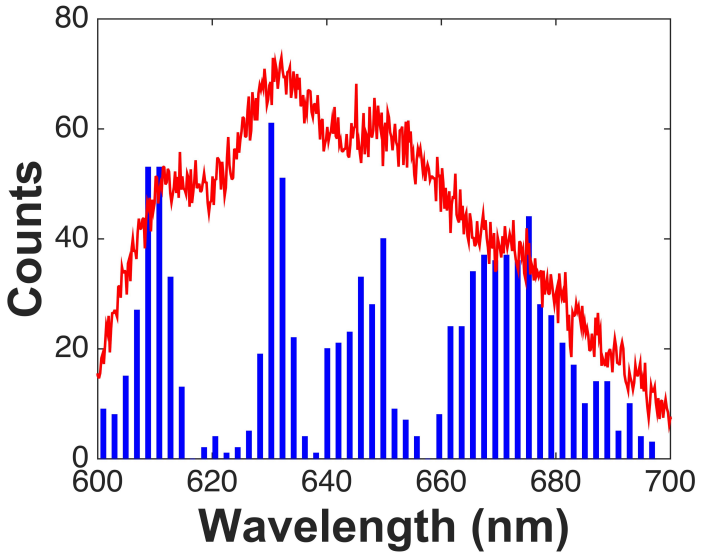

FIGURE 4.6: Statistical distribution of the dominant emission peak, recorded for PCDTBT single molecules. Overlapped: the bulk emission spectrum of a thin film recorded in Zeonex at a concentration of 5 ng/l.

4.1.5 Discussion on results

As seen in figures 4.3 and 4.5, the dominant feature in the PL spectra of single molecules is is shifted towards shorter wavelengths, compared to the fluorescence in bulk. This spectral shift is due to the large separation between individual polymer chains which will reduce interchain interactions as well as suppress energy transfers between PCDTBT and the surrounding Zeonex matrix. A very similar effect was observed for PFR in [16]. Having a structure somewhat similar to PCDTBT, in the form of a carbazole unit followed by a benzothiazole group delimited by thiophene

rings, the ensemble PL emission spectra as well as the SM emission spectra visibly shift to lower wavelengths when compared to the bulk emission of a pure film.

In this circumstance, the interchain energy transfers appear to be fully suppressed, which leaves intrachain transfers as the main means of energy transfer require to quench the exciton formed by the excitation source which reduces the number of sites accessible to the excited state. Also, the Zeonex matrix allows the polymer chain to assume an elongated conformation. Due to an increase in the polymer chain's statistical length, the red fluorescence emission is cancelled, relatively few molecules show a dominant fluorescence peak corresponding to that of the bulk emission, allowing lower energy features to become dominant.

This substantial variation in the material's optical properties at low concentration suggests that interchain energy transfers are the main method of energy transport in polymeric semiconductor devices.

4.2 Fluorescence lifetime imaging

4.2.1 Introduction

Fluorescence detection techniques have had wide applications in life sciences due to their sensitivity and ability to study interactions on a single-molecule scale. Several properties are important for characterising fluorescence signals [161, 162]:

- intensity. Dependant on the fluorophore concentration and its quantum efficiency, fluorescence intensity maps are used for determining the spatial structure of the sample and localising fluorophores;
- spectrum. Usually independent of concentration, it is an intrinsic characteristic of an emissive species, spectral images allow the identification of fluorohphores in a sample.
- lifetime. Not dependant on concentration but does depend on the fluorophore's nature and its molecular environment

There are various methods available for measuring and imaging fluorescence decay times, losing to a large number of instrumental methods of varying efficiencies,

acquisition times or resolution [163, 164]. In this section we make use of TCSPC (time-correlated single photon counting) in order to analyse the fluorescence decay distribution of PCDTBT.

Originating in astronomical imaging techniques, such as the Faint Object Camera mounted on the Hubble Space Telescope [165], TCSPC has clear advantages over conventional CCD techniques, mainly the ability to measure the arrival times of individual photons. The method relies on exciting the sample with a MHz range light source, which creates a train of single photon events which are then used to build a fluorescence decay curve. Although it provides a good signal to noise ratio and temporal resolution, it has the disadvantage of being strictly one dimensional. In order to solve this drawback, Becker & Hickl used a multidimensional approach to the TCSPC method which, besides measuring the arrival times of single photons, the method provides supplementary parameters like the location of a chromophore on the image or the wavelength of the detected photons [137]. The operating principle of multi-dimensional TCSPC is similar to the one dimensional variation. The sample is scanned with a focused laser with repetition rate in the MHz range. When a photon is detected, the detector will determine its arrival time and coordinates within the area that was scanned. A distribution of the arrival times of individual photons over the spatial coordinates is then built.

4.2.2 TCSPC measurements

For the purpose of further studying the energy transfer in single molecules, a series of fluorescence lifetime measurements were performed on PCDTBT films at two different concentrations. In this experiment, excitation was provided by a 473 nm pulsed laser and measurements were carried at the peak wavelengths observed in the histogram shown in figure 4.6, 609 nm, 632 nm, 647 nm and 675 nm respectively, through TCSPS methods (described in a previous chapter).

Figure 4.7 shows the typical data acquired in this experiment, in the form of fluorescence intensity maps, at the two studied concentrations: 400 µg/l and 5 ng/l. The area that was analysed was approximately 32 μm^2. The intensity maps were obtained by recording a series of fluorescence decay curves at the wavelengths mentioned above. Each measured decay curve was integrated and arranged in a 64 x 64 matrix, the result of which being a fluorescence intensity map of the PCDTBT

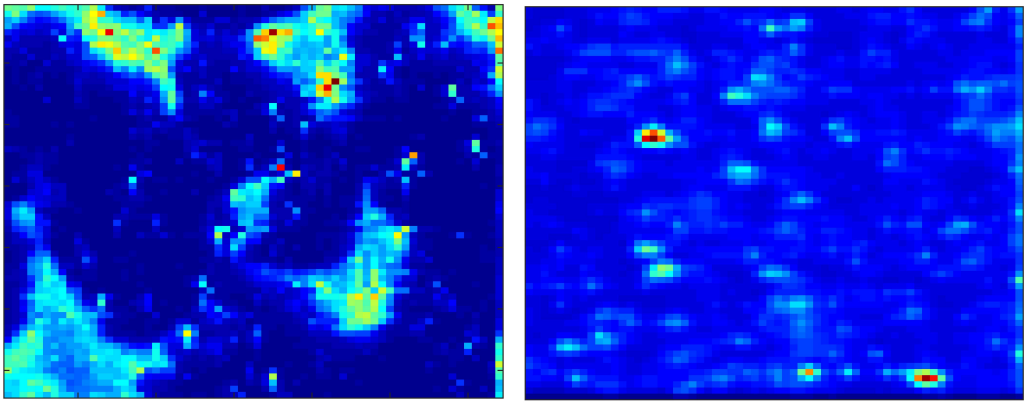

(a) (b)

FIGURE 4.7: Fluorescence lifetime maps of a PCDTBT film at 400 µg/l (a) and 5 ng/l (b).

film. Consistent with the PL intensity maps shown in figure 4.3, the morphology of the polymer film is dependent on concentration. At high concentration the material forms a series of large isolated islands (figure 4.7(a)) and as the concentration is reduced, the PCDTBT islands decrease in size until single molecule domain is reached (figure 4.7(b)).

4.2.3 Time-resolved analysis

After the sample surface was scanned at the wavelength of interest, areas containing single molecules were selected and the pixels associated with single molecules were analysed by using an exponential function (equation 4.1). An example of lifetime decay curve fitted with the exponential function was given in chapter 3, section 3.1.2.

$$I(t) = Ae^{\frac{-t}{\tau}} \tag{4.1}$$

where A represents the amplitude of the fluorescence emission, in arbitrary units; t is the time, in ns; and τ is the fluorescence lifetime, in nanoseconds.

Fluorescence lifetime was measured for both concentrations (bulk and SM level) and treated with the exponential function, as described above. After analysing a large number of emitters, a statistical analysis was performed, in which the occurrence of the acquired fluorescence lifetimes were plotted in a series of histograms. Figures

4.8 and 4.9 show the result of the statistical analysis, categorised by concentration and wavelength.

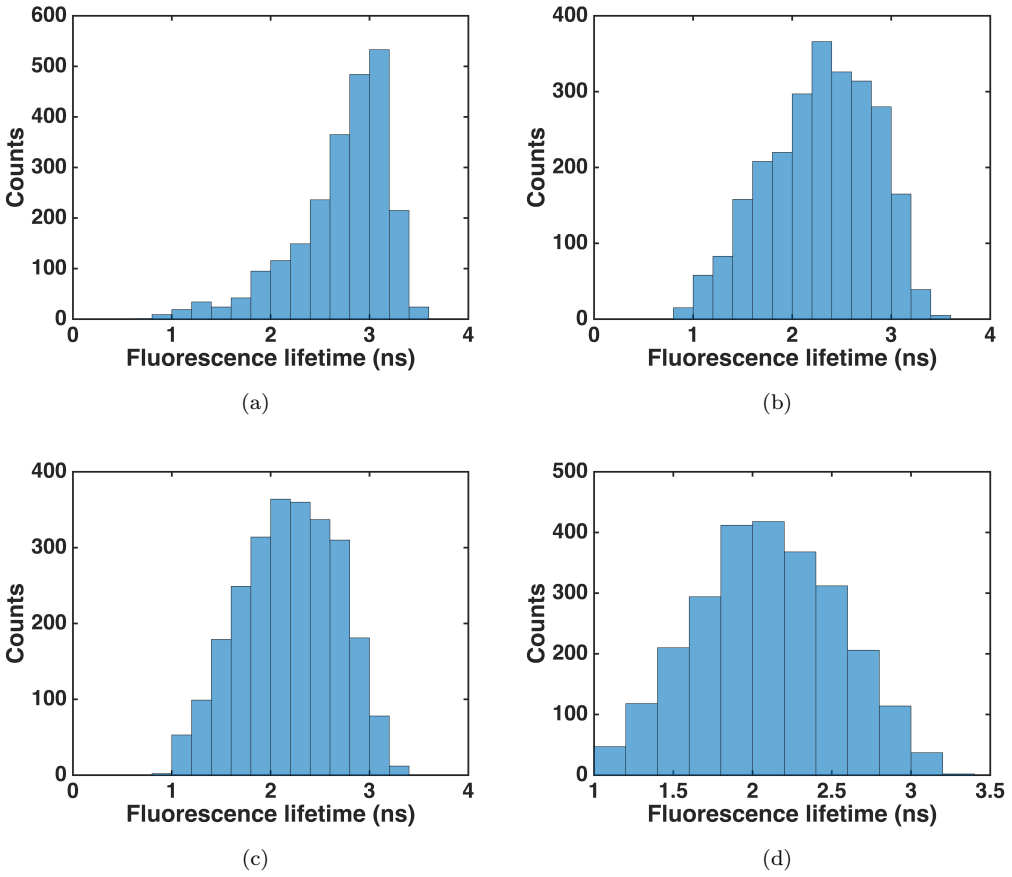

FIGURE 4.8: Statistical distributions of the fluorescence lifetimes corresponding to the four emission peaks observed in figure 4.6, for a PCDTBT film at 400 µg/l: a) 609 nm; b) 632 nm; c) 647 nm; d) 675 nm

After the mentioned histograms were built, the mean fluorescence lifetime was determined by fitting the above mentioned histograms with equation 4.2.

$$O = f(\tau|k,\mu,\sigma) = \left(\frac{1}{\sigma}\right) exp\left(-\left(1+k\frac{\tau-\mu}{\sigma}\right)^{-\frac{1}{k}}\right)\left(1+k\frac{\tau-\mu}{\sigma}\right)^{-1-\frac{1}{k}} \quad (4.2)$$

Equation 4.2 is the probability density function for a generalised extreme value distribution, where O is the occurrence of the fluorescence lifetime, τ represents the fluorescence lifetime, σ is the probability function's location parameter, σ is the scale parameter and k is the shape parameter.

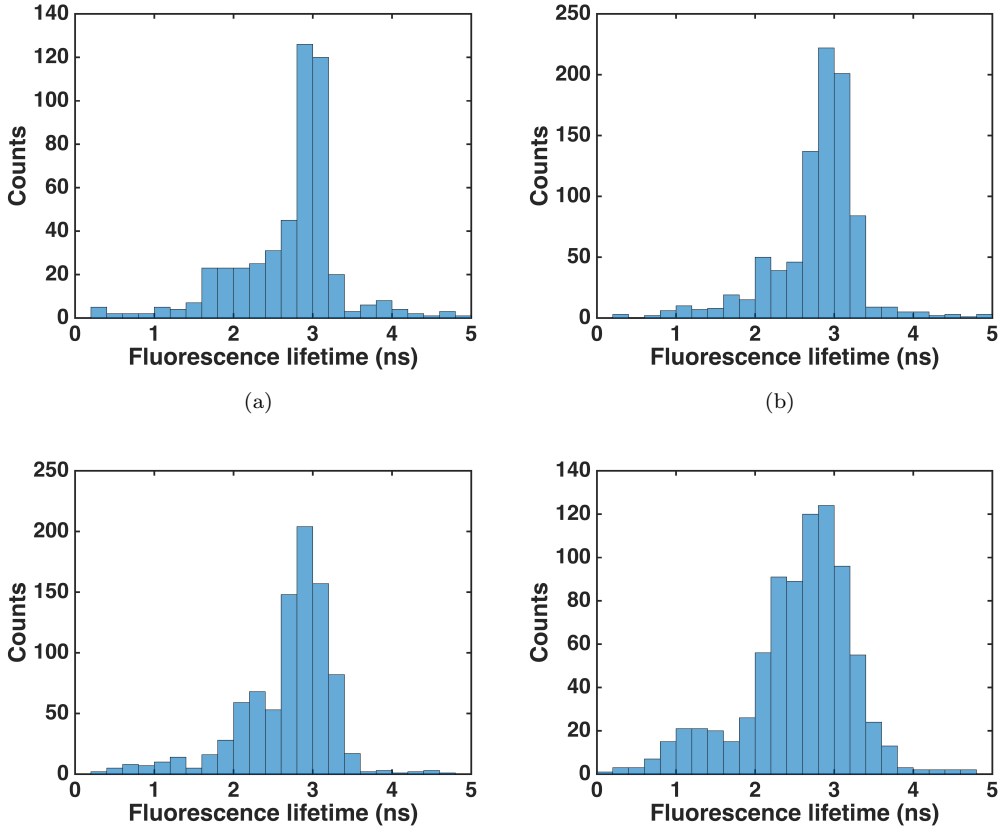

FIGURE 4.9: Statistical distributions of the fluorescence lifetimes corresponding to the four emission peaks observed in figure 4.6, for a PCDTBT film at 5 ng/l: a) 609 nm; b) 632 nm; c) 647 nm; d) 675 nm

Although the bulk measurements (400 µg/l) fit the generalised value distribution, in the case of SM fluorescence lifetime measurements the probability distribution function has the shape parameter k = 0, and equation 4.2 becomes:

$$O = f(\tau|k,\mu,\sigma) = \left(\frac{1}{\sigma}\right) exp\left(\frac{\tau-\mu}{\sigma}\right) exp\left(-exp\left(\frac{\tau-\mu}{\sigma}\right)\right) \tag{4.3}$$

4.2.4 Variation across concentration

The statistical analysis described in the previous section was performed on both concentrations. Afterwards mean fluorescence lifetime was determined, in the form of the probability distribution mean and plotted against wavelength and concentration.

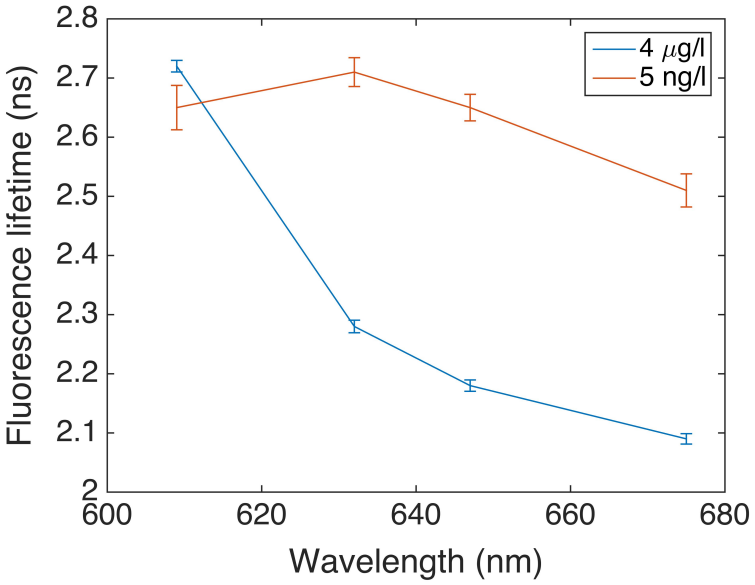

FIGURE 4.10: Variation of the fluorescence lifetime for PCDTBT with wavelength. Blue: 400 µg/l; black: 5 ng/l. The error bars were taken as one standard deviation.

As can be seen in figure 4.10, the mean fluorescence lifetimes at single molecule scale shows little to no variation across the wavelengths of interest. For the 4 µg/l films, decrease of almost 1 ns was observed. This similarity in the lifetimes at single molecule level, as opposed to the decay times in bulk, indicates that the main process which accompanies the studied polymer's optical properties in SM domain is an intramolecular energy transfer between the various chromophores in the monomer unit. Hence, energy transfers between chromophores is free and unrestricted in bulk samples and molecular aggregates, a degree of freedom which is not present in single molecules which are limited to energy transfers within the polymer chain.

The reduced lifetime in the bulk is an indication of transfer between molecules which allows the excited stated to access traps and defects, thus reducing their lifetime. This implies that energy transports in single chains are highly restricted.

Chapter 5

Blinking fluorescence of PCDTBT single molecules

5.1 Introduction

Conjugated polymers are a class of organic materials that gained interest in recent decades due to their application in developing and improving optoelectronic devices [1–11]. The relationship between the properties of π-conjugated polymers and their chemical structure in order to design materials for specific optoelectronic applications, since a material's chemical structure influences its electronic properties as well as chain morphology which can have powerful consequences on the optical and electronic properties of a molecule [166–170].

An important tool for analysing a molecule's photo physical properties and monitor the fluorescence of individual polymer chains is single-molecule spectroscopy, which can be used to reveal processes that would otherwise be hidden in bulk measurements. However, in spite of the method's efficiency, fluorescent properties of single molecules are sometimes impaired by a phenomenon called photoblinking, with severe effects on the efficiency of SMS. This phenomenon is characterised by a fluctuation of the fluorescent single, characterised by the presence of a dark (off) state alternating with a bright (on) state [106, 107, 171].

Since photoblinking is a process that hinders the efficiency of single-molecule spectroscopy, there have been many attempts at identifying the mechanism responsible

for fluorescence quenching, associated with the presence of dark states [83]. One candidate process which can explain the quenching process responsible for photoblinking is triplet state dynamics. As explained by Barbara et al. in [130], fluorescence intensity transient are a direct result of triplet quenching and triplet-triplet annihilation. According to this mechanism, the initial fluorescence emission of a species is one characteristic of a triplet-free molecule. As S_0 to S_1 transitions occur, a build up of triplet states also occurs. During the accumulation of triplets, reverse intersystem crossing decay back to ground state eventually becomes a dominant process. Since this mechanism reduces the photoluminescence yield of the emitting molecule, PL intensity suddenly drops, resulting in a dark state in the fluorescence time trace. Triplet-triplet annihilation eventually leads to a stable population of triplet states, leading to increased fluorescence emission and the presence of an "on" state. A similar triplet quenching mechanism has also been reported by Schindler and Lupton in [172]. Moreover, the authors also report a means of detecting triplet states at room temperature by purging the analysed samples with air, a process which leads to a strong PL flare followed by dynamic triplet quenching.

Besides triplet quenching, another process has been described as being responsible for photoblinking. This second mechanism involves a charge transfer between the studied single molecules and trap sites on the environment SM's are embedded in [100, 173–177]. According to this mechanism, described by a charge tunnelling model, a charge originating from a singlet or triplet state (an electron or perhaps a hole) is tunnelled towards an acceptor in the sample enviroment thus quenching the sample's emission. Subsequently, the charges will be recombined by back tunnelling thus restoring the sample's emission[173]. This process is characterised by a power law distribution of on and off states, which originates in the exponential dependence of electron tunnelling rates as well as donor/acceptor energy levels [173, 174].

5.2 Sample preparation and data collection

Samples for blinking fluorescence measurements have been prepared by means of the same procedure used for preparing samples for photoluminescence and fluorescence lifetime measurements. PCDTBT was dissolved in chlorobenzene and a 4 g/L Zeonex polymer matrix, at a concentration of 5 ng/L. A glass substrate was then coated with the dilute polymer solution and then spincoated at a constant speed for

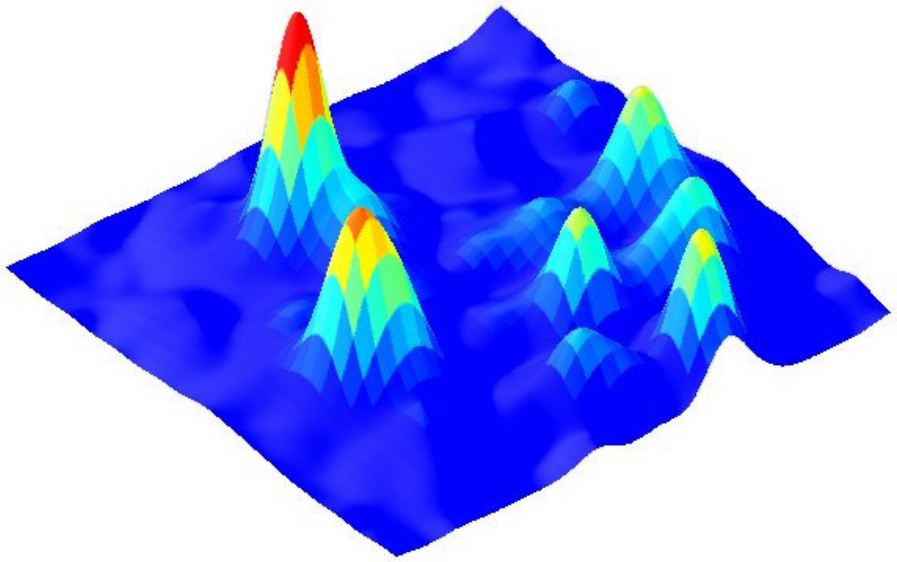

FIGURE 5.1: Confocal image of the polymer film surface at a concentration of 5 ng/l.

one minute, in order to obtain a constant film and to expel excess material. Due to the high rotational speed, the solvent used to diffuse the conjugated polymer evaporates, thus leaving on the substrate only PCDTBT molecules dispersed in a Zeonex matrix.

After preparation, samples were mounted on the experimental set-up and excited with a 80 MHz ultrafast laser. Unlike previous measurements, where a PL spectrum was recorded for each emitter, single molecules were directly imaged with a CCD camera and fluorescence time traces were measured by recording a series of consecutive confocal images of the film surface with an exposure time of 50 ms/frame. An example of such frame is shown in figure 5.1. Fluorescence time traces were generated from the acquired stacks by selecting the bright features in the image, identified as single molecules. The fluorescence intensities of selected single molecules were integrated and the obtained values were plotted against time.

5.3 Results and discussion

Examples of blinking data is shown in figure 5.2, in the form of several randomly selected fluorescence time traces for single PCDTBT molecules embedded in Zeonex acquired as described in the previous section. The fluorescence trajectories reveal a

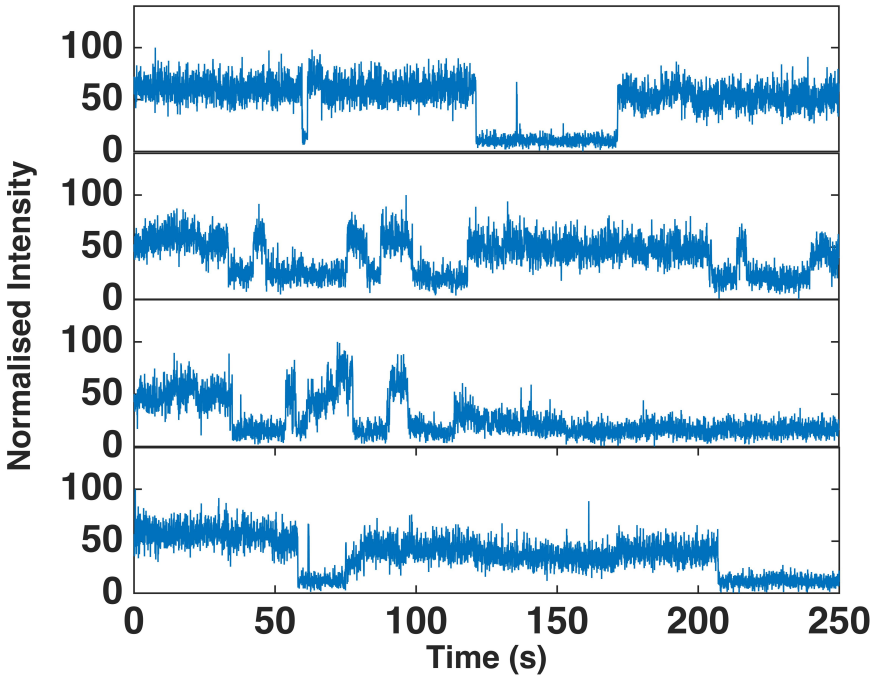

FIGURE 5.2: Examples of fluorescence time traces characteristic for PCDTBT single molecules.

clear fluorescence intermittency which is evidenced by the presence of bright on states alternating with dark states, characterised by low (most of the times negligible) fluorescence emission. Data was collected over a time of 250 seconds, with a sampling resolution of 50 milliseconds.

Due to the relatively infrequent nature of the blinking behaviour, analysing individual molecules is not possible. Therefore, fluorescence intensity fluctuations of over several hundred individual molecules were acquired and analysed. For this purpose, the fluorescence intensity of a total of 275 trajectories was normalised and combined. Figure 5.3 shows a cumulated histogram of the normalised fluorescence intensity values. Three intensity levels are noticed, illustrated by coloured Gaussian peaks, associated with a dark level (blue curve), an intermediate level (red curve) and a bright level (green curve), a behaviour also shown by Vanden Bout in [83] for a PPV-PPyV copolymer. Furthermore, histograms of the intensity levels for each individual fluorescence transient was built. As seen in figure figure 5.4, although there are three separate intensity levels, individual time traces only show two distinct levels, in the form of a bright level and a dark or intermediate level. A similar behaviour has been reported in [106] for MEH-PPV.

Since fluorescence blinking on the studied material occurs rather infrequently and

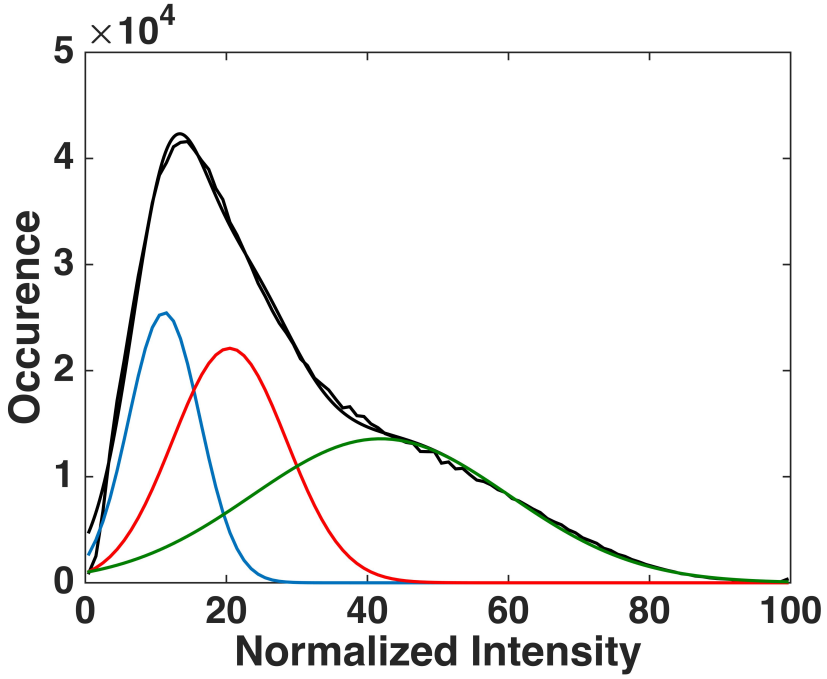

FIGURE 5.3: Cumulated intensity histogram of a collection of single molecule fluorescence intensity transients.

analysing individual molecules is not possible, all following analysis has been done for the entire population of 275 PCDTBT molecules.

We first analyse the distribution of blinking times. For this purpose, on and off times have been plotted on a logarithmic scale. The data follows a linear fit, therefore the distribution of on and off times can be described by the power law function shown in equation 5.1.

$$P(\tau) = P_0 \tau^{-m} \tag{5.1}$$

where P(τ) represents the distribution of on and off times, τ is the on or off blinking time for a population of 275 PCDTBT single molecules and m is the power law exponent.

As seen in figure 5.5, both on and off times are power law distributed, with a power law exponent m_{on}=1.21 for on times and m_{off}=1.06 for off times respectively. As also indicated in [175–179], power law exponent values between 1 and 2 are an indication of a charge tunnelling model. According to this model, a charge transfer takes place between the PCDTBT molecules and certain localised states in the Zeonex polymer

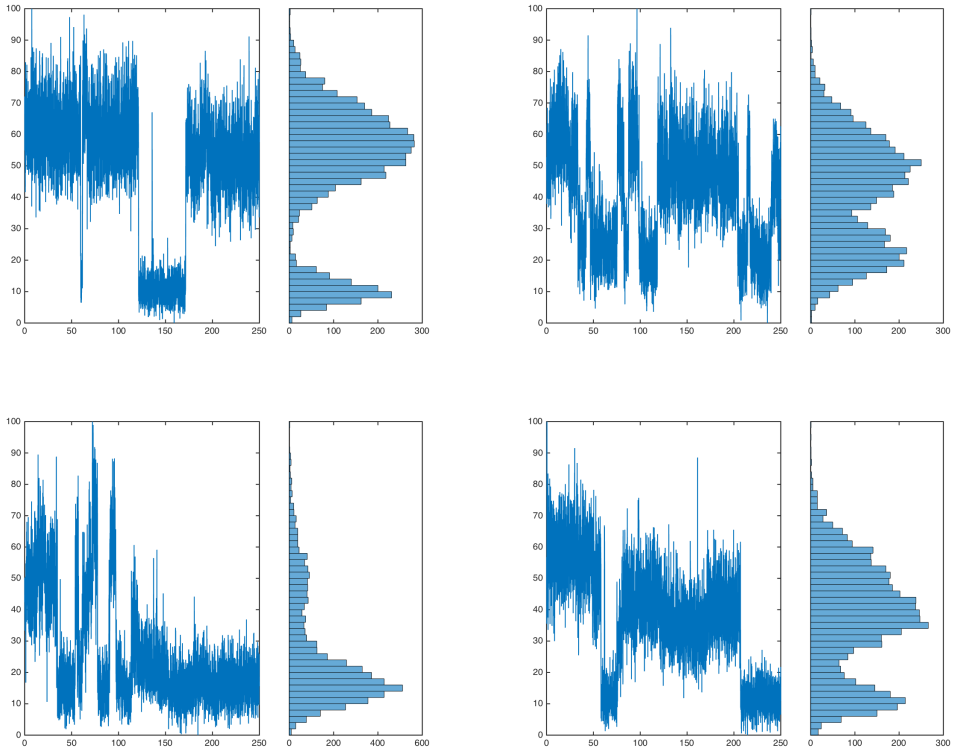

FIGURE 5.4: Fluorescence time traces of four PCDTBT single molecules and corresponding intensity histograms.

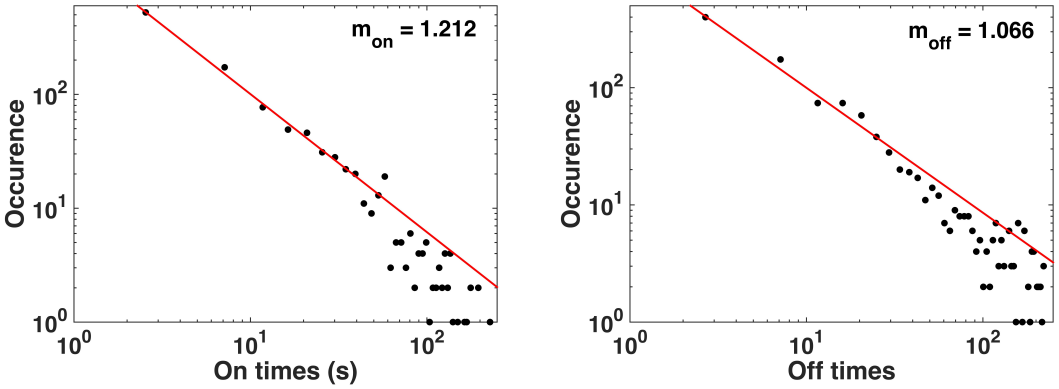

FIGURE 5.5: On and off time distributions for 275 PCDTBT molecules.

matrix. Following the electron tunnelling process, charges will recombine by reverse tunnelling thus restoring the fluorescence of PCDTBT single molecules. A similar result has been obtained by Clifford et. al in [100] for a population of Atto647N fluorescent dye molecules.

Figure 5.6 shows histograms of the on and off time frequencies recorded form fluorescence transients corresponding to PCDTBT single molecules. Statistical analysis of blinking time occurrence was performed by means of a power law function in the form of a Generalised Pareto probability distribution, described by equation 5.2.

$$P(\tau) = \frac{1}{\sigma}\left(1 + k\frac{\tau - \theta}{\sigma}\right)^{-1-\frac{1}{k}} \tag{5.2}$$

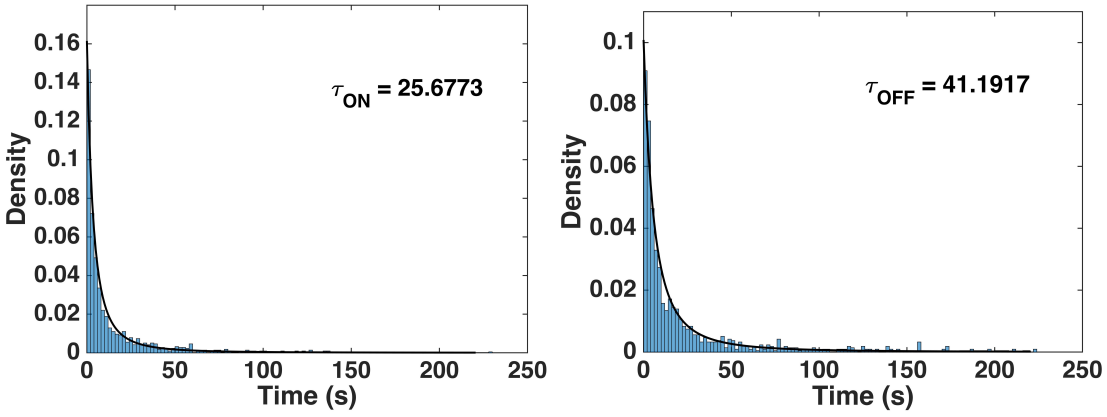

FIGURE 5.6: Histograms of on and off times for PCDTBT single molecules.

where P(τ) represents the frequency of on and off times, σ is a scale parameter, characteristic for the distribution's spread, θ is a threshold (or location), which determines the value with which the distribution shifts from zero and k is a shape parameter, responsible for stretching/shrinking the distribution curve. As seen in figure 5.6, the histograms show a clear power law behaviour with τ_{on}=25.67 s and τ_{off}=41.19 s.

The value recorded for the mean off time (41.19 s) is significantly higher than the corresponding on time (25.67 s). This likely indicates a photobleaching effect which, unlike fluorescence blinking, is an irreversible mechanism. Due to the power of the excitation source, chemical transformations are induced in the analysed material which significantly (and permanently) lowers a fluorophore's emission probability. This photobleaching process, commonly an undesirable process, establishes a useful time limit of a certain fluorophore [95].

The photoluminescence transients presented in figures 5.2 and 5.4 may seem random at first but they follow a very well defined statistical distribution, that can be of use in identifying the source of the emission. For this purpose, there is a means

of analysing the time trace data, by calculating a shift in the fluorescence intensity of the measured points. The analysis was performed for over 200 PCDTBT time traces and in figure 5.7 we show histograms containing the statistical distribution of fluorescence intensity differences for a few selected PCDTBT single molecules.

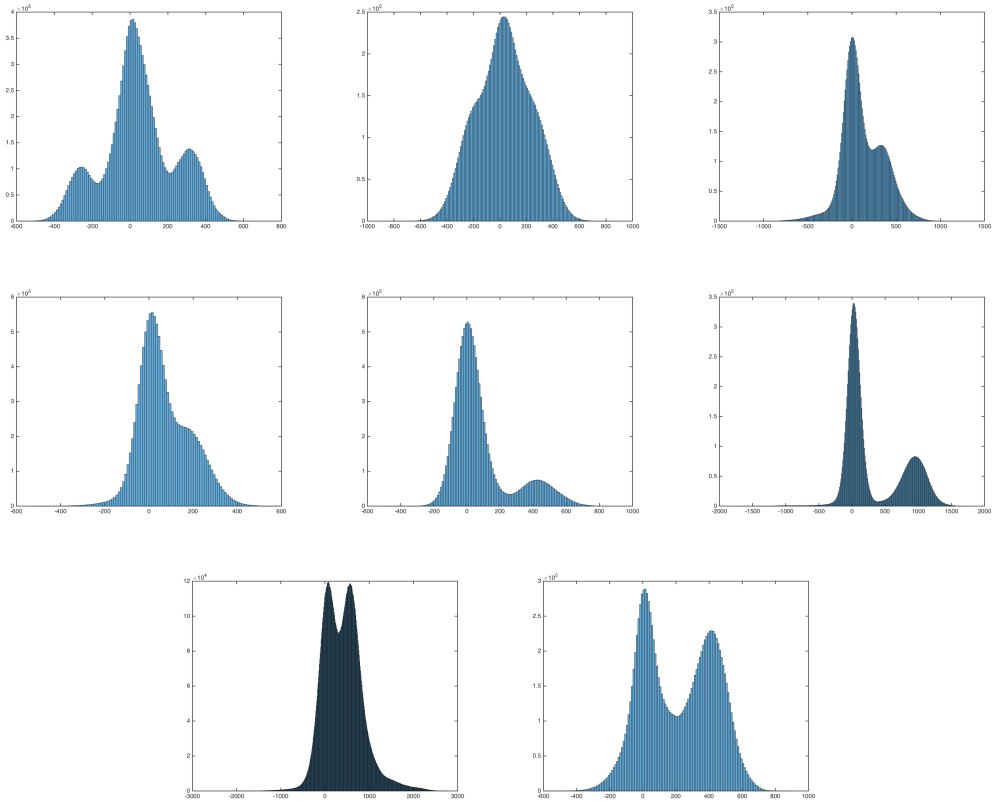

FIGURE 5.7: Histograms of the intensity difference between points from measured individual fluorescence time traces.

As seen, the histograms are characterised by a main gaussian peak at zero, with a width of approximately 50 intensity units, and one or two side peaks. There are two sets of side chains, one category at +/- 200 and a second category, above 500 intensity units. In good accordance with data presented earlier (figures 5.3 and 5.4), this analysis shows the presence of three states: an "off" state, and two separate "on" states. As also seen in figure 5.4, although there are three states, only two are present at any given time.

One likely cause for the features observed in figure 5.7 is a fluorescence emission originating from a single chromophore. In this case, the jumping events can be associated with a single chromophore reversibly switching between two different states, as also seen for certain dye SM's [180]. Also, another equally likely mechanism is

multiple chromophore emission, equating with two chromophores with similar properties. In this situation, the light source does not directly excite the fluorophore, but another chemical group in a high energy state. The created excited state will then migrate through the polymer chain by means of an intramolecular energy transfer.

The triplet states responsible for the blinking behaviour are usually extremely short lived (with lifetimes in the range of a few ms). Due to the sample rate of 50 ms used in this study, only the deep states were analysed, characterised by a long lifetime. Considering the fluorescence blinking analysis in this chapter, as well as the relatively broad SM fluorescence emission presented in chapter 4, this switching behaviour can be associated with the presence of an intramolecular aggregate resulting from a folding of the polymer backbone which allows direct interactions between different chemical groups on the same chain, which case the appearance of deep traps. Folded polymer chains, leading to the presence of an intramolecular aggregate has been reported previously [112, 181].

Chapter 6

Conclusions

6.1 Summary

6.1.1 Automation

Since single molecule experiments are usually rather slow, due to the time required to manually measure a sufficient number of emitters for any significant investigation, a first goal of the project was to automate and optimise the single molecule fluorescence experimental procedure as well as the data analysis method. The rationale behind this goal is to allow the acquisition and analysis of data from a large number of single molecules in a reasonable amount of time. Results of this optimisation are shown in chapter 3.

Initially, a series of LabVIEW based applications have been devised and carried out, to verify the utility of the proposed task. The original application shown to be feasible but there were certain obstacles, related to the application's speed due to problems of compatibility between the toolkits and packages used in designing the application. This lead to replacing the initial LabVIEW application with a new sequence of hardware and software packages that solved earlier design issues. In order to test the performance of the now automated set-up and the reproducibility of any obtained results, PL emission from a sample of polystyrene microspheres has been measured and compared to the manufacturer's data sheet. Experiments yielded a PL spectrum with a main emission peak at 560 nm, which accurately matches the fluorescence properties provided by the manufacturer.

Analysing the large quantity of data provided by the experimental set-up was achieved by means of a series of Matlab applications (presented in appendix A and B). The code uses the data file generated by the set-up in order to build fluorescence maps as well as detect, generate and characterise the PL spectra of emissive features of significance.

Automating the data acquisition and analysis provided us with an exceptionally flexible experimental set-up and procedure, allowing the investigation of various types of samples such as polymer films and biological samples. Depending on the mode of operation, several experiments can be performed: mapping the sample surface, image acquisition, photoluminescence spectroscopy and fluorescence lifetime imaging.

6.1.2 Single molecule photoluminescence

A second objective of this project was studying the photoluminescence properties in single molecule domain and revealing possible mechanisms responsible for the emission of light when exciting a polycarbazole deviated conjugated polymer, commercially known as PCDTBT. This has been achieved in chapter 4, by means of photoluminescence spectroscopy and fluorescence lifetime imaging.

Firstly, the materials; properties in bulk were determined. The polymer's absorption is characterised by the presence of two main peaks at 380 nm and 570 nm respectively, attributed to π-π^* transitions of an excited state. The PL properties of a pure PCDTBT film are in the form of a broad spectrum containing a main peak at 700 nm and a series of side shoulders corresponding to double C - C bond vibrations.

Low concentration PCDTBT films were analysed by means of fluorescence spectroscopy. The measurements reveal complex PL spectra for individual molecules, containing four main emission peaks at 609 nm, 632 nm, 647 nm and 675 nm. A statistical analysis of over 1000 single molecules suggests that the majority of SMs exhibit fluorescence emission at energies higher than that of the bulk material. This is due to the large separation between individual emitters which effectively suppresses intermolecular energy transfers, leaving intrachain transfers as the dominant mechanism.

Fluorescence lifetime imaging shows little variation of PCDTBT single molecule decay times, indicating an intramolecular energy transfer between the polymer's repeating units. Compared to fluorescence lifetime at single molecule level, fluorescence decay measured in bulk shows a visible decrease of the measured decay times. This is an indication that the energy of formed excited states is transferred without restrictions between individual chromophores in a concentrated film. The observed reduction in the fluorescence lifetime of the bulk material can be explained by the ability of the excited state to recombine by accessing various traps present in the sample, a mechanism not available for single molecules which are limited to transitions within the molecule.

6.1.3 Photoblinking

The final experiment performed in this study has been a fluorescence time trace experiment, which is presented in chapter 5. This experiment is important for revealing the source of the fluorescence emission as well as possible mechanisms regarding the infrequent fluorescence emission encountered in single molecule photoluminescence. To this end, the fluorescence blinking of over 250 PCDTBT single molecules has been acquired and analysed.

Power law distribution analysis of the observed time traces yielded a power law exponent of 1.21 and 1.06 for on and off times respectively. This indicates a tunnelling mechanism in which charges, represented by excited electrons or holes, are transferred from the polymer molecules to trap sites on the surrounding matrix, thus quenching the fluorescence emission. Following this transfer, charges will then be recombined and fluorescence is restored.

The high value of the average off time, nearly double that of on time, reveals the presence of a photoblinking reaction. A side effect of the excitation power, photobleaching permanently annihilates PL emission by inducing certain chemical changes in the emitting structure.

Results also show that although the presence of three separate intensity levels has been shown, individual emitters only displaying two events (in the form of a dark state and one bright state). A possible mechanism that can explain the presence of this behaviour is an emission originating from two chromophores with nearly

identical properties. This can be correlated with SM spectroscopy results, showing the presence of an intramolecular aggregate. Intramolecular aggregates are a direct result of a folding of the polymer chain, a process that allows direct interactions between various chemical groups within the molecule.

6.2 Conclusions and future work

In conclusion, SM spectroscopy as well as fluorescence lifetime measurements revealed a suppression of interchain energy transfers, leaving intramolecular transfers as the dominant mechanism which controls the polymer's fluorescence properties. This is supported by the higher fluorescence emission in single molecule domain compared to PL emission in bulk as well as an apparent lack of variation in the fluorescence decay times of single molecules.

Photoblinking experiments show that the most likely mechanism responsible for fluorescence quenching involves electron/hole tunnelling between PCDTBT chains and the host matrix. Fluorescence time traces also display the presence of three distinct states (one dark state and two separate bright states) but only two jumping events for a given molecule. This indicates that excitation and emission take place in different sections of the polymer backbone. A means of explaining this phenomenon is by associating the polymer's photoblinking with the presence of intramolecular clusters, a direct consequence of folding the polymer chain, thus allowing a direct interaction between different fluorophores on the molecule.

There are several approaches that can be taken in order to improve upon and expand the work presented in this report. One such possible improvement is to upgrade and accelerate the experimental set-up's automation as well as the data analysis code. This will allow us to measure and analyse more single molecules in one sitting, which will lead to a more precise statistical treatment of a certain material?s photo physical properties.

Furthermore, another approach for future research would be an attempt at correlating the photophysical properties of PCDTBT with morphological data, mainly the shape and folding of single polymer chains. There are a number of experiments which can achieve a correlation between optical and morphological properties. One possibility is to analyse the optical properties of conjugated polymers with a chemical

structure similar to that of PCDTBT, which will help in establishing a relationship between he structure and function of a conjugated system.

Also, the inclusion of new experiments can achieve in establishing a structure-function correlation, such as polarisation anisotropy, scanning probe microscopy (AFM or STM) and even various sample preparation methods (such as using different types of polymer matrix to dissolve the conjugated polymer of interest).

Appendix A

Fluorescence Data Analysis Code

A.1 Main Script

```
%load data

data=readSPE('...');
imnum=5;

%get the summed image and the summed stack
XWidth=100;
YWidth=100;
maxarea=9;
store_threshold = 9000000;
frames=length(data)./(XWidth*YWidth);


[summed_stack,summed_image] = SM_build_image_spectra(data,XWidth,...
 YWidth,frames );

%get the points of interest;
threshold = store_threshold;
number_points=zeros(1,100);
```

```
for Q=1:100
threshold=threshold-(Q*(1000));
[ stats1,temp1,temp2 ] = SM_slected_SM( summed_image,threshold );
number_points(Q)=size(find([stats1.Area] <maxarea),2);
end

[x, i ]= max(number_points);

threshold = store_threshold;
threshold=threshold-(i*(1000));
[ stats,holdall,BT ] = SM_slected_SM( summed_image,threshold );



%get the background
if frames==1
    [ summedb,summedbs ] = SM_calculate_background_spectra( data );
end

if frames==1
   [ Corrected ] = SM_return_corrected_spec( data,summedbs,holdall,...
      XWidth,YWidth );
end

disp(size(Corrected));

% get fluorescence spectra
centw=650;
w=1:1:size(Corrected,2);
Xdata=centw-54+(w*(108/512));

Sections=[10 15];

fitres=zeros(size(Corrected,3),4,3);
fitresults=zeros(size(Corrected,3),12);
for Q=1:size(Corrected,3)
    Spectra(:,1)=Xdata;
```

```
    int=smooth(sum(Corrected(:,:,Q),1));
    spec=int;
    Spectra(:,2)=(spec-min(spec))/(max(spec)-min(spec));
    [fitresults(Q,:) ] = SM_fit_spectra( Spectra );
    disp(100*Q/size(Corrected,3));
end

% get dominant peaks
a=fitresults(:,[1:4]);
b=fitresults(:,[5:8]);

A=transpose(a);

maxValue=zeros(Q,1);
rowIdx=zeros(Q,1);

for n=1:Q
[maxValue(n,:), rowIdx(n,:)] = max(A(:,n),[],1);
end

row=transpose(1:Q);
col=rowIdx;
v{imnum}=b(sub2ind(size(a),row,col));

plot histogram
if numel(v)>2
for k=1:numel(v)
    peaks=cat(1,v{1:k});
end
histogram(peaks,'BinWidth',1);
end

clear n; clear rowIdx; clear A; clear row; clear col; clear maxValue;
clear a; clear b; clear imnum; clear k; clc;

imagesc(summed_image)
```

```
hold on
plot(holdall(:,1),holdall(:,2),'y*')
```

A.2 Secondary Functions

A.2.1 Building the image

```
function [summed_stack,summed_image] = SM_build_image_spectra(data,...
XWidth,YWidth,frames )

for I = 1:frames
summed_stack(:,:,I)=...
     sum(data(:,:,1+((I-1)*XWidth*YWidth):((I)*XWidth*YWidth)),3);
end

summed_image=sum(sum(data,1),2);
summed_image=reshape(summed_image,XWidth, YWidth);


end
```

A.2.2 Selecting points of interest

```
function [ stats,holdall,BT ] = SM_slected_SM( summed_image,Threshold )

indx=find(summed_image > Threshold);

blank=zeros(size(summed_image,1),size(summed_image,2));
blank(indx)=1;
BT= im2bw(blank,0.5);
stats=regionprops(BT,'PixelList','Area');

for Section_number=1:size(stats,1);
```

```
clear positions;
positions(:,1)=stats(Section_number).PixelList(:,1);
positions(:,2)=stats(Section_number).PixelList(:,2);

values=zeros(1,size(stats(Section_number).PixelList,1));

for Q=1:size(stats(Section_number).PixelList,1)
    values(Q)=summed_image(positions(Q,2),positions(Q,1));
end

[q,indy]=max(values);

holdall(Section_number,1)=positions(indy,1);
holdall(Section_number,2)=positions(indy,2);
end

end
```

A.2.3 Selecting and subtracting the background

```
function [ summed,summeds ] = SM_calculate_background_spectra( data )

%bottom 10%
section_range=floor(length(data)/10);

back=sum(sum(data,2),1);
background=sort(back);
background=reshape(background,1,[]);
background_min=background(section_range);
ind=find(back<background_min);

for J=1:length(ind)
summed(:,:,J)=data(:,:,ind(J));
end
summeds=sum(summed,3)./section_range;
```

```
end
```

A.2.4 Generating PL spectra

```
function [Corrected] = SM_return_corrected_spec(data,summedbs,...
holdall,XWidth,YWidth )

for J=1:size(holdall,1)

    indx=sub2ind([XWidth,YWidth],holdall(J,2),holdall(J,1));
    Corrected(:,:,J)=data(:,:,indx)-uint16(summedbs);


end
```

A.2.5 Fluorescence spectra and peak fitting

```
function [ fitresults ] = SM_fit_spectra( Spectra )

ft = fittype( 'gauss4' );
opts = fitoptions( 'Method', 'NonlinearLeastSquares' );
opts.Display = 'Off';
opts.Lower = [0 600 0 0 620 0 0 640 0 0 660 0];
opts.Upper = [Inf 620 Inf Inf 640 Inf Inf 660 Inf Inf 700 Inf];
[fitresult, gof] = fit( Spectra(:,1), Spectra(:,2), ft, opts );



fitresults(1)=fitresult.a1;
fitresults(2)=fitresult.a2;
fitresults(3)=fitresult.a3;
fitresults(4)=fitresult.a4;
```

```
fitresults(5)=fitresult.b1;
fitresults(6)=fitresult.b2;
fitresults(7)=fitresult.b3;
fitresults(8)=fitresult.b4;

fitresults(9)=fitresult.c1;
fitresults(10)=fitresult.c2;
fitresults(11)=fitresult.c3;
fitresults(12)=fitresult.c4;

end
```

Appendix B

Fluorescence Time Trace Data Analysis Code

B.1 Main Script

```
load('data.mat');

t=transpose([0.05:0.05:250]);

T = [.1:1e-1:.4];
S = [1:50];

curve=data(:,2);
new_curve=(curve-min(curve))/(max(curve)-min(curve));

newdata=smooth(new_curve);

[deriv,minmax,stats,time]=AnalyzeEdges(newdata,S,T);
time2=time*0.05;
res=[time2(1,1);diff(time2)];

states(:,1) = res(1:2:end,:);
states(:,2) = res(2:2:end,:);
```

```
disp(sprintf('State 1\t State 2'));
for i=1:length(states)
disp(sprintf('%5.2f\t%5.2f', states(i,1), states(i,2)));
end
```

B.2 Edge Analyzer

```
function [dData,minmax,stats,time2] = ...
AnalyzeEdges(data,scales,thresholds,timestep,startTime,endTime,tranRad )

t=transpose([0.05:0.05:250]);
if (nargin < 7)
    tranRad = 1;
end
if (nargin < 6)
    endTime = 10;
end
if (nargin < 5)
    startTime = 0;
end

% time scale
if (nargin < 4)
    timestep = 1;
    format = '%5d\t%5.2f\t%5.2f';
else
    format = '%5.2f\t%5.2f\t%5.2f';
end

if (nargin < 3)
    thresholds = T;
end
if (nargin < 2)
```

```
    scales = S;
end

% Limit analysis to time region specified
if (nargin < 4)         % no time data specified
    time = 1:length(data);
elseif (nargin < 5)     % scale specified, but no range
    time = 0:timestep:(length(data)-1)*timestep;
elseif (nargin < 6)     % scale and start time specified
    data = data((startTime/timestep)+1:end);
    time = startTime:timestep:(length(data)-1)*timestep + startTime;
else                    % scale and region specified
    data = data((startTime/timestep)+1:(endTime/timestep)+1);
    time = startTime:timestep:(length(data)-1)*timestep + startTime;
end

% Create the derivative scale space--minima and maxima of the derivative
% correspond to transitions
dData = CreateGaussScaleSpace(data, 1, scales);

% Find the position of local minima and maxima of the most coarse scale
minmax = FindLocalExtrema(dData(:, end), thresholds(end), scales(end));
minmaxIdx = find(minmax);

% Refine min/max positions through scale space
for i = size(scales)-1:-1:1
  minmax=FindLocalExtrema(dData(:,i),thresholds(i),scales(i),minmaxIdx);
  minmaxIdx = find(minmax);
end

% Find the data statistics in each region
stats = RegionStats(data, minmaxIdx, tranRad);

% Plot detected transitions over original data
figure;
plot(t, data,'k');
```

```
hold on;
plot(t, 1.0 * minmax * max(data(:,end)), 'b');
hold off;

time2 = NaN(length(minmaxIdx)+1,1);

% Print region statistics
% disp(sprintf(' Time\t Mean\t Stdv'))
for i = 1:length(minmaxIdx);
%     disp(sprintf(format, time(minmaxIdx(i)), stats(i,1), stats(i,2)));
    time2(i) = time(minmaxIdx(i));
end
% disp(sprintf(format, time(length(data)), stats(end,1), stats(end,2)));
time2(i+1) = time(length(data));
```

References

[1] J. E. Zhi, X. L. Xu, J. B. Shen, W. Zhao, B. Tong, and Y. P. Dong. Application of fluorescent conjugated polymers in detecting biomacromolecules. *Progress in Chemistry*, 21:739–746, 2009.

[2] G. Bidan. Electroconducting conjugated polymers: New sensitive materials to build up chemical and electrochemical sensors. a review. *Sensors and Actuators B: Chemical*, 6:45–56, 1992.

[3] K. I. Tsuji, H. Eguchi, K. Yasukouchi, M. Uroki, and I. Taniguchi. Enzyme immunosensors based on electropolymerized polytyramine modified electrodes. *Bioelectronics*, 5:87–101, 1990.

[4] A. J. Frank. Photoelectrochemical solar cells: Stabilization of small band-gap semiconductor in aqueous solution by surface attached organic conductor polymer. *Molecular Crystals and Liquid Crystals*, 83:341–352, 1982.

[5] K. Nakatani, K. Suzuki, and H. Okanima. A monolithic series-connected solar cell on an organic polymer film substrate. *Solar Energy Materials*, 17:265–277, 1988.

[6] Z. L. Yang, Y. L. Bu, and Q. Y. Chen. High efficiency low band gap conjugated polymer materials for solar cells. *Progress in Chemistry*, 23:2607–2616, 2011.

[7] G. Grem, G. Leditzky, B. Ullrich, and G. Leising. Realisation of a blue emitting device using poly(p-phenylene). *Adv. Mater*, 4:36–37, 1992.

[8] R. H. Friend. Conjugated polymer semiconductor devices: characterization of charged and neutral excitations. *Synth. Met.*, 51:357–371, 1992.

[9] J. A. Osaheni and S. A. Jenekhe. New red light emitting conjugated rigid-rod polymer: Poly(benzibisthiazole-1,4-phenylene-bisvynilene). *Macromolecules*, 26:4726–4728, 1992.

[10] M. Aktic, Y. Segui, and B. Ai. A new polymer insulated gate field effect transistor. *J. Appl. Phys*, 51:5055–5057, 1980.

[11] H. Koezuka and A. Tsumura. Field-effect transistor utilizing conducting polymers. *Synth. Met.*, 28:753–760, 1989.

[12] D. C. Watters, J. Kingsley, H. Yi, T. Wang, A. Iraqi, and D. Lidzey. Optimising the efficiency of carbazole co-polymer solar-cells by control over the metal cathode electrode. *Organic Electronics*, 13:1401–1408, 2012.

[13] H. Yi, S. Al-Faifi, A. Iraqi, D. C. Watters, and J. Kingsley. Carbazole and thienyl benzo[1,2,5]thiadiazole based polymers with improved open circuit voltages and processability for application in solar cells. *J. Mater. Chem.*, 21:13649, 2011.

[14] T. Basche, W. E. Moerner, M. Orrit, and U. P. Wild. *Single-Molecule Optical Detection, Imaging and Spectroscopy*. VCH Verlagsgesellschaft mbH, 2007.

[15] M. Vacha and S. Habuchi. Conformation and physics of polymer chains: a single-molecule perspective. *NPG Asia Mater.*, 2:134–142, 2010.

[16] G. E. Khalil, A. M. Adawi, A. M. Fox, A. Iraqi, and D. G. Lidzey. Single molecule spectroscopy of red- and green-emitting fluorene-based copolymers. *J. Chem. Phys*, 130(4):044903, 2009.

[17] Alan Owens. *Compound Semiconductor Radiation Detectors*. Series in Sensors. CRC Press-Taylor & Francis Group, 6000 Broken Sound Parkway NW, STE 300, Boca Raton, FL 33487-2742 USA, 2012.

[18] C. Kittel. *Introduction to Solid State Physics*. John Wiley & Sons, Wiley 8th Edition, 2005.

[19] W. T. Wenckenbach. *Essentials of Semiconductor Physics*. John Wiley & Sons, Hoboken N.J., 1999.

[20] N. Bohr. On the constitution of atoms and molecules. *Philosophical MAgazine*, 26(6):1–25, 1913.

[21] J. P Colinge and C. A. Colinge. *Physics of Semiconductor Devices*. Springer Science & Business Media, October 2005.

[22] T. W. Kelley, P. F. Baude, C. Gerlach, D. E. Ender, M. A. Hasse, D. E. Vogel, and S. D. Theiss. Recent progress in organic electronics: Materials, devices amnd processes. *Chem. Mater.*, 16:4413–4422, 2004.

[23] S. R. Forrest. The path to ubiquitous and low-cost organic electronic appliances on plastic. *Nature*, 428:911–918, 2004.

[24] T. Tsuitsui and K. Fujita. The shift from "hard" to "soft" electronics. *Adv. Mater*, 14:949–952, 2002.

[25] J. M. Shaw and P. F. Seidler. Organic electronics: Introduction. *IBM J. Res. Dev.*, 45:3–10, 2001.

[26] A. Facchetti. Pi-conjugated polymers for organic electronics and photovoltaic cell applications. *Chem. Mater.*, 23:733–758, 2011.

[27] N. Karl. Charge carrier transport in organic semiconductors. *Synth. Met.*, 133-134:649–657, 2003.

[28] H. E. Katz. Recent advances in semiconductor performance and printing processes for organic transistor-based electronics. *Chem. Mater.*, 16:4748–4756, 2004.

[29] R. Hamilton, C. Bailey, W. Duffy, M. Heeney, M. Shkunov, D. Sparrowe, S. Tierney, I. McCulloch, R. J. Kline, D. M. DeLongchamp, and M. Chabinyc. The influence of molecular weight on the microstructure and thin film transistor characteristics of pbttt polymers. *Proc. SPIE-Int. Soc. Opt. eng.*, 6336: 158, 2006.

[30] Frank C. Spano. Temperature dependent exciton emission from herringbone aggregates of conjugated oligomers. *J. Chem. Phys.*, 120(16), 2004.

[31] Luiz A. Ribeiro, Pedro H. Oliveira Neto, Wiliam F. da Cunha, Luiz F. Roncaratti, Ricardo Garano, Demetrio A. da Silva Filho, and Geraldo M. e Silva. Exciton dissociation and charge carrier recombination processes in organic semiconductors. *J. Chem. Phys.*, 135(22), 2011.

[32] W. J. D. Beenken and T. J. Pulleritis. Spectroscopic units in conjugated polymers: A quantum chemically founded concept? *J. Phys. Chem. B*, 108 (20):6164–6169, 2004.

[33] Ivan G. Scheblykin. Conjugated macrocycles: Excitations get random. *Nature Chemistry*, 4(11):903–904, 2013.

[34] Y. Berlin, A. Burin, J. Friedrich, and J. Kohler. Low temperature spectroscopy of proteins. part ii: Experiments with single protein complexes. *Phys. Life Rev.*, 4(1):64–89, 2007.

[35] M. Ariu, M. Sims, M. D. Rahn, J. Hill, A. M. Fox, D. G. Lidzey, M. Oda, J. Cabanillas-Gonzalez, and D. D. C. Bradley. Exciton migration in -phase poly(9,9-dioctylfluorene). *Phys. Rev. B*, 67(19), 2003.

[36] W. H. Carothers. Studies on polymerization and ring formation. i. an introduction to the general theory of condensation polymers. *J. Am. Chem. Soc.*, 51:2548–2559, 1929.

[37] G. Odian. *Principles of Polymerisation 4th ed.* Wiley Interscience, Hoboken (NJ), 2004.

[38] L. Reh. Challenges for process industries in recycling. *China Particuology*, 4 (2):47–59, 2006.

[39] E. Saldivar-Guerra and E. Vivaldo-Lima. *Handbook of Polymer Synthesis, Characterisaton and Processing.* John Wiley and Sons, Inc., first edition edition, 2013.

[40] W. H. Ray. On the mathematical modeling of polymerization reactors. *J. Macromol. Sci. PArt C*, 8(1):1–56, 1972.

[41] J. Kahovec, R. B. Fox, and K. Hatada. Nomenclature of regular single-strand organic polymers. *Pure Appl. chem.*, 74(10):1921–1956, 2002.

[42] G. Natta, G. Mazzanti, and P. Corradini. *Atti Accad. naz. Lincei, Cl, Sci. Fis. Mat. Nat. r.*, 25:3, 1958.

[43] H. Shirakawa, E. J. Louis, A. G. MacDiarmid, C. K. Chiang, and A. J. Heeger. Synthesis of electrically conducting organic polymers: halogen derivatives of polyacetylene, (ch)x. *J. Chem. Soc. Chem. Commun.*, 16:578–580, 1977.

[44] The nobel prize in chemistry 2000, nobel media ab. URL `http://www.nobelprize.org/nobel_prizes/chemistry/laureates/2000/`.

[45] T. J. Skotheim and J. r. Reynolds. *Handbook of Conducting Polymers*. CRC Press, Boca Raton, USA, third edition edition, 1997.

[46] T. Johansson, W. Mammo, M. Svensson, M. R. Andersson, and O. Inganas. Electrochemical bandgaps of substituted polythiophenes. *J. Mater. Chem.*, 13 (6):1316–1323, 2003.

[47] H. Kishida, K. Hirota, T. Wakabayashi, and H. Okamoto. Third-order optical nonlinearity in regio-controlled polythiophene films. *Appl. Phys. Lett.*, 87(12): 121902, 2005.

[48] Y. TAdesse, R. W. Grange, and S. Priya. Synthesis and cyclic force characterization of helical polypyrrole actuators for artificial facial muscles. *Smart Mater. Struct.*, 18(8):085008, 2009.

[49] A. Pron and P. Rannou. Processible conjugated polymers, from organic semiconductors to organic metals and superconductors. *Prog. Polym. Sci.*, 27: 135–190, 2002.

[50] F. Wudl, M. Kobayashi, and A. J. Heeger. Poly(isothianaphthene). *J. Org. Chem.*, 49(18):3382–3384, 1984.

[51] F. L. Klavetter and R. H. Grubbs. Polycyclooctatetraene (polyacetylene) synthesis and properties. *J. Am. Chem. Soc.*, 10:7807–7813, 1988.

[52] J. H. Edwards and W. J. feast. A new synthesis of poly(acetylene). *Polym. Commun,*, 21:595–596, 1980.

[53] R. L. Elsenbaumer, K. Y. Jen, and R. Oboodi. Processible and environmentally stable conducting polymers. *Synth. Met.*, 15:169–174, 1986.

[54] K. Kaeriyama, M. Sato, and S. tanaka. Electrochemical preparation of conducting polyalkythiophene ®lms. *Synth. Met.*, 18:233–236, 1987.

[55] R. D. McCullough and R. D. Lowe. Enhanced electrical conductivity in regioselectively synthesized poly 3-alkylthiophenes). *J. Chem. Soc. Chem. Commun.*, 1:70–72, 1992.

[56] R. D. McCullough, S. Tristam-Nagle, S. P. Williams, R. D. Lowe, and M. Jayaraman. Self-orienting head-to-tail poly 3-alkylthio- phenes): new insights on structure-property relationships in conducting polymers. *J. Am. Chem. Soc.*, 115:4910–4911, 1993.

[57] T. A. Chen and R. D. Rieke. The first regioregular head-to-tail poly 3-hexylthiophene-2,5-diyl) and a regiorandom isopolymer: Ni vs. pd catalysis of 2 5)-bromo-5 2)- bromozincio)-3-hexylthiophene polymerization. *J. Am. Chem. Soc.*, 114:10087–10088, 1992.

[58] T. A. Chen, X. Wu, and R. D. Rieke. Regiocontrolled synthesis of poly 3-alkylthiophenes) mediated by rieke zinc: their characterization and solid-state properties. *J. Am. Chem. Soc.*, 117:233–244, 1995.

[59] M. Sauer, J. Hofkens, and J. Enderlein. *Handbook of Fluorescence Spectroscopy and Imaging*. Wiley-VCH Verlag GMBh & Co. KgaA, Weinheim, 2011.

[60] M. Shirai, T. Yamamoto, and M. Tsunooka. Ablative photodegradation of poly(methyl methacrylate and its homologues by 185-nm light. *Polymer Degradation and Stability*, 63:481–487, 1999.

[61] J. A. Woollam, C. Bungay, J. Hilfiker, and T. Tiwald. Vuv and ir spectroellipsometric studies of polymer surfaces. *Nuclear Instruments and Methods in Physics Research B*, 208:35–39, 2003.

[62] W. Pauli. Uber den zusammenhang des abschlusses der elektronengruppen im atom mit der komplexstruktur der spektren. *Z. Physik*, 31:765–783, 1925.

[63] A. Jablonski. Uber den mechanisms des photolumineszenz von farbstoffphosphoren. *Z. Physik*, 94:38–46, 1935.

[64] J. R. Lakowicz. *Principles of Fluorescence Spectroscopy*. Springer Science+Business Media, New York, NY 10013, USA, 3rd edition. edition, 2006.

[65] M. Kasha. Collisional perturbation of spin-orbital coupling and the mechanism of fluorescence quenching. a visual demonstration of the perturbation. *J. Chem. Phys*, 20:71–74, 1952.

[66] M. Tabachnyk, A. H. Karani, K. Broch nd L/ M. Pazos-Outon, J. Xiao, T. C. Jellicoe, J. Novak, D. Harkin, A. J. Pearson, A. Rao, N. C. Greenhan, M. L. Bohm, and R. H. Friend. Efficient singlet exciton fission in pentacene prepared from a soluble precursor. *Apl. Materials*, 4:16112, 2016.

[67] V. I. Arkhipov, H. Bassler, M. Deussen, E. O. Gobel, U. Lemmer, and R. F. Mahrt. Field-induced dissociation of optical excitations in conjugated polymers. *Journal of Non-Crystalline Solids*, 198-200:661–664, 1996.

[68] M. Nothaft, S. Hohla, F. Jelezko, J. Pflaum, and J. Wrachtrup. Single molecule electrical excitation. *Phys. Status Solidi B*, 249(4):653, 660 2012.

[69] A. Kohler and H. Bassler. Triplet states in organic semiconductors. *Mat. Sci. Eng. R*, 66:71–109, 2009.

[70] P. W. Atkins and R. Friedman. *Molecular Quantum Mechanics 4th Edition.* Oxford University Press, Great Clarendon Street, Oxford, 1983.

[71] A. Kohler and D. Beljonne. The singlet-triplet exchange energy in conjugated polymers. *Adv. Func. Mater.*, 14(1):11–18, 2004.

[72] S. Kraner, R. Scholz, F. Plasser, C. Koerner, and K. Leo. Exciton size and binding energy limitations in one-dimensional organic materials. *J. Chem. Phys.*, 143:244905, 2015.

[73] O. V. Mikhnenko, P. W. Blom, and T-Q. Nguyen. Exciton diffusion in organic semiconductors. *Energy Envirom. Sci.*, 8:1867–1888, 2015.

[74] S. D. Dimitrov, B. C. Schroeder, C. B. Nielsen, H. Bronstein, Z. Fei, I. McCulloch, M. Heeney, and J. R. Durrant. Singlet exiton lifetimes in conjugted polymer films for organic solar cells. *Polymer*, 8(1):14, 2016.

[75] N. J. Turro. *Modern Molecular Photochemistry.* University Science Books, Mill Valey, CA, USa, 1991.

[76] M. K. K. Nakaema and R. Sanches. Frequency-domain fluorometry. *Quimica Nova*, 22(3):412–416, 1999.

[77] F. V. Bright and C. A. Munson. Time-resolved fluorescence spectroscopy for illuminating complex systems. *Anal. Chim. Acta*, 500:71–104, 2003.

[78] E. Schrodinger. Are there quantum jumps? part 2. *Brit. Soc. Phil. Sci.*, 3 (11):233–242, 1952.

[79] W. E. Moerner and L. Kador. Optical detection and specroscopy of single molecules in a solid. *Phys. Rev. Lett.*, 62(21):2535–2538, 1989.

[80] M. Orrit and J. Bernard. Single pentacene molecuels detected by fluorescence excitation in a p-terphenyl crystal. *Phys. Rev. Lett.*, 65(21):2716–2719, 1990.

[81] A. Yildiz, M. Tomishige, R. D. Vale, and P. R. Selvin. Kinesin walks hand-over-hand. *Science*, 303(5658):676–678, 2004.

[82] G. Seisenberger, M. U. Reid, T. Endress, H. Buning, M. Hallek, and C. Brauchle. Real-time single-molecule inaging of hte infection pathway of an adeno-associated virus. *Science*, 294(5548):1929–1932, 2001.

[83] D. A. Vanden Bout, W-T Yip, D. Hu, D-K Fu, T. M. Swager, and P. F. Barbara. Discrete intensity jumps and intramolecular electronic energy transfer in the spectroscopy of single conjugated polymer molecules. *Science*, 277: 1074–1077, 1997.

[84] S. Westenhoff, W. J. D. Beenken, A. Yartsev, and N. C. Greenhan. Conformational disorder of conjugated polymers. *J. Chem. Phys.*, 125:154903, 2006.

[85] G. Rossi, R. R. Chance, and R. Silbey. Conformational disorder in conjugated polymers. *J. Chem. Phys.*, 90(12):7594–7601, 1989.

[86] A. Thiessen, J. Vogelsang, T. Adachi, F. Steiner, and D. A. Vanden Bout. Unraveling the chromophoric disorder of poly(3-hexylthiophene). *P. Natl. Acad. Sci. USA*, 110(38):E3550–E3556, 2013.

[87] M. J. Walter, J. M. Lupton, K. Becker, J. Feldmann, G. Gaefke, and S. Hoeger. Simultaneous raman and fluorescence spectroscopy of single conjugated polymer chains. *Phys. Rev. Lett.*, 98:137401, 2007.

[88] E. J. J. Martin, N. Berube, F. Provencher, M. Cote, C. Silva, S. K. Doom, and J. K. Grey. Resonance raman spectroscopy and imaging of push-pull conjugated polymer-fullerene blends. *J. Mater. Chem. C*, 3:6058–6066, 2015.

[89] M. L. Shand, R. R. Chance, M. LePostollec, and M. Schott. Raman photoselection and conjugation-length dispersion in conjugated polymer solutions. *Phys. Rev. B*, 25(7):4431–4436, 1982.

[90] Z. Wang and L. J. Rothberg. Structure and dynamics of single conjugated polymer chromophores by surface-enhanced raman spectroscopy. *ACS Nano*, 1(4):299–306, 2007.

[91] P-Y. chen, A. Rassamesard, H-L. chen, and S-A. Chen. Conformation and fluorescence property of poly(3-hexylthiophene isolated chains studied by single

molecule spectroscopy: effects of solvent quality and regioregularity. *Macromolecules*, 46:5657–5663, 2013.

[92] B. Fuckel, G. Hinze, G. Diezemann, F. Nolde, K. Mullen, J. Gauss, and T. Bache. Flexibility of phenilene olygomers revealed by single molecule spectroscopy. *J. Chem. Phys.*, 125:144903, 2006.

[93] S. Habuchi, H. Fujita, T. Michinobu, and M. Vacha. Twist angle plays an important role in photophysical properties of a donor-acceptor-type conjugated polymer: a combined ensemble and single-molecule study. *J. Phys. Chem. B*, 115:14404–14415, 2011.

[94] J. M. Lupton. Single-molecule spectroscopy for plastic electronics: materials analysis from the bottom-up. *Adv. Mater.*, 22:1689–1721, 2010.

[95] T. Gensch, M. bohmer, and P. F. Aramendia. Single molecule blinking and photobleaching separated by wide-field fluorescencem icroscopy. *J. Phys. Chem. A*, 109:6652–6658., 2005.

[96] S. Rocha, J. A. Hutchinson, K. Peneva, A. Herrmann, K. Mullen, M. Skjot, C. I. Jorgensen, A. Svendsen, F. C. De Schryver, J. Hofkens, and H. Uji-i. Linking phospholipase mobility to activity by single-molecule wide-field microscopy. *ChemPhysChem*, 10:151–161, 2009.

[97] H. Lin, Y. tian, K. Zapadka, G. Persson, D. Thomsson, O. Mirzov, P. O. Larsson, J. Widengren, and I. G. Scheblykin. Fate of excitations in conjugated polymers: single-molecule spectroscopy reveals nonemissive dark regions in meh-ppv individual chains. *Nano Letters*, 9(12):4456–4461, 2009.

[98] S. Chattoraj and K. Bhattacharyya. Spatial inhomogeneity in spectra and exciton dynamics in porphyrin micro-rods and micr-brushes: confocal microscopy. *J. Chem. Sci.*, 128(11):1717–1724, 2016.

[99] M. F. Zickler, F. A. Feist, J. Jacob, K. Mullen, and T. Basche. Single molecule studies of a ladder type conjugated polymer: vibronic spectra, line widths and energy transfer. *Macromol. Rapid Commun.*, 36:1096–1102, 2015.

[100] J. N. Clifford, T. D. M. Bell, P. Tinnefeld, M. Heilemann, S. M. Melnikov, J i Hotta nad M. Sliwa, P. Dedecker, M. Sauer, J. Hofkens, and E. K. L. Yeow. Fluorescence of single molecules on polymer films: sensitivity of blinking to local environment. *J. Phys. Chem. B*, 111(25):6987–6991, 2007.

[101] R. M. Dickinson, A. B. Cubitt, R. Y. Tsien, and W. E. Moerner. On/off blinking and switching behaviour of single molecules of green fluorescent protein. *Nature*, 388:355–358, 1997.

[102] G. E. Khalil, A. M. Adawi, B. Robinson, A. J. Cadby, W. C. Tsoi, J-S. Kim, A. Charas, J. Morgado, and D. G. Lidzey. Spectroscopy and single-molecule emission of a fluorene-terthiophene oligomer. *J. Phys. Chem. B*, 115(12028-12035), 2011.

[103] Y. Tian, A. Merdasa, M. Peter, M. Abdellah, K. Zheng, C. S. Ponseca Jr, T. Pulleritis, A. Yartsev, V. Sundstrom, and I. G. Scheblykin. Giant photoluminescence blinking of perovskite nanocrystals reveals single-trap control of luminescence. *Nano Lett.*, 15:1603–1608, 2015.

[104] T. Stangl, P. Wilhelm, K. Remmerssen, S. Hoger, J. Vogelsang, and J. M. Lupton. Mesoscopic quantum emitters from deterministic aggregates of conjugated polymers. *Proc. Natl. Acad. Sci. U.S.A.*, 112(41):E5560–E5566, 2015.

[105] J. Vogelsang, T. Adachi, J. Brazard, D. A. Vanden Bout, and P. F. Barbara. Self-assembly of highly ordered conjugated polymer aggregates with long-range energy transfer. *Nature Materials*, 10:942–946, 2011.

[106] F. Schindler and J. M. Lupton. Single chromophore spectroscopy of mehppv. homing-in on the elementary emissive species in conjugated polymers. *ChemPhysChem*, 6:926–934, 2005.

[107] F. Schindler, J. M. Lupton, J. Feldmann, and U. Scherf. A universal picture of chromophores in pi-conjugated polymers derived from single-molecule spectroscopy. *P. Natl. Acad. Sci. Usa*, 101(41):14695–14700, 2004.

[108] T. Basche, W. E. Moerner, M. Orrit, and H. Talon. Photon antibunching in the fluorescence of a single dye molecule trapped in a solid. *Phys. Rev. Lett.*, 69(10):1516–1519, 1992.

[109] H. J. Kimble, M. Dagenais, and L. Mandel. Photon antibunching in resonance fluorescence. *Phys. Rev. Lett.*, 39:691–695, 1977.

[110] P. Kumar, T-H. Lee, A. Mehta, B. G. Sumpter, R. M. Dickinson, and M. Barnes. Photon antibunching from oriented semiconducting polymer nanostructures. *J. Am. Chem. Soc.*, 126:3376–3377, 2004.

[111] A. J. Wise and J. K. Grey. Understanding the structural evolution of single conjugated polymer chain conformers. *Polymers*, 8(11):388, 2016.

[112] P. Kumar, A. Mehta, M. D. Dadmun, J. Zheng, L. Peyser, A. P. Bartko, R. M. Dickinson, T. Thundat, B. G. Sumpter, D. W. Noid, and M. D. Barnes. Narrow-bandwidth spontaneous luminescence from oriented semiconducting polymer nanostructures. *J. Phys. Chem. B*, 107:6252–6257, 2003.

[113] M. Vacha and S. Habuchi. Conformation and physics of polymer chains: a single-molecule perspective. *NPG Asia Mater.*, 2(4):134–142, 2010.

[114] C. Eggeling, J. R. Fries, L. Brand, R. Gunther, and C. A. M. Seidel. Monitoring conformational dynamics of a single molecule by selective fluorescence spectroscopy. *Proc. Natl. Acad. Sci. U.S.A.*, 95:1556–1561, 1998.

[115] H. Lin, S. R. Tabaei, D. Thomsson, O. Mirzov, P. O. Larsson, and I. G. Scheblykin. Fluorescence blinking, exciton dynamics, and energy transfer domains in single conjugated polymer chains. *J. Am. Chem. Soc.*, 130:7042–7051, 2008.

[116] F. J. Hofmann, J. Vogelsang, and J. M. Lupton. Impact of charge carrier injection on single chain photophysics of conjugated polymers. *Appl. Phys. Lett.*, 108:263301, 2016.

[117] A. Kiraz, M. Ehrl, C. Brauchle, and A. Zumbusch. Low temperature single moelcule spectroscopy using vibronic excitation and dispersed fluorescence detection. *J. Chem. Phys.*, 118(24):10821–10824, 2004.

[118] R. Hildner, U. Lemmer, U. Scherf, M. van Heel, and J. Kohler. Revealing the electron-phonon coupling in a conjugated polymer by single-molecule spectroscopy. *Adv. Mater.*, 19:1978–1982, 2007.

[119] C. Ronne, J. Tragardh, D. Hessman, and V. Sundstrom. Temperature effect on single chain meh-ppv spectra. *Chem. Phys. Lett.*, 388(1):40–45, 2004.

[120] T. Guillet, J. Berrehar, R. Grousson, J. Kovensky, C. Lapersonne-Meyer, and V. Voliotis. Emission of a single conjugated polymer chain isolated in its single crystal monomer matrix. *Phys. Rev. Lett.*, 87(8):087401, 2001.

[121] F. A. Feist, M. Zickler, and T. Basche. Origin of the red sites and energy transfer rates in single meh-ppv chains at low temperature. *ChemPhysChem*, 12:1499–1508, 2011.

[122] Y. Ebihara, S. Habuchi, and M. Vacha. Conformation-dependent room-temperature emission spectra of single meh-ppv chains in different polymer matrices. *Chem. Lett.*, 38(11):1094–1095, 2009.

[123] J. kim, M. H. Yun, G-H. Kim, J. Lee, S. M. Lee, S-J. Ko, Y. Kim, G. K. Dutta, M. Moon, S. Y. Park, D. S. Kim, J. Y. Kim, and C. Yang. Synthesis of pcdtbt-based fluorinated polymers for high open-circuit voltage in organic photovoltaics: towards an udnerstanding of relationships between polymer energy levels engineering and ideal morphology control. *ACS Appl. Mater. Interfaces*, 6:7523–7534, 2014.

[124] R. Alqurashi, J. Griffin, A. Alsulami, and A. buckley. Open-circuit voltage in inverted polycarbazole:fullerene bulk heterojunction solar cells. *IEEE Journal of Photovoltaics*, 6(4):918–923, 2016.

[125] S. Cho, J. H. Seo, S. H. Park, S. Beauport, M. Leclerc, and A. J. Heeger. A thermally stable semiconducting polymer. *Adv. Mater.*, 22:1253–1257, 2010.

[126] C. H. Peters, I. T. Sachs-Quintana, J. P. Kastrop, S. Beaupre, M. Leclerc, and M. D. McGehee. High efficiency polymer solar cells with long operating lifetimes. *Adv. Energy Mater.*, 1:491–494, 2011.

[127] Y. sun, J. H. Seo, C. J. Takacs, J. Seifter, and A. J. Heeger. Inverted polymer solar cells integrated with a low-temperature-annealed sol-gel-derivated zno film as an electron transport layer. *Adv. Mater.*, 23:1679–1683, 2011.

[128] X. Sun, J. Ni, C. Li, L. Huang, R. Xu, Z. Li, H. Cai, J. Li, and J. Zhang. Air-processed high performance ternary blend solar cells based on ptb7-th:pcdtbt:pc70bm. *Organic Electronics*, 37:222–227, 2016.

[129] Y. Xiao, H. Wang, S. Zhou, K. Yan, W. Xie, Z. Guan, S-W. T, and J-B. Xu. Efficient ternary bulk heterojunction solar cells with pcdtbt as hole-cascade material. *Nano Energy*, 19:476–485, 2016.

[130] P. F. Barbara, A. J. Gesquiere, S-J PArk, and Y. J. Lee. Single-molecule spectroscopy of conjugated polymers. *Acc. Chem. Res.*, 38:602–610, 2005.

[131] W. E. Moerner. Those blinking single molecules. *Science*, 277(5329):1059–1060, 1997.

[132] Edge detector 1d tutorial, 2017. URL `http://cismm.web.unc.edu/resources/tutorials/edge-detector-1d-tutorial/`.

[133] J. Canny. A computational approach to edge detection. *IEEE Trans. Pattern Anal. Mach. Intell.*, 8(6):679–698, 1986.

[134] T. Peter So and C. Y. Dong. Fluorescence spectrophotometry. *Encyclopedia of Life Sciences*, 2002.

[135] Dh-2000 family. deuterium-halogen light sources for the uv-vis-nir, 2016. URL `http://oceanoptics.com/product/dh-2000-family/`.

[136] C. Vasilev, M. P. Johnson, E. Gonzales, L. Wang, A. V. Ruban, G. Montano, A. J. Cadby, and C. N. Hunter. Reversible switching between nonquenched and quenched states in nanoscale linear arrays of plant light-harvesting antenna complexes. *Langmuir*, 30(28):8481–8490, 2014.

[137] Wolfgang Becker. *The bh TCSPC Handbook. Sixth Edition.* Becker & Hickl GmbH, 2014.

[138] L. M. Bollinger and G. E. Thomas. Measurement of the time dependence of scintillation intensity by a delayed coincidence method. *Rev. Sci. Instrum*, 32: 1044–1050, 1961.

[139] S. Cova, M. Bertolaccini, and C. Bussolati. The measurement of luminescence waveforms by single-photon techniques. *Phys. Stat. Sol.*, 18:11–61, 1973.

[140] B. Leskovar and C. C. Lo. Photon counting system for subnanosecond fluorescence lifetime measurements. *Rev. Sci. Instrum*, 47:1113–1121, 1976.

[141] H. C. Gerritsen, M. A. H. Asselbergs, A. V. Agronskaia, and W. G. J.H.M. van Sark. Fluorescence lifetime imaging in scanning microscopes: acquisition speed, photon economy and lifetime resolution. *J. Microsc.*, 206:218–224, 2002.

[142] K. Carlsson and J. P. Philip. Theoretical investigation of the signal-to-noise ratio for different fluorescence lifetime imaging techniques. *Proc. SPIE 4622*, pages 70–78, 2002.

[143] R. M. Balew and J. N. Demas. An error analysis of the rapid lifetime determination method for the evaluation of single exponential decays. *Anal. chem.*, 61:30, 1989.

[144] J. W. Kingsley, P. P. Marchisio, H. Yi, A. Iraqi, C. J. Kinane, S. Langridge, R. L. Thompson, A. J. Cadby, A. J. Pearson, D. G. Lidzey, R. A. Jones, and A. J. Parnell. Molecular weight dependent vertical composition profiles of pcdtbt:pc71bm blends for organic photovoltaics. *Scientific Reports*, 4(5286): 1–7, 2014.

[145] Spin coating: A guide to theory and techniques, 2016. URL `https://www.ossila.com/pages/spin-coating#spin-coating-thickness-equation`.

[146] T. P. Burghardt, J. E. Charlesworth, M. F. Halstead, J. E. Tarara, and K. Ajtai. In situ fluorescent protein imaging with metal film-enhanced total internal reflection microscopy. *Biophysical Journal*, 90(12):4662–4671, 2006.

[147] T.P.Burghardt, K.Ajtai, and J.Borejdo. In situ single-molecule imaging with attoliter detection using objective total internal reflection confocal microscopy. *Biochemistry*, 45(13):4058–4068, 2006.

[148] M.Sergeev, S.Constantino, and P.W.Wiseman. Measurement of monomer-oligomer distributions via fluorescence moment image analysis. *Biophysical Journal*, 91(10):3884–3896, 2006.

[149] Fluospheres fluorescent microspheres, October 2005.

[150] T. P. Burghardt, K. Ajtai, and J. Borejdo. In situ single-molecule imaging with attoliter detection using objective total internal reflection confocal microscopyinternal reflection confocal microscopy. *Biochemistry*, 45:4058–4068, 2006.

[151] G. D. Scholes and G. Rumbles. Excitons in nanoscale systems. *Nature Materials*, 5:683–696, 2006.

[152] I. Bugiel, K. Konig, and H. Wabnitz. Investigation of cells by fluorescence laser scanning microscopy with subnanosecond time resolution. *Lasers Life Sci.*, 3:47–53, 1989.

[153] L. D'Olieslaeger, M. Pfannmoller, E. Fron, I. Cardinaletti, M. Van Der Auweraer, G. Van Tendeloo, S. Bals, W. Maes, D. Vanderzande, J. Manca, and

A. Ethirajan. Tuning of pcdtbt:pc71bm blend nanoparticles for eco-friendly processing of polymer solar cells. *Solar Energy Materials and Solar Cells*, 159: 179–188, 2017.

[154] H. Nie, Y. Zhao, M. Zhang, Y. Ma, M. Baumgarten, and K. Mullen. Detection of tnt ex[plosives with a new fluorescent conjugated polycarbazole polymer. *Chem. Commun.*, 47:1234–1236, 2011.

[155] H. Nie, G. Sun, M. Zhang, M. Baumgarten, and K. Mullen. Fluorescent conjugated polycarbazoles for explosives detection: Side chain effects of tnt sensor sensitivity. *J. MAter. Chem.*, 22(2129-2132), 2012.

[156] B. Zhang, Z. hu, M. Wang, H. Xiao, X. Gong, W. Yang, and Y. Cao. Highyefficient polymer soalr cells baed on poly(carbazole-alt-thiophene-benzofurazan). *New. J. Chem.*, 36:2042–2047, 2012.

[157] N. Banerji, S. Cowan, M. Leclerc, E. Vauthey, and A. J. Heeger. Exciton formation, relaxation, and decay in pcdtbt. *J. Am. Chem. Soc.*, 132:17459–17470, 2010.

[158] C. Duan, W Cai, B. B. Y. Hsu, C. Zhong, K. Zhang, C. Liu, Z. Hu, F. Huang, C. C. Bazan, A. J. Heeger, and Y. Cao. Toward green solvent processable photovoltaic materials for polymer solar cells: the role of highly polar pendant groups in charge carrier transport and photovoltaic behavior. *Energy Environ. Sci.*, 6:3022–3034, 2013.

[159] A. J. Heeger. Semiconducting polymers: the third generation. *Chem. Soc. Rev.*, 39:2354–2371, 2010.

[160] Y. Zhu, L. Yang, Z. Zhao, Y. Huang, Z. Xu, Q. Yang, P. Wang, Y. Li, and X. Xu. Improved performances pf pcdtbt:pc7y1bm bhj solar cells through incorporating small molecule donor. *Phys. Chem. Chem. Phys.*, 17:26777–26782, 2015.

[161] W. Becker. Fluorescence lifetime imaging by multi-dimensional time correlated single photon counting. *Medical Photonics*, 27:41–61, 2015.

[162] K. Suhling, L.M. Hirvonen, J. A. Levitt, P-H. Chang, C. Tregidgo, A. Le Marois, D.A. Rusakov, K. Zheng, S. Ameer-Beg, S. Poland, S. Coelho, R. Henderson, and N. Krstajic. Fluorescence lifetime imaging (flim). basic concept sand some recent developments. *Medical Photonics*, 27:3–40, 2015.

[163] R. M. Ballew and J. N. Demas. An error analysis of the rapid lifetime determination method for the evaluation of single-exponential decays. *Anal. Them.*, 61:30, 1989.

[164] J. P. Philip and K. Carlsson. Theoretical investigation of the signal-to-noise ratio in fluorescence lifetime imaging. *J. Opt. Soc. Am.*, A20:368–379, 2003.

[165] H. W. Kroger, G. K. Schmidt, and N. Paller. Faint object camera: European contribution to the hubble space telescope. *Acta Astronaut.*, 26:827–834, 1992.

[166] A. Kraft, A. C. Grinsdale, and A. B. Holmes. Electroluminescent conjugated polymers - seeing polymers in a new light. *Angew. Chem., Int. Ed*, 37:402–428, 1998.

[167] B. J. Schwartz. Conjugated polymers as molecular materials: how chain conformation and film morphology can influence energy transfer and interchain interactions. *Annu. Rev. Phys. Chem*, 54:141–172, 2003.

[168] U. Scherf and E. J. W. List. Semiconducting polyfluorene - towards reliable structure-property relationships. *Adv. Mater*, 14:477–487, 2002.

[169] D. hu nad J. Yu, K. Wong, B. Bagchi, P. J. Rossky, and P. F. Barbara. Collapse of stiff conjugated polymers with chemical defects into ordered, cylindrical conformations. *Nature*, 405:1030–1033, 2000.

[170] T. Huser, M. Yan, and L. J. Rothberg. Single chain spectroscopy of conformational dependence of conjugated polymer photophysics. *Proc. Natl. Acad. Sci. U.S.A.*, 97(21):11187–11191, 2000.

[171] J. G. Muller, U. Lemmer, G. Raschke, M. Anni, U. Scherf, J. M. Lupton, and J. Feldmann. Linewidth-limited energy transfer in single conjugated polymer molecules. *Phys. Rev. Lett.*, 91(26):267403, 2003.

[172] F. Schindler, J. M. Lupton, J. Feldmann, and U. Scherf. Controlled fluorescence bursts from conjugated polymers induced by triplet quenching. *Adv. Mater.*, 16(7):653–657, 2004.

[173] J. P. Hoogenboom, J. Hernando, E. M. H. P. van Dijk, N. F. van Hulst, and M. F. Garcia-Parajo. Power-law blinking in the fluorescence of single organic molecules. *ChemPhysChem*, 8:823–833, 2007.

[174] J. P. Hoogenboom, W. K. den Otter, and H. L. Offerhaus. Accurate and unbiased estimation of power-law exponents from single-emitter blinking data. *J. Chem. Phys.*, 125:204713, 2006.

[175] M. Kuno, D. P. Fromm, H. F. Hamann, A. Gallagher, and D. J. Nesbitt. On off fluorescence intermittency of single semiconductor quantum dots. *J. Chem. Phys.*, 11(2):1028–1040, 2001.

[176] M. Kuno. Modeling distributed kinetics in isolated semiconductor quantum dots. *Phys. Rev. B*, 67:125304, 2003.

[177] J. B. Hoogenboom, E. M. H. P. van Dijk, J. Hernando, N. F. van Hulst, and M. F. Garcia-Parajo. Power-law-distributed dark states are the main pathway for photobleaching of single organic molecules. *Phys. Rev. Lett.*, 95:097401, 2005.

[178] M. A. Tachiya and A. Mozumder. Kinetics of geminate-ion recombination by electron tunnelling. *Chem. Phys. Lett.*, 34(1):77–79, 1975.

[179] R. Verberk, A. M. van Oijen, and M. Orrit. Simple model for the power-law blinking of single semiconductor nanocrystals. *Phys. Rev. B*, 66:233202, 2002.

[180] W. P. Ambrose and W. E. Moerner. Fluorescence spectroscopy and spectral diffusion of single impurity molecules in a crystal. *Nature*, 349:225–227, 1991.

[181] R. Chang, J. H. Hsu, W. S. Fann, J. Yu, S. H. Lin, Y. Z. Lee, and S. A. Chen. Aggregated states of luminescence conjugated polymers in solutions. *Chem. Phys. Lett.*, 317:153–158, 2000.